

PULP

---

- 1      **Pine resin components are degraded at different rates during outdoor seasoning for dissolving wood pulp production**  
*Sebastian España Orozco, Elisabeth Fitz, Jürgen Ritzberger, Susanne Möderl and Robert H. Bischof*
- 9      **Innovative dissolving pulps for application in cellulose MMF production**  
*Birgit Kosan, Frank Meister, Ina Sigmund, J. Paulitz*

CELLULOSE COMPOUNDS

---

- 15     **Convenient preparation of methyl cellulose using trimethylsulfonium hydroxide electrolytes**  
*Gabriel Julian Partl, Kateryna Huemer, Robert Bischof, Danuta Aigner, Christian Sperger, and Herwig Schottenberger*

PROCESSING

---

- 23     **Alkali-Blau (Anilin-Blau) für die Färbung textiler PAC-Fasern**  
*Manfred Hähnke*

FIBERS

---

- 29     **Lyocell fibers from pulps with high mannan and xylan content – Part 1: Fiber cross section**  
*Gabriele Schild, Martina Opietnik, Sandra Schlader*
- 39     **Processing of metal sulfide/cellulose nanocomposite fibers in core-shell configuration**  
*Michael Weißl, Mike Pelzmann, Armin Zankel, Brigitte Bitschnau, Helmar Wiltsche, Gregor Trimmel, and Stefan Spirk*

ANALYTICS

---

- 49     **Effect of packing density on zeta potential of cellulosics**  
*Adisak Jaturapiree, Avinash P. Manian, Thomas Bechtold*

## Editorial

Today's global society is based on the use of fossil resources, primarily oil, natural gas and coal. The entire chemical industry – and thus all dependent industries – rely on fossil energy and material carriers. It is imperative to think not only about fossil fuels in this regard – as is often done in the media in a simplifying way. Of course, oil and natural gas are used to produce fuel oil, fuel gas, gasoline, diesel and kerosene. More importantly (and often forgotten) are all the materials and substances that are naturally available to us in everyday life: plastics of all kinds, colors, chemicals, packaging or pharmaceuticals. Many of these everyday necessities have undergone various processing steps and chemical transformations, and behind some of them is even the complexity of entire industries. Ultimately, however, as diverse as they may be, they all come from the same fossil resources.



Two of today's global and future problems followed directly from the exploitation and utilization of these fossil fuels: the climate change issue and the environmental pollution problem. The burning of fossil fuels generates carbon dioxide. This process can to a certain extent be counterbalanced by photosynthesis, the quasi-natural "back-reaction" of combustion processes: atmospheric CO<sub>2</sub> and water are converted into glucose and oxygen, and ultimately new organic matter, prompted by solar energy. However, the increasing amounts of released carbon dioxide can no longer be compensated for by natural photosynthesis, which leads to an overall increase in the CO<sub>2</sub> content of the atmosphere – with all the known negative climatic effects. The environmental problem is also a direct consequence of the processing of fossil resources, namely the occurrence of side reactions and waste products along the production lines and the low recyclability of many products with their high environmental persistence. Fossil resources are therefore the foundation of today's global production – the current world economy and high-tech society are based on their use – but their overutilization also puts us in grave danger.

It is an undisputable scientific fact that one day the fossil resources will be used up. While the exact timing of this cannot be accurately predicted – neither the exact amount of fossil resources nor the evolution of their consumption is well known – the certainty of this event is beyond doubt. If the global society does not want to fall back into a rudimentary state of preindustrial development at that time, it must be able at that time to completely replace fossil resources in their entirety and in all applications – and the only option to do this are renewable resources. This is not just about producing energy and fuels based on other fuels, but rather the entire production lines, material fluxes, and processes of the chemical industry and its downstream industries must be converted to be based on the new starting materials. All the materials, basic and fine chemicals, plastics, paints and pharmaceuticals as products of the petroleum-based industry, which today are naturally part of our lives, must then be produced on the basis of renewable raw materials. This is such a fundamental process of change at all levels of society and economy that it is often compared to such fundamental changes as the change of hunters and gatherers to sedentariness or the transitions of the Stone Age to Bronze Age and Iron Age. While the use of renewable raw materials is already starting today and will increase more and more in the future, the train of thought is today rarely completed in its entirety: fossil resources are definitely finite, even if the time when they are being used up is not fixed, at the latest by that time the whole global chemistry will have to be based on renewable resources, or the consequences for human development would be catastrophic.

It is the natural scientists', and especially the chemists' privilege to anticipate these future developments, to analyze and prepare them on a factual basis. Thus, worldwide, and especially in research, a focus on renewable resources is noticeable, but on a large scale, i.e. when replacing fossil resources on industrial scale, this does not yet seem to be on full swing. All refineries of the future will be complex biorefineries, even today we have walked already a good share of the way toward this goal, let's just take all the developments in pulping and lignin utilization and cellulose fiber manufacture as good examples for the transition of low-grade pulp mills, which use only one component of wood or other natural starting materials, to high-tech biorefineries of the future that try to make use of those renewable resources as completely as possible.

This special issue in *Lenzinger Berichte* illustrates the current research endeavors in the field of biorefineries and reflects their complexity and breadth. It is to be hoped that the aspects of biorefinery research presented here will be informative and educational for the reader. In summary, the contributed articles should show how challenging and sometimes arduous, but above all how rewarding and instructive the work with renewable resources for future biorefineries and manmade cellulose can be.

**Univ.-Prof. Dr. Dr. Thomas Rosenau**

*Head of Institute of Chemistry of Renewable Resources  
University of Applied Life Sciences, Vienna*

Vienna, December 2019

# Pine resin components are degraded at different rates during outdoor seasoning for dissolving wood pulp production

---

**Sebastian España Orozco<sup>1</sup>, Elisabeth Fitz<sup>1</sup>, Jürgen Ritzberger<sup>2</sup>, Susanne Möderl<sup>2</sup> and Robert H. Bischof<sup>2</sup>**

<sup>1</sup> WOOD Kplus Kompetenzzentrum Holz GmbH, Altenberger Strasse 69, A-4040 Linz, Austria c/o Lenzing AG, Werkstraße 2, A-4860 Lenzing, Austria

<sup>2</sup> Lenzing AG, Werkstraße 2, A-4860 Lenzing, Austria

## Abstract

Wood based cellulose fibers are a sustainable alternative to crude oil derived fibers. They are produced from highly pure, wood derived dissolving pulp. Spruce is the standard pulp wood for dissolving pulp production at Lenzing Biocel Paskov. However, to support the use of biodiverse forests, other wood species are tested as pulp wood source. Pine wood is available in relevant quantities, but is particularly rich in wood extractives, also known as pitch or resin, which can disturb pulp production and reduce pulp quality.

We used outdoor seasoning of pine sapwood chips as a method to reduce their resin content, a prerequisite for blending pine chips with spruce chips for dissolving pulp production. Fresh pine sapwood chips contained higher amounts of acetone soluble extractives (4.4 % w/w) than the reference spruce wood (1.8-2.3 % w/w). Triglycerides and sterol esters, as well as fatty and resin acids were particularly elevated in pine wood, while we detected less sterols and lignans than in spruce wood chips. During storage in a flat pure pine pile, the total extractives content was reduced at a rate of ca. 0.47% per month, from January to July. Triglycerides and sterol esters showed a high initial rate of degradation, with reductions of about 75 % and 58 %, respectively, within the first month of storage and a slow decline during the rest of the storage period. Seasoned pine chips (10%) were blended with spruce chips (90%) to produce dissolving wood pulp at mill scale and viscose was prepared from the respective pulp, as well as from 100% spruce pulp. The extractives levels in the pine containing pulp and the purity of viscose produced from such pulp were found to be indistinguishable from the reference 100% spruce pulp and viscose.

In this work we provide a detailed analysis of the kinetics of resin degradation in pine wood during outdoor seasoning. Our results indicate that measuring wood extractives purely gravimetrically is not an appropriate tool to evaluate resin degradation during wood seasoning.

## Introduction

Every year 100 million tons of fibers are produced globally to make textiles and technical products. Currently, only one third of these fibers are made from renewable resources such as cotton or wood [1]. Having the 2020 and 2030 environmental goals of the EU in mind, the market for sustainable goods is growing fast. The production of cellulose fibers such as Vis-

cose, Modal or Lyocell in an integrated fiber plant emits less green house gases compared to terephthalate fiber production from petroleum-based or bio-based processes [2]. Besides the beneficial environmental footprint, wood-based fibers have superior properties with respect to softness, while using less ecotoxic chemicals and water in the process compared

to cotton derived cellulose fibers [1,3,4]. All three types of wood-based cellulose fibers, Viscose, Modal and Lyocell, are produced from dissolving pulp, which has high purity requirements as prerequisite for spinning high quality fibers [5].

The amount of lipophilic wood extractives, commonly referred to as pitch or resin, is one important purity parameter of dissolving pulp. Extractives are non-structural wood components from the tree's metabolism and make up about 2 to 5 % of the total carbon [6]. They protect the plant from oxidation or biotic and abiotic attacks, and have storage functions [7]. The composition of the different extractives groups in wood differs between tree species and wood tissues and depends on the climate and season [8]. Fluctuations in extractive composition alter the chemical, physical and optical properties of the tree and the pulp, respectively [6]. Softwood species such as spruce (*Picea abies*) or pine (*Pinus sylvestris*) are particularly rich in lipophilic wood extractives such as resin acids, fatty acids, triglycerides, sterols, sterol esters and phenolic substances [9].

Extractives can be, as the name suggests, extracted by water or organic solvents. While water soluble extractives are removed by washing during the pulping process, lipophilic extractives remain as deposits on the pulp or in the plant. Various extractives reduce product quality as well as production plant performance, the latter being caused by increased maintenance and operating cost [10,11]. For example, the phenolic pine wood extractive pinosylvin is known to interfere with acid sulfite pulping by condensation with the lignin molecule [12,13,14]. The pinosylvin content of spruce is high in knot and heartwood and low in sapwood [16].

Storage of wood logs and wood chips can reduce the content of pitch in pulp wood by promoting the hydrolysis of esters and triglycerides [16,17,18]. Moreover, outside storage, or air-seasoning, is more effective in reduction than kiln-drying [19]. During open-air storage in chip piles, wood extractives are degraded in several phases [18]. In the first 14 days, living cells inside the wood parenchyma, bark and foliage respire and produce heat. This leads to a build-up of temperature inside the wood pile, thereby creating suitable conditions for bacteria and fast growing sap-stain fungi to thrive on wood extractives [16,20]. The metabolic heat generated by these microbes leads to a further increase of temperature. Wood degrading fungi, on the other hand, grow more slowly and are only able to thrive, when the temperature inside the pile stays below 50°C [20]. In recent years, deliberate application of bacteria or sap-stain fungi was proposed to make microbial conversion of wood pitch

during air seasoning more controllable and quicker [21-25].

In this study we aimed to investigate the extractives content of pine sapwood and the degradation of resin components over time during air seasoning. A sufficiently low content of extractives in the wood and the resulting pulp could enable a mixing of these two wood types at Lenzing Biocel Paskov in order to support biodiversity and flexibility of the production.

## Materials and methods

### Wood seasoning and sampling

Industrial whole tree spruce chips, spruce chips from sawmill residues and pine sapwood chips were used in the study. Pine chips were piled on a dedicated flat pine wood chips pile with dimensions of 75x55x5 meters and sampled directly from the pile after unloading from a truck (before storage) or dug out from the pile, digging ca. 1 meter below the surface (during and after storage). Samples were taken roughly once per month between December 2016 and June 2017 from 8-12 different sectors of the pile, to get a representative sample of the whole pile. Both types of spruce chips, whole tree chips and sawmill residue chips, were stored and air seasoned on standard piles with approximate dimensions of 130 meters diameter and 20 m height. Fresh spruce chips were sampled from the conveyer belt that feeds the chip piles (after chip screening). Stored chips were sampled from the conveyer belt feeding the pulp cooker. The residence time of the chips on each of the spruce piles was about 4 weeks. The outside temperature and temperature in the pine pile (at half height) were monitored using temperature probes. Temperatures inside the spruce chips piles were measured by burying temperature sensors inside the pile.

### Processing of wood chip samples prior to extractives analysis

All chips samples were frozen prior to analysis. After thawing the chip samples, subsamples of 100 g were dried in crystallizing dishes in an oven at 50°C for three days and were coarsely ground with a cutting mill SM 100 (Retsch, Germany) and selected with a 6 mm quadratic-perforated sieve. Subsequently, the samples were finely ground by a cutting mill Model (Arthur H. Thomas Co., USA) and selected with a 60 mesh sieve prior to extraction of extractives. In the case of pulp samples, frozen samples were thawed prior to analysis. Samples were diluted with acetic acid so as to reach a pH of 3 and a consistency of ca. 15 % dry solids. Samples were then lyophilized and extracted as described below.

## Extraction and analysis of extractives from wood and pulp

The accelerated solvent extraction was done with 5-7 g of ground wood or dried acidified pulp using a SpeedExtractor E-916 (Büchi, Essen, Germany). 40 mL acetone was used as solvent and the extraction was performed twice for five minutes at 100 bar and 100°C. The extract was transferred into a volumetric flask and filled to 100 ml with acetone. An aliquot of the acetone extract, spiked with 200  $\mu$ l of an internal standard, was dried under vacuum at 40°C and taken for the analyses of extractive groups, e.g. fatty and resin acids, sterols and lignans, sterol esters and triglycerides, with GC-FID after trimethylsilylation with BSTFA:TMCS 9:1 % v/v for 20 min at 70°C. The representative standards were heneicosanoic acid, cholesterol, cholesteryl palmitate and 1,3-Dipalmitoyl-2-oleoylglycerol dissolved in acetone with concentrations of 80-160 mg L<sup>-1</sup>. 2  $\mu$ l were injected into a 6890N Network GC System (Agilent Technol.) and transferred to a Zebtron Capillary GC column ZB-5HT Inferno (15 m x 0.25 mm ID and 0.1  $\mu$ m film thickness) with a cold split injection. Helium was used as carrier gas with a gas flow of 2.5 ml/min and a split-ratio of 1:30. The programmable temperature vaporizer was heated from 35°C to 440°C at 12°C/s, subsequently from 440°C to 450°C at 1°C/s and held for 1.5 min. The GC oven temperature program, started at 60°C and held for 1.8 min, was raised to 150°C at 64°C/min, then to 250°C at 43.5°C/min, finally reaching 410°C at 35°C/min and held for 2 min. The total extractives content was determined gravimetrically. Therefore, the residual extract was dried with a speed vaporizer for 20 min and subsequently 1 h at 105°C. [26,27].

## Dissolving pulp and viscose production

Dissolving pulp containing pine sapwood chips was produced under standard conditions used at Lenzing Biocel Paskov during a nine-day campaign. The pine campaign was followed by an equally long reference phase without pine wood. Pine campaign: 10 % seasoned pine sapwood chips from pine pile, 50 % spruce chips from sawmill residues, 40 % spruce whole tree chips. Reference phase: 60 % spruce chips from sawmill residues, 40 % spruce whole tree chips. Chips were subjected to acid sulfite pulping using the Magnesium bisulfite process and a totally chlorine free bleaching sequence. Treiber tests were performed as described previously [28].

## Results

### Temperature assessment

The temperature within the flat pine pile was between 4 and 8°C respectively from January to mid-March, which can be explained by the ambient temperature <0° during this period and the low height of the pile. In the following month the temperature rose to ca. 26°C at a rate of about 4°C/week. Temperature then stayed just below 30°C for another month before it once more started to decline to 18°C until mid of May, as depicted in figure 1. In comparison, the rate of temperature increase in the standard spruce piles was higher as were the maximum temperatures. As expected, the maximum temperature was strongly influenced by the position of the sample within the pile, whereby the maximum temperature was reached below the peak of the pile, and lower temperatures were found towards the edges of the pile.

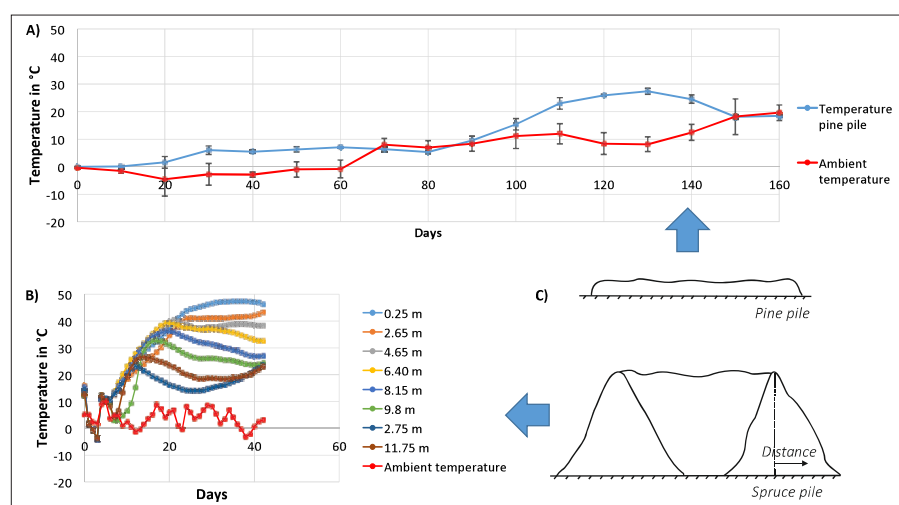


**Figure 1:** Figure 1: Temperature profiles of the wood chip piles. **A)** Temperature profile (at half height) during outside seasoning in the 5m high dedicated pine pile. **B)** Temperature profile at 4 meters height and ambient temperature during outside seasoning on the „Guglhupf“ shaped spruce pile. Distances in meters, as resolved in the legend, represent the distance of the temperature probes to the highest point of the pile, as shown in the bottom right sketch. **C)** Cross-section of both piles drawn at scale. The arrow labelled with „distance“ indicates the position of sensors in the spruce pile. Zero meters is where the arrow meets the dotted line. Longer distances are closer to the pointy end of the arrow.

Longer distances are closer to the pointy end of the arrow.

## Pine sapwood chips have strongly elevated levels of triglycerides compared to spruce chips

We performed extractives analyses by gravimetric determination of acetone soluble extractives and more detailed analysis of extractive groups by GC-FID. The results were compared with the extractives content of the two types of spruce wood chips that are used to produce dissolving pulp, which are spruce sapwood chips and spruce sawmill residues. As shown in figure 2, both types of spruce chips were found to have an extractive content of roughly 2-3 % (w/w). Between 21-32 % of the gravimetrically determined

extractives of the acetone extract were identified in the GC-FID runs, as depicted in figure 2B. Among the extractive groups, the group “fatty and resin acids” was most abundant, followed by the group “sterols and lignans”. Pine chips had comparably higher total extractives and triglyceride contents in the fresh woods, which is consistent with literature. Triglycerides, resin acids and fatty acids made up the biggest portion of extractives in GC-FID measurements, while sterol esters and sterols and lignans were found to be substantially less abundant or less detectable with our method.

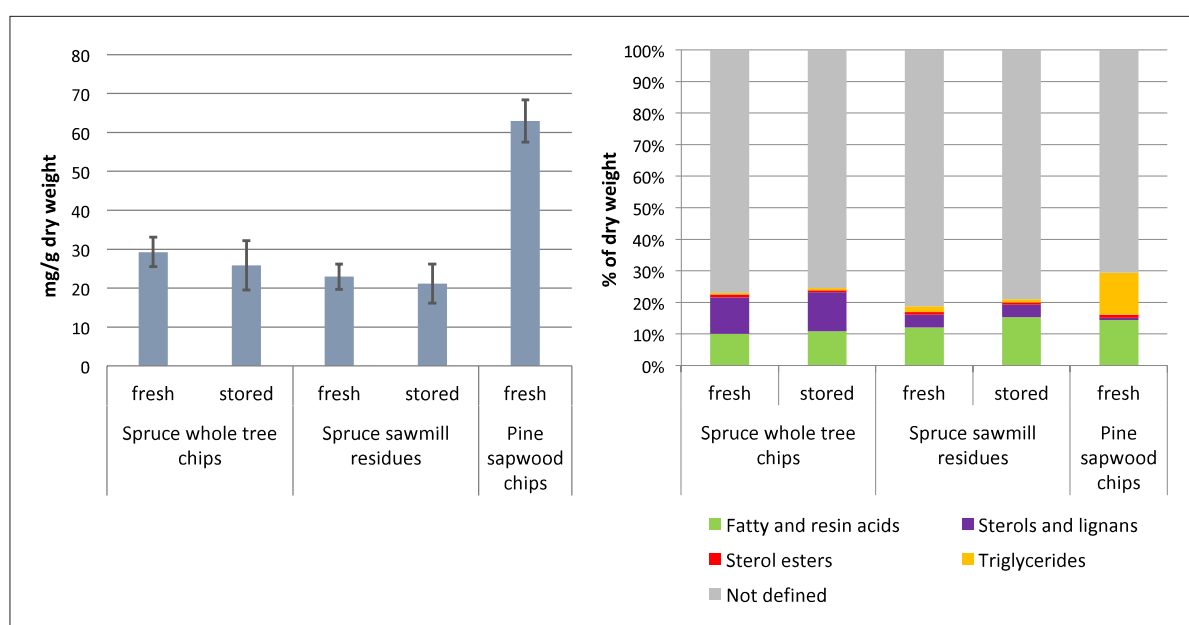


**Figure 2:** Extractives in different wood chips. **A)** The total height of the bar corresponds to the gravimetric acetone extractives determined gravimetrically. **B)** The percentage content of the different extractives groups as indicated in the legend, determined by GC-FID. Averages of three independent samples are reported.

## Resin components degrade at different rates

To follow the extractives reduction during storage, samples from several sectors of the pine chips pile were drawn representing the average extractive level of the pile. An extractive content of or below 2 % w/w was set as threshold to start production of dissolving wood pulp from 10 % pine chips, since this level roughly corresponds to the one of extractives in spruce chips currently used for dissolving pulp production. As shown in figure 3, the extractives content of the pine sapwood chips pile samples fell about 50 % from December 2016 to June 2017. The high standard deviation of the extractives content can be explained by the fact, that the pine chip intake was from end of November until mid of February and therefore the chips had different storage duration.

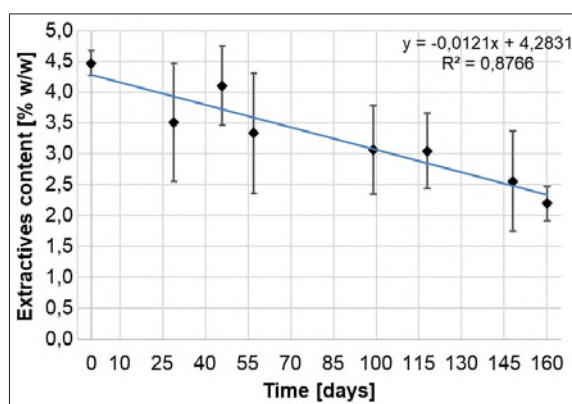


**Figure 3:** Extractives content in acetone extract of pine wood chips from 01.12.2016 until 24.05.2017 or 160 days. Values represent the mean and standard deviation of all on average about 8 samples at a given sampling point, thus representing the whole pile.

Figure 4 shows the concentrations of the four extractives group during the seasoning. Both, hydrolysable and neutral types of extractives (triglycerides and sterol esters) had a high initial degradation rate. More specifically, triglycerides and sterol esters were reduced by about 75 % and 58 %, respectively, within the first month of storage. At the last sampling after 100 days, triglycerides and sterol esters were reduced by 93 % and 70 %, respectively. On the other hand, fatty and resin acids, increased during the first two months. This is probably caused by the hydrolysis of sterol esters and triglycerides, as previously observed [16]. The content of sterols and lignans did not change during the sampling period.

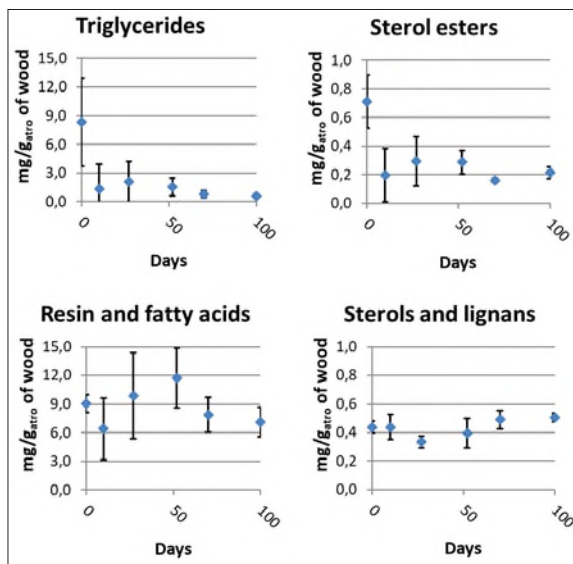


**Figure 4:** Degradation of extractives during pine sapwood chips storage. Values represent the mean and standard deviation of all samples at a given sampling time point, representing the whole pile.  $g_{\text{atro}}$  stands for grams on an absolute dry basis.

### Effect of pine sapwood addition on pulp and viscose quality

We also wanted to learn whether inclusion of 10% pine sapwood chips for dissolving pulp production would cause detectable rise of impurities in pulp or a decrease of the quality of viscose made from such pine containing pulp. To monitor if the extractives content of the pine chips was below the set threshold level of 2 % throughout the trial, daily samples were taken of both types of spruce chips and the pine chips. Extractive contents were gravimetrically determined daily throughout the trial from acetone extracts and results are shown in figure 5. As can be seen, pine sapwood chips had the same average extractives content

as spruce whole tree chips. Sawmill chips, on the other hand, had a significantly lower content of extractives. To analyze whether the relatively high residual extractive content in the pine chips would lead to an enrichment of extractives in the final pulp, we determined the extractives content of never dried, fully bleached pulp once every two days. The total amounts of the four extractives groups analyzed by GC-FID of  $0.198 \pm 0.015 \text{ mg/g}_{\text{atro}}$  for 9-day period with pinewood addition and  $0.214 \pm 0.043 \text{ mg/g}_{\text{atro}}$  for the pine-free reference phase were not significantly different ( $p > 0.05$ , paired t-test for all extractive groups). It is therefore concluded, that the seasoning reduced the pitch content of pine wood strongly enough to avoid an increase of residual extractives in final pulp.

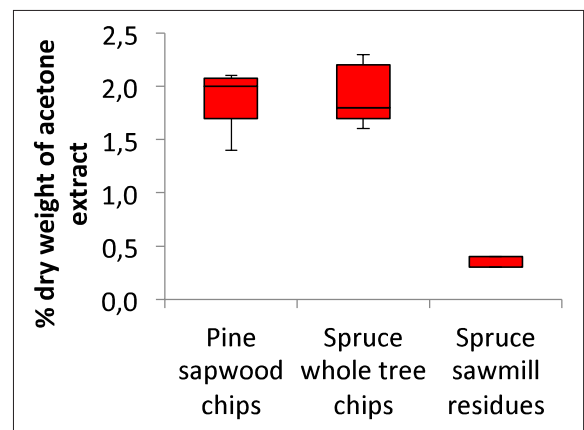


**Figure 5:** Box plot representation of extractives content of acetone extracts in two different types of spruce whole tree chips during the 9-day pine trial. Box plots represent the 9 independent samples ( $n = 9$ ) taken once daily during the campaign.

Lastly, we used the “Treiber test” to determine the filter value and particle content of viscose (xanthogenated cellulose) prepared from both types of dissolving wood pulp (with and without pine). The filter value or filterability and particle content (in ppm) are key quality characteristics of the viscose process and directly correlated with the dissolving pulp quality. The filter value was indistinguishable for viscose produced from pulps representing both wood mixtures, being  $382 \pm 16.9$  with pulp prepared during pine addition and  $378 \pm 16.9$  for pulp produced during the pine-free reference phase. Particles in the viscose were on the same level with pine addition ( $4.1 \pm 0.7 \text{ ppm}$ ) than without pine ( $4.3 \pm 0.8$ ).

## Discussion

The fresh pine sapwood chips had strongly elevated levels of extractives compared to spruce chips usually pulped at Lenzing Biocel Paskov, which is in accordance with literature [9]. In general, our analysis detected a comparably low percentage of lipophilic extractives (<30% of gravimetric amount), but the pattern of extractive groups for pine was consistent with literature values. The relatively low levels of triglycerides and sterol esters of spruce wood is likely caused by their previous hydrolysis during log storage. Triglyceride levels in fresh pine were particularly high and are known to often be responsible for deposits [16]. Therefore, the degradation of extractives during storage was monitored and the pine trial only started after the averaged extractive content in the pile was below 2 %. We found that extractives in the pine pile were degraded at a rate of approximately 0.5 % (w/w) per month. While this value might be used as a rule of thumb for future storage of pine chips, it must be noted that the rate of extractives degradation might be considerably different, depending on the temperature inside the chip pile. The temperature inside the pile, on the other hand, is influenced by the pile's ability to dissipate metabolic heat which is governed by (i) the height of the pile and (ii) the compactness of the pile [13]. The ambient temperature likewise has an influence on a pile's ability to dissipate metabolic heat [23]. It is to be expected that the degradation rate of pine chips in the 130x20m spruce piles would be higher than for the smaller flat pine pile. Should it be necessary to further accelerate the extractives degradation rate, e.g. because pine chips need to be dosed at a high proportion, extractive degrading micro-organism can be applied to accelerate the seasoning process [15,16,20,21]. Further downstream in the operation, extractive degrading lipases could be applied to make unseasoned wood processable at mill scale [24].

Triglycerides and sterol esters were degraded quickly during the initial month of storage giving rise to an increase in fatty acid concentrations, which is in agreement with previous results [9]. Remarkably, the same trend could not be observed for sterols. For the sterols it rather appeared as if there was an initial reduction of sterol compounds, with a later buildup that appears to not be correlated to sterol ester hydrolysis. While we cannot exclude that this merely accounts for “over-interpreting“ a limited set of data with considerable error, there is another explanation. The rise of the sterol concentration corresponds nicely with the rise of the temperature inside the pile (from 6°C to 30°C), which might be indicative of increased

microbial activity. Ergosterol in particular is the most abundant sterol in fungal cell membranes [29] and concentrations of 0.4 mg/g are typical values for wood chips that are overgrown by fungal cultures [30]. We therefore consider it possible that the degradation of the wood sterols is “masked” by a build-up of sterols originating from the fungi growing on the wood.

## Conclusion

Pine wood is a challenging type of pulp wood for processing with the sulfite process due the risk of pinosylvin triggered lignin polymerization events that may lead to “black cooks”, meaning failed pulp cooks. The high resin content of pine wood has the potential to decrease pulp purity also in successful cooks and, in further consequence, lead to complications in the produced viscose. Here we show that selection of pine sapwood, having lower contents of pinosylvin, and thorough seasoning of pine wood allows production of 10% pine containing dissolving pulp and viscose without a noticeable negative effect on (i) the extractive level in the final bleached pulp and (ii) the key quality parameters (Treiber value, contaminating particles) of viscose prepared from such pulps, compared to 100% spruce pulp. We also show that the distinct extractive groups of pine resin are degraded at different rates. Hydrolysis of esters occurred first, followed by a decrease of fatty and resin acids, while very little change in the amount of sterols and lignans was visible during an almost half year long storage trial.

## References

- [1] Shen L., Worrell E. and Patel M. K. Environmental impact assessment of cellulosic fibres. *Resour. Conserv. Recy.*, 2010. 55:260-274
- [2] Shen L., Worrell E. and Patel M. K. Comparing life cycle energy and GHG emissions of biobased PET, recycled PET, PLA, and man-made cellulose. *Biofuels Bioprod. Bioref.*, 2012. 6:625-639
- [3] Bredereck K. and Hermanutz F. Man-made cellulose. *Rev. Prog. Color*, 2015. 35:59-75
- [4] Abu-Rous M., Liftinger E., Innerlohninger J., Malengier B. and Vasile S. A new physical method to assess handle properties of fabrics made from wood-based fibers. Publication pending. Paper presented at Autex 2017 World Textile Conference, Corfu, Greece, 29-31 May 2017 (pp. 281-289). Bristol, UK, IOP publishers.
- [5] Kumar H. and Christopher L. P. Recent trends



- and developments in dissolving pulp production and application. *Cellulose*, 2017. 24:2347-2365
- [6] Sjoström, E. (2013). *Wood chemistry: fundamentals and applications*, San Diego: Academic Press Inc., 1993. pp92-108
- [7] Witzell J., Martín J. A. Phenolic metabolites in the resistance of northern forest trees to pathogen – past experiences and future prospects. *Can. J. For Res.*, 2008. 38: 2711-2727
- [8] Nimz H. H. Wood-chemistry, ultrastructure, reactions. *Holz als Roh-und Werkstoff* (1984) 42:314
- [9] Ekman R. and Holmbom B. The chemistry of wood resin. In: Back E. L. and Allen L. H. (eds) *Pitch control, wood resin and deresination*. TAPPI, Atlanta, 2000. pp 37-76
- [10] Allen L. H. Pitch control in paper mills. In: Back E. L. and Allen L. H. (eds) *Pitch control, wood resin and deresination*. TAPPI, Atlanta, 2000a. pp 307-328
- [11] Allen L. H. Pitch control in paper mills. In: Back E. L. and Allen L. H. (eds) *Pitch control, wood resin and deresination*. TAPPI, Atlanta, 2000b. pp 265-288
- [12] Erdtmann H. Heartwood extractives of conifers. *Tappi*, 1949. 31:305–310
- [13] Erdtmann H. Compounds inhibiting the sulphite cook. *Tappi*, 1949. 32:303–305
- [14] Willför S., Hemming J., Reunanen M. and Holmbom B. Phenolic and Lipophilic Extractives in Scots Pine Knots and Stemwood. *Holzforschung*, 2005. 57: 359-372
- [15] Belt T., Keplinger T., Hänninen T. and Rautkari L. Cellular level distributions of Scots pine heartwood and knot heartwood extractives revealed by Raman spectroscopy imaging. *Industrial Crops and Products*, 2017. 108:327-335
- [16] Fuller W. S. Chip pile storage – a review of practices to avoid deterioration and economic losses. *Tappi*, 1985. 68(8):48-52
- [17] Strand A., Sundberg A., Vähäsalo L. and Holmbom B. Influence of pitch composition and wood substances on the phase distribution of resin and fatty acids at different pH levels. *J. of Dispersion Science and Technology*, 2011. 32(5): 702-709.
- [18] Silvério F. O., Barbosa L. C. A., Maltha C. R. A., Fidêncio P. H., Cruz M. P., Veloso D. P., Milanez A. F. Comparative study on the chemical composition of lipophilic fractions from three wood tissues of *Eucalyptus* species by gas chromatography-mass spectrometry analysis. *J. of Wood Science*, 2007. 53(6): 533-540.
- [19] Myronycheva O., Karlsson O., Sehlstedt-Persson M., Öhman M. and Sandberg D. Distribution of low-molecular lipophilic extractives beneath the surface of air- and kiln-dried Scots pine sapwood boards. *PLoS ONE*, 2018. 13(10): e0204212.
- [20] Farrell R. L., Hata K. and Wall M. B. Solving pitch problems in pulp and paper processes by the use of enzymes and fungi. *Adv. Biochem. Eng. Biotechnol.*, 2007. 57:197-212
- [21] Gutiérrez A., del Rio J. C. and Martínez A. T. Fungi and their enzymes for pitch control in the pulp and paper industry. In: Hofrichter M. (ed) *The Mycota X*. Berlin, 2010. pp 357-353
- [22] Gutiérrez A., del Rio J. C. and Martínez A. T. Microbial and enzymatic control of pitch in the pulp and paper industry. *Appl. Microbiol. Biotechnol.*, 2009. 82(6):1005-18
- [23] Kallioinen A, Vaari A., Rättö M., Konn J., Siika-aho M. and Viikari L. Effects of bacterial treatments on wood extractives. *J. Biotechnol.*, 2003. 103:67-76
- [24] Burnes T. A., Blanchette R. A. and Farrell R. L. Bacterial Biodegradation of extractives and patterns of bordered pit membrane attack in pine wood. *Appl. Env. Microbiol.*, 2000. 66(12):5201-05
- [25] Ekman R. Resin during storage and in biological treatment. In: Back E. L. and Allen L. H. (eds) *Pitch control, wood resin and deresination*. TAPPI, Atlanta, 2000. pp 185-204
- [26] Ferrero F., Lohrer C., Schmidt B. M., Noll M. and Malow M. A mathematical model to predict the heating-up of large-scale wood piles. *J. Loss Prevent. Proc.*, 2009. 22(4):439-448
- [27] Hata K., Matsukura M. and Fujita J. Mill-Scale Application of Enzymatic Pitch Control During Paper Production. In: Jeffries TW and Viikari L (eds) *Enzymes for pulp and paper processing*. American Chemical Society, Washington, 1996. pp 280-296
- [28] Friebel C., Bischof R. H., Schild G., Fackler K. and Gebauer I. Effects of Caustic Extraction on Properties of Viscose Grade Dissolving Pulp. *Processes*, 2019. 7(3):122
- [29] Pasanen A.-L., Yli-Pietilä K., Pasanen P., Kalliokoski P. and Tarhanen J. Ergosterol content in various fungal species and biocontaminated building materials. *Appl. Env. Microbiol.*, 1999. 65(1):138-142
- [30] Van Kuijk S. J. A., Sonnenberg A. S M., Baars J. J. P., Hendriks W. H. and Cone J. W. The effect of particle size and amount of inoculum on fungal treatment of wheat straw and wood chips. *J. Anim. Sci. Biotechnol.*, 2016. 7:39-48



# Innovative dissolving pulps for application in cellulose MMF production

---

Birgit Kosan<sup>1</sup>, Frank Meister<sup>1</sup>, Ina Sigmund<sup>2</sup>, J. Paulitz<sup>3</sup>

<sup>1</sup> Thuringian Institute for Textile and Plastics Research, Breitscheidstraße 97, 07407 Rudolstadt, Germany,

<sup>2</sup> Saxonian Textile Research Institute (STFI), Annaberger Straße 240, 09125 Chemnitz, Germany

<sup>3</sup> INNtexas Innovation Netzwerk Textil GmbH, Annaberger Straße 240, 09125 Chemnitz, Germany

## Abstract

Within agriculture, more than half the globally harvested dry mass consists of agricultural residues and inedible biomass. Locally available waste-based raw materials have huge potential in the circular economy. In the future, the biomass could instead be used to produce paper and sustainable natural and man-made fibre for textile application. Beside pineapple leaf fibres hemp could be another approach, especially in the temperate zone all over the world.

The paper demonstrates Bast fibre material, mostly free of wooden particles (Hemp tow) and dried hemp bark strips (HBS), which could be profitably applied for fabrication of dissolving pulp in direct dissolution process, when would be downgraded organic and inorganic impurities. Purified hemp pulp exhibit an excellent dissolution and spinning behaviour and Lyohemp<sup>®</sup> fibres could be processed very comfortable into yarns of high tenacity and low unevenness. Fabrics made of Lyohemp<sup>®</sup> proved excellent processability and moisture management.

**Keywords:** *organic grown hemp, pulp cooking, dissolving-grade hemp pulp, Lyocell fibre, Lyohemp<sup>®</sup>*

## Introduction

Recently, approximately 72 % of the net annual increment of forests is currently harvested, pointing at a limited potential for the increased sourcing of wood biomass as required for worldwide improving fibre demand. By shifting to alternative sources of biomass and more effectively using bio-waste or residues, the resource base could be extended without any need for additional land for biomass production [1].

Within agriculture, more than half the globally harvested dry mass consists of agricultural residues and inedible biomass, such as cereal and legume straw, vegetable crop stalks, leaves and shoots, etc. It is estimated that 121 million tonnes of agricultural crop residues (mainly straw) could be generated annually in Europe, together with 46 million tonnes of forestry residues and 31 million tonnes of grass [2]. Moreover, a massive amount of straw is burned in Asian countries, causing significant CO<sub>2</sub> and dust emissions that may strongly contribute to climate change and acidic rain.

The major barrier to increasing the use of agricultural

and forestry residues is the cost associated with harvest logistics, which often exceeds that for primary fossil materials. Local bio-refining systems that match residue supply and material demand in a smart way need to be developed, as the wide dispersal of residues does not fit the economies of scale of the already existing industrial oil-based production system. Nevertheless, locally available waste-based raw materials have huge potential in the circular economy. In the future, the biomass could instead be used to produce paper and sustainable natural and man-made fibre for textile application.

As only one example, the Ananas Anam Company has developed an innovative non-woven textile called *Piñatex<sup>TM</sup>*, made from pineapple leaf fibres. These fibres are the by-product of the pineapple harvest, meaning that no extra land, water, fertilisers or pesticides are required to produce them. The original development was carried out in the Philippines, with finishing, research and continuing development now being undertaken in Spain and the United Kingdom.

This private initiative provides additional income for farmers, while creating a new industry for pineapple-growing countries [3].

Cultivation and harvesting of hemp could be another approach, especially in the temperate zone all over the world. Hemp is an example of a multipurpose crop, delivering natural fibres, seeds, pharmaceuticals and woody by-products [4]. Hemp seeds have been the major force driving cultivation growth. Hemp is considered to be environmentally friendly due to a decrease of land use and other environmental impacts, like water requirement of only 300 - 500 l/kg dry matter (around 7 % that of cotton), indicating a possible decrease of ecological footprint. It is also claimed to require few pesticides and no herbicides, and it has been called a carbon negative raw material. Further advantages are high weed suppression and soil loosening by the large hemp root system. Since hemp is very self-compatible, it can also be grown several years in a row in the same fields (monoculture). Finally, there is a large progress in automated hemp harvesting, sorting and processing.

It is the target of this paper to demonstrate the suitability of hemp stems for dissolving pulp manufacturing and its application in cellulose man-made fibre manufacturing according to the Lyocell process.

## Material and Procedures

Bast fibre material, mostly free of wooden particles (Hemp tow) and dried hemp bark strips (HBS) was delivered by Bast & Faser GmbH, Adelsdorf, Germany and was used as received. All other chemicals and solvents were used as delivered at technical (caustic soda, NMMO) or analytical grade.

### Pulp Fabrication

Dried HBS and hemp fibre tow (as reference), which was mechanical pre-processed for elimination about 20 % hurds, were treated in pre-tests by different concentrated aqueous caustic soda solution at 160°C for approximately 60 minutes. Beside caustic soda, a surface active additive (Ashland Infinity™ DA 2724) was applied in the cooking liquor. The reduction of the Kappa number was used for determination of that caustic soda concentration, which was required for minimising of lignin content. A Kappa number of about 5 had been targeted.

Additional, a P-H-P fibre bleaching sequence has to be applied for adjustment of hemp pulp DP at 550 up to 700 using subsequently hydrogen peroxide (P) and sodium hypochlorite (H) at 55°C for 120 minutes each. Within the pulping procedures, suitable sequen-

trants (Synthron's Actiron DP 950 and / or Masquol™ FEO) were added for elutriation of high metal ion contents [5]. The resulting pulp was finally dried to a solid content of 80 % and was used without any further treatment for dope preparation.

### Dope preparation and characterization

Laboratory dope preparation using hemp pulp samples was carried out at cellulose concentrations between 10 and 12 % (w/w). The dopes were prepared, starting from an aqueous suspension of the pulp in 50 % aqueous NMMO which was transferred into a discontinuous laboratory scaled stirring and kneading reactor.

The pulp was dissolved by evaporation of excess water at elevated temperatures of 100 °C in maximum and decreased pressure of 4 kPa in minimum and a rotational speed up to 20 rpm.

At the moment when excess water was fully evaporated and a mixture of one mole of water per mole of NMMO was achieved, the pulp dissolved immediately. A transparent, brownish, honey like spinning dope was generated. The shearing was continued another 60 minutes at 10 rpm for dope homogenization.

The prepared dope was characterized finally by

- refraction index for determination of NMMO monohydrate concentration,
- intrinsic viscosity of precipitated cellulose for determination of cellulose DP in dope,
- daylight microscopy for determination of non-dissolved fibrous particles,
- particle analysis by laser diffraction for characterisation of jelly-like particle concentration as well as PSD and
- rheological characterisation of viscoelastic dope behaviour at rotation and oscillation tests,

as described earlier [6-8].

### Continuous fibre spinning

For larger scale trials, dope was continuously manufactured using a List Master Conti kneading system (List Technology AG, Arisdorf, Switzerland). After dissolution at approximately 100 °C, the molten dope was continuously transferred to the filtration unit and then to the spinning bar. While proceeding through the dry-wet spinning process, the dope was extruded through the holes of spinnerets by means of spinning pumps and formed the spinning capillaries. In the air gap, spinning capillaries were drafted until achieving the intended fibre fineness and were regenerated when passing the surface of the spinning bath. In the last process section, the solvent was removed from the fibres again by pure water counter flow extraction. Fibres were machine-cut, finished and dried to

equilibrium moisture content. Removed solvent was recovered by anion and cation exchange processes and distillation off the excess water.

### Fibre processing

Characterization of fibre properties were conducted as described previously [9]. Lyocell fibres thus obtained were further processed by opening, carding, drawing and roving. Afterwards, ring spun yarn of different counts were linked into circular knitted fabrics, dyed and finished by common textile procedures [10, 11].

## Results and Discussion

### Pulp Fabrication

It was intended to convert the major part of hemp raw materials (HBS and hemp tow) into pulp suitable for dissolving and dry-wet solution spinning of cellulose man-made fibres.

For that purpose a cooking procedure had to be developed for the dried and pre-treated hemp substrates. This study was conducted in close connection with the well experienced paper pulp mill OP Papirna s.r.o., Olšany, Czech Republic, a subsidiary of Delfort Group Traun, Austria.

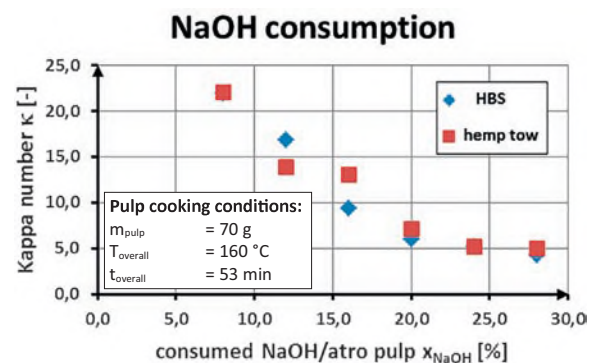
For an application in solution spinning dissolving pulp has to meet specific properties regarding molecular weight and MWD, but for concentration of organic and inorganic impurities, too. Table 1 summarizes the most important parameters in this regard.

**Table 1:** Molecular and purity requirements of dissolving pulp applied in Lyocell process

<b>Pulp characteristics:</b>		
<b>DP<sub>Cuoxam</sub> (measured in Cuoxam solution)</b>	[-]	550 - 650
<b>a-cellulose content (insoluble in 17.5 % caustic soda)</b>	[%]	> 90
<b>Contents of sensitive inorganic impurities:</b>		
<b>iron and copper, each</b>	[mg/kg]	< 10
<b>other heavy metal cations (Mn, Cr, Ni)</b>	[mg/kg]	≤ 20
<b>sodium</b>	[mg/kg]	≤ 500
<b>potassium</b>	[mg/kg]	≤ 100
<b>calcium</b>	[mg/kg]	≤ 100
<b>magnesium</b>	[mg/kg]	≤ 100
<b>ash content</b>	[%]	< 1

The primary DP and impurities of hemp material is too high and should be reduced by pulping procedures. For that reason both raw material samples were pre-tested in laboratory scale. About 70 grams of each, hemp tow and HBS, were treated by increasing concentration of aqueous caustic solution at 160 °C for about 60 minutes. After the end of the cooking procedure Kappa number was determined according to DIN ISO 302:2004. The targeted value of Kappa number was around 5. The results of laboratory pre-tests are summarized in figure 1.

**Figure 1:** Caustic soda consumption in hemp pulp cooking process



In conclusion from the effect of increasing caustic soda concentration, 24 % aqueous solution of caustic soda was applied in all pulp cooking procedures. In the end, the conducted cooking trials generally confirmed, that the increase of cooking liquor concentration and of cooking time could acceptably increase polymer degradation down to the intended pulp DP. However, increased pulp cooking time lowered significantly the overall pulp yield.

Therefore also the adaptation of bleaching sequences was investigated in a second step. Conventional bast fibre pulp bleaching procedures for paper manufacturing use successively hydrogen peroxide (P-sequence) or chlorine dioxide (D-sequence). They end up with an extraction sequence at presence of hydrogen peroxide (EP-sequence).

Because of the environmental toxicity of elementary chlorine containing agent chlorine dioxide should be removed in more recent procedures. For the intended DP reduction an additional sequence was identified using sodium hypochlorite (H) as bleaching agent.

DP as well as alpha-cellulose content, that means organic impurities corresponds well with required values for solution spinning from NMMO solutions. A specific challenge in the developed manufacturing of hemp derived dissolving pulp was the separation from higher amounts of inorganic impurities (alkali, earth-alkali and heavy metal salts as well as ash con-

tent). In subsequent dope preparation step higher amounts of salt particles might originate in spinning dopes, if such impure pulp would be used.

The arising salt particles might clog up the spinning holes and acutely disrupt the ongoing fibre spinning process. Furthermore, high concentration of metal ions also pollutes the ion exchange columns when the used solvent is recovered again. Another challenge, also arising from high metal salt contents, is the chemical sensitivity of the solvent NMMO. Especial, the pulp immanent heavy metal complexes based on iron and copper ions, might generate a serious solvent decomposition, what could be autocatalytic pushed on by means of addressed ions.

For that reason crude pulps were washed with deionised water in order to isolate most of the included hazardous metal ions. After washing of the pulp the iron and copper metal ion content decreased down to no longer relevant amounts. Ongoing problems arise from the extremely high  $\text{Ca}^{2+}$  and  $\text{Mg}^{2+}$  ions concentration, even in purified pulp samples.

But problems could be solved when cooking was transferred into commercial scale and pulp manufacturing was combined with pulp purification by means of deionised water containing suitable sequestrants (see material and methods section). The sequestrants might irreversibly bind the ions by formation of complex compounds, even under caustic and/or oxidative conditions. In the end  $\text{Ca}^{2+}$  ion concentration dropped down below 200 and  $\text{Mg}^{2+}$  ion concentration was found below 50 ppm.

At the end of cooking process investigation a 5.3 metric ton OG hemp tow sample should be converted into dissolving pulp applying the identified process parameter. Five different cooking batches were performed in commercial scale equipment. Intrinsic viscosity of the produced five pulp samples was in the range of 370 ml/g up to 450 ml/g, what correlates with pulp DP's of about 500 up to 650, respectively.

The accepted iron ion concentration in semi-technical scale was appointed below 10 ppm. Unfortunately the content of iron ion was nearly twice the number. For that reason the so-called onset-temperature, what means that temperature at what thermal induced sol-

vent decomposition occur, has had to be measured, if the iron ion content is higher than allowed. In case of dope derived from OG hemp pulp it was determined at the same temperature as of dopes prepared of common wooden pulp and was located at higher temperatures than 170 °C. That temperature is high enough to release the prepared pulp for further processing of man-made cellulose fibres. In the last step the pulp was dried to solid content of 80 % and was handed over for further investigation of direct dissolution in NMMO monohydrate. Table 2 summarizes the typical properties found in dissolving hemp pulp.

**Table 2:** Hemp pulp properties at the end of cooking and bleaching steps.

Measured Parameter		OG Hemp Pulp
DP <sub>cuoxam</sub>		670
a-cellulose content	%	97.8
carboxyl group	$\mu\text{mol/g}$	13.3
carbonyl group	$\mu\text{mol/g}$	12.5
heavy metal ions	ppm	25
thereof Fe/Cu/	ppm	20 / 0.26
Ni/Cr/Mn	ppm	0.26 / 3.0 / 0.87
alkali/earth alkali ions	ppm	452
thereof Na/K	ppm	207 / < 1
Mg/Ca	ppm	41 / 203

### Dope preparation and dry wet fibre spinning

Spinning dopes were produced as described in material and method section. After finishing dissolution and homogenization dopes were characterized by daylight microscopy, laser light scattering, particle analysis and rotation/oscillation rheometry. Incomplete pulp dissolution as present in figure 2, what even could be detected by daylight microscopy, might occur whenever fibrous particles are insoluble in case of high molecular weight cellulose shares or unsuitable pulp is used or solid particles are formed in case of higher amounts of inorganic impurities.

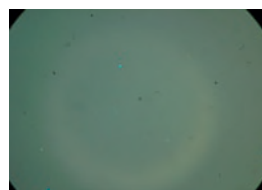
**Figure 2:** Dissolution state of hemp dissolving pulps identified by day-light microscopy



2a) bad solution state caused by solid salt particles



2b) bad solution state caused by non-dissolved fibrous particles



2c) sufficient dissolution state

Bad solution state as shown in fig. 2a could be caused by extreme high  $\text{Ca}^{2+}$  and  $\text{Mg}^{2+}$  ions concentration. Visible particles are generated by calcium and magnesium salts, which precipitate, if concentration of excess water in dopes comes to nearly monohydrate state of NMMO. Because those particles are incompressible danger arises for clogging of spinning holes, if dopes are extruded through the spinneret.

Another bad solution state caused by non-dissolved pulp fibres is presented in Fig. 2b. The elongated particles represent non dissolved fibre fragments, which could not be sufficiently solvated by NMMO monohydrate. Even after extension of dissolution time, increase of dissolving temperature or shearing forces inside kneader or List Master Conti aggregate those particles would not be dissolved sufficiently and would also cause spinning disruption or even spinning capillary breaks.

Fig. 2c shows a good dissolution state in day-light microscopic image, when DP is well adjusted and pulp is well separated from the inorganic contamination by application of sequestrants. Such kind of purified pulp could be easily shaped into cellulose man-made fibres by dry-wet spinning procedure.

Table 3 summarises the properties of typical spinning dopes, what are prepared of manufactured OG Hemp pulp and is used for fibre spinning trials up to semi-technical scale.

**Table 3:** Dope properties of optimal manufactured OG Hemp Pulp

Dope characteristics		OG Hemp Pulp
<b>Cuoxam -DP (fibre)</b>		618
<b>Cellulose concentration</b>	%	10.4
<b>Zero shear viscosity at 85°C</b>	Pas	4,926

Due to the elevated DP of the hemp pulp the cellulose concentration in the dope have had to be degraded down to 10.4, instead of 12 %. Nevertheless the prepared spinning dope could be very well transferred into Lyocell fibres having very good physical data of textile fibre properties (see table 4) and an excellent textile processing behaviour.

**Table 4:** Textile physical properties of Lyocell fibres made of hemp pulp

Fibre testing		OG Hemp Pulp
<b>Fineness</b>	dtex	1.9
<b>Fibre tenacity, cond.</b>	cN/tex	41.6
<b>Elongation, cond.</b>	%	13.1
<b>Loop tenacity</b>	cN/tex	12.5

Obtained fibres were further processed into yarns and present a very satisfied processing behaviour, too. Results of characterization of yarn strength and unevenness was done by STFI Chemnitz and look well and could adjust at the same level as for typical cellulose MMF based on wooden pulp. Typical yarn counts down to 10 tex (Nm 100 / Ne 165) could be achieved during ring spinning process. Compared to state of the art such yarn counts really offer new perspectives for textile applications of MMF based on annual plant pulps. The yarn also exhibits a significant better evenness according to the 100 % native hemp yarn at sufficient yarn tenacity.

This order of properties is also assessed in yarn dyeing and finishing as well as in further fabric knitting. Leading textile costumers were very positively surprised by the improved coloration behaviour and excellent moisture management when deep black dyed *Lyohemp*<sup>®</sup> fabrics were handed over to them.



**Figure 3:** Registered Trademark of new Lyohemp<sup>®</sup> textiles made of innovative hemp pulp

## Conclusion

Locally available plant-based or waste-based raw materials might have huge potential in the circular economy. Degummed HBS as well as conventionally processed hemp fibre tow as a control could be successfully transformed into dissolving grade pulp by an adapted paper pulp cooking process and integrated pulp purification for separation from high amount of ash, alkali and earth-alkali impurities. Iron and copper ions concentration could also be decreased down to process conformed ppm-range. The well purified pulp could be easily dissolved in NMMO monohydrate as solvent. Spinning dopes exhibit satisfying properties and were dry-wet spun into Lyocell type fibres. The Lyocell fibres proposed sufficient mechanical properties for further textile processing. Yarns made of these fibres represented fine yarn counts as well as convincing mechanical and evenness properties, which appear in favourable yarn dyeing and finishing. *Lyohemp*<sup>®</sup> fabrics manufactured from such kind of yarns seem to be of surprisingly good quality for textile clothing application.

## Acknowledgements

The presented results were gathered in the NaFaTech project, which was financially supported by the Federal Ministry for Economic Affairs and Energy under the supported code 16KN034824. The authors would like to express their cordial thank for granted allowance and all involved consortia members and subcontractors from industry and research institutions for their active technical support of the complex project subjects.



## References

- [1] EEA Report: The circular economy and the bio-economy - Partners in sustainability, No 8/2018, p. 38
- [2] Iqbal, Y., Lewandowski, I., Weinreich, A., Wipfel, B., Pforte, B., Hadai, O., Tryboi, O., Spöttle, M. and Peters, D.; Maximising the yield of biomass from residues of agricultural crops and biomass from forestry, Final Report, Ecofys, Berlin, **2016**
- [3] Ananas Anam, Introducing Piñatex (<http://www.ananas-anam.com/pinatex>), accessed August 10, **2019**
- [4] European Industrial Hemp Association: Record cultivation of industrial hemp in Europe in 2016, **2017**, (<http://www.eiha-conference.org/pressrelease?id=183>), accessed August 10, 2019
- [5] Synthron, Safety Data Sheet ACTIRON® DP 950 and Safety Data Sheet MASQUOL® FEO (**2016**)
- [6] Ch. Michels, B. Kosan: Lyocell process - material and technological restrictions, Chemical Fibers International 50, (**2000**), 556-561
- [7] Ch. Michels, B. Kosan: Contribution to dissolution state of cellulose in aqueous amine oxide characterized by optical and rheological methods, Lenzinger Berichte, 82 (**2003**), 128-135
- [8] F. Meister, B. Kosan: A tool box for characterization of pulps and cellulose dopes in Lyocell technology, in Cellulose Dissolution and Regeneration: Systems and Interactions, Nordic Pulp & Paper Research Journal Vol. 30 no. (1), (**2015**), 112-120
- [9] *DIN EN ISO 1973:1995-12* - Textiles - Determination of linear density - Gravimetric method and vibroscope method, *DIN EN ISO 5079:1996-02* - Textiles - Fibres - Determination of breaking force and elongation at break of individual fibres, *DIN 53843-2:1988-03* - Testing of textiles; loop tensile test for staple fibres
- [10] R. B. Chavan, A. K. Patra: Development and processing of Lyocell, Indian Journal of Fibre & Textile Research 29, (**2004**), 483-492
- [11] J. Bischofberger: Processing of Lyocell from fiber to end use, Lenzinger Berichte 77, (**1997**), 19-22



# Convenient preparation of methyl cellulose using trimethylsulfonium hydroxide electrolytes

Gabriel Julian Partl<sup>1,2</sup>, Kateryna Huemer<sup>2</sup>, Robert Bischof<sup>3</sup>, Danuta Aigner<sup>2</sup>, Christian Sparger<sup>3</sup>, and Herwig Schottenberger<sup>1\*</sup>

<sup>1</sup> Faculty of Chemistry and Pharmacy, University of Innsbruck, Innrain 80-82, 6020 Innsbruck, Austria

<sup>2</sup> Kompetenzzentrum Holz GmbH, Altenberger Straße 69, 4040 Linz, Austria

<sup>3</sup> Lenzing AG, Werkstraße 2, 4860 Lenzing, Austria

\* Contact: Herwig.Schottenberger@uibk.ac.at

## Abstract

In this communication, a simple and scalable synthesis method for highly pure, halide-free aqueous trimethylsulfonium hydroxide electrolytes, as well as their application as derivatizing cellulose solvents, is disclosed. Utilization of co-solvents such as DMSO enables the dissolution of celluloses with varying degrees of polymerization under exceptionally mild conditions. The derivatization extent is controllable via several reaction parameters, *e.g.* temperature, time, stoichiometry and presence/absence of a co-solvent. The products' degree of substitution was determined using quantitative <sup>13</sup>C-NMR spectroscopy. In addition, the possible use of other sulfonium and sulfoxonium hydroxide electrolytes in this context is touched on.

**Keywords:** methyl cellulose, trimethylsulfonium hydroxide, electrolyte, derivatizing cellulose solvent, co-solvent

## Introduction

Methyl cellulose is one of the most widely used cellulose ethers, with applications spanning from several medical uses such as in ophthalmological preparations or laxatives, utilization in consumer products, *e.g.* as rheological modifier or food additive (E461), to its use as supplement in construction materials [1]. In part due to this industrial importance, several methods of synthesizing methyl cellulose with varying degrees of substitution (DS) have been explored. The most widely used pathway involves the heterogeneous reaction of cellulose with a biphasic mixture of aqueous sodium hydroxide and methyl chloride or methyl iodide [1].

Homogeneous synthesis procedures are based around dissolution of unsubstituted cellulose in *i.e.* onium hydroxide electrolytes or dry dimethylacetamide/lithium chloride mixtures before etherification with a suitable methylating agent.

Depending on the DS, methyl cellulose may be dissolved in (cold) water or organic solvents. When prepared under homogeneous conditions, methyl celluloses with DS > 0.9 are soluble in water (for

heterogeneously prepared products: DS > 1.3), while a DS > 2.5 restricts applicable solvents to the organic realm. Specifically, a DS greater than 2.1 allows for dissolution in ethanol, a DS > 2.4 results in acetone- and ethyl acetate-soluble species, and a DS higher than 2.7 gives methyl celluloses that dissolve in certain aromatic hydrocarbons [1].

Water-soluble methyl cellulose exhibits some special properties, one of the most notable being its lower critical solution temperature (LCST) behavior: at high temperatures (typically > 60 °C), it precipitates from aqueous solution in form of a thermoreversible gel [1].

Trimethylsulfonium hydroxide (Me<sub>3</sub>S-OH), too, has found several applications, almost all of them capitalizing on its alkylating properties. Exemplarily, Me<sub>3</sub>S-OH is used in highly efficient O-, S-, and N-methylations [2], in pyrolytic methylation reactions for analytical purposes [3–8], or solid phase micro-extractions with *in situ* transesterification [9]. Notably, trimethylsulfonium species are important precursors for the preparation of sulfur ylides, which

in turn are famous epoxidation agents used in the Johnson-Corey-Chaykovsky reaction [10–12].

Generally, sulfonium salts are not regarded as good cellulose solvents in literature [13]. However, as early as in 1941, several trialkylsulfonium hydroxide electrolytes, most notably triethylsulfonium hydroxide and di-*n*-butylmethylsulfonium hydroxide, have been claimed to dissolve substantial amounts of cellulose [14]. Yet, there is no description of whether the dissolution takes place under derivatization or not, and Me<sub>3</sub>S-OH is not mentioned as a suitable solvent either. Additionally, the reaction of Me<sub>3</sub>S-OH with cellulose derivatives has been described, but it was solely employed as a transesterification agent: by utilizing Me<sub>3</sub>S-OH, cellulose esters were cleaved, forming free cellulose and fatty acid methyl esters [15]. Thus, to the best of our knowledge, direct methylation and dissolution of cellulose using Me<sub>3</sub>S-OH electrolytes has not been reported as of yet.

## Materials & Methods

### Materials

Celluloses used in this communication were commercially available Avicel PH-101 (Sigma-Aldrich) and cellulose from Lenzing AG (hereinafter called LenCel, degree of polymerization approx. 400, water content roughly 8 wt%).

Aqueous solutions of trimethylsulfonium hydroxide were prepared in three reaction steps:

*a) Trimethylsulfonium methylsulfate, Me<sub>3</sub>S-MeSO<sub>4</sub>:* to 15.6 g (250 mmol) of dimethyl sulfide in 100 ml of acetonitrile, 30.0 g (237.8 mmol) of dimethyl sulfate were added slowly and the resulting mixture stirred at 4 °C for 3 h, followed by stirring at room temperature (RT) for 16 h (with reflux condenser and balloon attached, in case an exothermal event occurs). Subsequently, 150 ml of diethyl ether were added to the reaction solution and the precipitated product filtered off, washed with diethyl ether and dried *in vacuo*. 43.4 g (230.5 mmol) of pure-white, slightly odorous, powdery Me<sub>3</sub>S-MeSO<sub>4</sub> were isolated, corresponding to 97% of theoretical yield.

<sup>1</sup>H-NMR (300 MHz, (CD<sub>3</sub>)<sub>2</sub>SO) δ= 3.40 (s, 3H), 2.87 (s, 9H) ppm. <sup>13</sup>C{<sup>1</sup>H}-NMR (75 MHz, (CD<sub>3</sub>)<sub>2</sub>SO) δ= 53.03, 26.00 (3C) ppm.

*b) Trimethylsulfonium bisulfate, Me<sub>3</sub>S-HSO<sub>4</sub>:* 43.4 g (230.5 mmol) of Me<sub>3</sub>S-MeSO<sub>4</sub> were dissolved in 100 ml of deionized water (dissolution process is strongly endothermal). To this solution, 0.5 ml (9.0 mmol) of

96% sulfuric acid were added and the resulting reaction mixture stirred without a stopper at 100 °C for 16 h. Upon cooling to RT, the virtually pure Me<sub>3</sub>S-HSO<sub>4</sub> crystallizes as a colorless mass. The yield was practically quantitative, and the product directly reacted to the hydroxide without further purification.

<sup>1</sup>H-NMR (300 MHz, (CD<sub>3</sub>)<sub>2</sub>SO) δ= 8.27 (s, 1H), 2.88 (s, 9H) ppm. <sup>13</sup>C{<sup>1</sup>H}-NMR (75 MHz, (CD<sub>3</sub>)<sub>2</sub>SO) δ= 26.10 (3C) ppm.

*c) Trimethylsulfonium hydroxide, Me<sub>3</sub>S-OH:* 40.1 g (230 mmol) of Me<sub>3</sub>S-HSO<sub>4</sub> (as prepared in step b)) were dissolved in 100 ml of water, followed by the addition of a hot solution of 77.7 g (239 mmol) of barium hydroxide octahydrate (purity: 97%) in 200 ml of water, under vigorous stirring. The resulting heterogeneous mixture was left to cool to RT, and then the fine precipitate of barium sulfate filtered off. Subsequently, the filtrate was concentrated to approx. 50 g, cooled and filtered again (glass frit, pore size 5). This gave 42.6 g of a practically colorless, slightly viscous solution. Via acid-base titration, a hydroxide content of 4.25 mmol/g was determined, corresponding to an approximately 40 wt% solution of Me<sub>3</sub>S-OH (79 % yield).

<sup>1</sup>H-NMR (300 MHz, (CD<sub>3</sub>)<sub>2</sub>SO) δ= 2.53 (s, 9H) ppm.

<sup>1</sup>H-NMR (300 MHz, D<sub>2</sub>O) δ= 2.60 (s, 9H) ppm.

<sup>13</sup>C{<sup>1</sup>H}-NMR (75 MHz, (CD<sub>3</sub>)<sub>2</sub>SO) δ= 26.09 (3C) ppm.

Alternatively, and much more conveniently, Me<sub>3</sub>S-OH solutions may also be prepared directly via combination of aqueous solutions of commercially available trimethylsulfonium iodide and tetra-*n*-butylammonium hydroxide, followed by filtration of precipitated tetra-*n*-butylammonium iodide and extraction of the aqueous filtrate with dichloromethane in order to remove residual impurities [16]. In this communication, we opted for a halide-free process in order to avoid complications during cellulose dissolution and thus used the above-described 3-step process.

### Preparation of methyl celluloses:

Set amounts of Avicel or LenCel were mixed intimately with fixed amounts of a 40 wt% Me<sub>3</sub>S-OH solution. In experiments where a co-solvent was employed, one mass equivalent of dimethyl sulfoxide (DMSO) was added at the end in order to avoid clumping of the cellulose. All samples were stirred for either 3 h or 24 h at 25, 60 or 100 °C, as listed in Table 1. Samples 1-6 were stirred in small glass vials fitted with plastic screw caps, while samples 7 and 8 were prepared using thick-walled glass vessels fitted with PTFE seals.

**Table 1:** Sample numbering and reaction parameters for the preparation of methyl celluloses.

Sample	Cellulose type	Cellulose (mg)	40% Me <sub>3</sub> S-OH (mg)	DMSO (mg)	Final cellulose conc. (wt%)	t (h)	T (°C)
1	LenCel	100	900	1000	5	24	25
2	Avicel	200	800	1000	10	24	25
3	LenCel	100	900	-	10	3	60
4	LenCel	100	900	1000	5	3	60
5	Avicel	200	800	-	20	3	60
6	Avicel	200	800	1000	10	3	60
7	Avicel	1000	4000	-	20	3	100
8	Avicel	1000	4000	5000	10	3	100

**Regeneration and purification of the products:**

**Samples 1 and 2:** After the reaction, the products were precipitated with 5 ml of ethanol and the samples stirred for another 3 h. Subsequently, the products were filtered off, washed twice with ethanol and diethyl ether each and dried *in vacuo*. As an additional purification step, the samples were dissolved in DMSO to make a 5 wt% solution, and the viscous solutions added dropwise to a tenfold volume excess of ethanol. The resulting dispersions were stirred overnight, followed by filtration of the precipitated products, washing with ethanol, acetone and diethyl ether, and drying *in vacuo* for 40 h.

**Samples 3-6:** After the reaction, the mixtures were left to cool to RT and their volume diluted to approximately 5 ml with water. The colored, viscous solutions were syringe-filtered (1.1  $\mu$ m, glass-based) and the products precipitated with 50 ml of a 4:1 mixture of acetone and ethanol (for **4** and **6**, an extra 30 ml of diethyl ether were needed to induce precipitation). The products were filtered off, washed twice with acetone and diethyl ether each, and then dried *in vacuo*. As an additional purification step, the samples were dissolved in DMSO to make a 5 wt% solution, and these viscous solutions added dropwise to a tenfold volume excess of ethanol. The resulting dispersions were stirred overnight, followed by filtration of the precipitated products, washing with ethanol, acetone and diethyl ether, and drying *in vacuo* for 40 h.

**Samples 7 and 8:** After the reaction, the mixtures were left to cool to RT, followed by treatment with 10 ml of ethanol and filtration of the products. For purification purposes, sample **7** was dissolved in 10 ml of water and regenerated via dropwise addition of the solution

to 200 ml of acetone. Sample **8** was dissolved in 10 ml of a 1:1 mixture of ethanol/chloroform and regenerated via dropwise addition to 200 ml of acetone as well. The products were dried *in vacuo*.

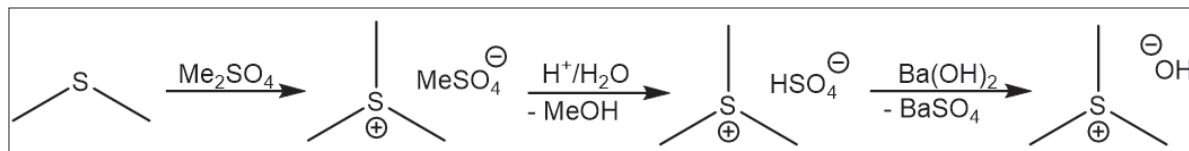
**Methods**

For Me<sub>3</sub>S-MeSO<sub>4</sub>, Me<sub>3</sub>S-HSO<sub>4</sub> and the Me<sub>3</sub>S-OH electrolyte, <sup>1</sup>H and <sup>13</sup>C NMR spectra were recorded on a Bruker Avance DPX 300 spectrometer (300 MHz) and analyzed using the software MestReNova (version 9.0.1). Samples **1-8** were investigated by <sup>1</sup>H-NMR (500 MHz, data not shown) and quantitative <sup>13</sup>C-NMR at 80°C in DMSO-*d*<sub>6</sub>. All NMR measurements were carried out on a 500 MHz Bruker AVIII 500 spectrometer using a 5 mm probe. Chemical shifts are given in ppm. For <sup>1</sup>H-NMR experiments, a cellulose concentration of approximately 10 g/l was employed; <sup>13</sup>C-NMR sample concentration was approximately 60 g/l. <sup>1</sup>H-NMR spectra were recorded with the following acquisition parameters: 10  $\mu$ s 90° pulse, 4.1 s acquisition time, 8 ppm spectral width and a relaxation delay of 1 s. 32 scans were accumulated. The spectra were referenced to the DMSO-*d*<sub>6</sub> peak at 2.50 ppm. Inverse-gated decoupled <sup>13</sup>C-NMR spectra were recorded with 11.25  $\mu$ s 90° pulses, 1.31 s acquisition time, 2.0 s relaxation delay, 199 ppm spectral width and 4 dummy scans. 8192 scans were accumulated. The spectra were referenced to the DMSO-*d*<sub>6</sub> peak at 39.52 ppm. Deconvolution and visualization of the spectra was performed with the Bruker program TopSpin (version 4.0.3). Acid-base titrations were done using a 1.0 M *p*-toluenesulfonic acid solution.

## Results & Discussion

Aqueous trimethylsulfonium hydroxide solutions were prepared via a 3-step process (Scheme 1): methylation of dimethyl sulfide with dimethyl sulfate and subsequent hydrolysis of the methyl sulfate moiety gave trimethylsulfonium bisulfate, which was reacted to the hydroxide by using an aqueous barium hydroxide solution and filtering off precipitated barium sul-

fate. Concentration of the resulting trimethylsulfonium hydroxide solution is possible up to at least 40 wt% without encountering significant formation of dimethylsulfonium methylide, or rather, owing to the marked thermal instability thereof [17], decomposition products. When stored at 4 °C for 4 months, a noticeable smell of ethene builds up, yet the hydroxide content of the solution remains practically unchanged.



**Scheme 1:** Preparation of trimethylsulfonium hydroxide electrolytes.

Initial tests with aqueous  $\text{Me}_3\text{S-OH}$  solutions as cellulose solvents were not very encouraging: at RT, even 40 wt%  $\text{Me}_3\text{S-OH}$  solutions did not dissolve any cellulose. However, distinct swelling of the cellulosic material was observed, along with minor (in case of LenCel) to significant coloration of both the liquid and solid phase (in case of Avicel). Moderate heating with a heat gun quickly led to dissolution of up to at least 20 wt% of Avicel and 10 wt% of LenCel, with higher concentrations resulting in gel-like phases. Upon attempted regeneration of the cellulose via addition of an excess of water, it was noted that most of the cellulose remained in solution, as evidenced by both low regeneration yield and the aqueous phase retaining relatively high viscosity. After precipitation of the rest of the cellulosic material with acetone and NMR analysis of the material, it was apparent that low-DS methyl cellulose had formed. Thus, it may be concluded that trimethylsulfonium hydroxide electrolytes belong to the group of derivatizing, aqueous cellulose solvents [18]. The formation of methyl cellulose is not that unexpected: in literature, the use of trimethylsulfonium hydroxide as methylating agent is well documented [2, 19].

Interestingly, when one mass equivalent of DMSO (relative to the total weight of cellulose + 40 wt%  $\text{Me}_3\text{S-OH}$ ) was employed as a co-solvent, dissolution of cellulose was rapid even at RT. Specifically, 5 wt% of Avicel dissolved in under a minute, and 10 wt% of Avicel (Fig. 1a) or 5 wt% of LenCel (Fig. 1b) were solubilized in approximately two hours. Currently, the role of the co-solvent is not entirely clear. While it is

certainly possible that DMSO is methylated to give a cationic intermediate which in turn alkylates the cellulosic substrate, there is no spectroscopic evidence in favor of such a mechanism. Thus, at present, DMSO is thought to act purely as a co-solvent.

Regarding the dissolution mechanism, it appears that solubilization is not solely achieved by quick derivatization of cellulose and concomitant formation of water-soluble species ( $\text{DS} > 0.9$  for homogeneously prepared methyl cellulose) [1]. This hypothesis is corroborated by the observation that for several minutes after cellulose dissolution, addition of an excess of water still leads to precipitation of most of the cellulosic material. In the presence of DMSO and directly after dissolution at RT, 60-70% of the cellulosic materials are readily regenerated upon dilution. Thus, we believe  $\text{Me}_3\text{S-OH}$  electrolytes to act both as a derivatizing (via methylation) and a non-derivatizing solvent (via providing a strongly basic environment) at the same time; low-DS methyl celluloses are known to solubilize in strongly basic media.

Especially at RT, methylation is comparatively slow: after 24 hours, the DS of the products was approximated to be roughly 0.9 for Avicel and 1.2 for LenCel (determined via residual hydroxide concentration of the electrolytes; more accurate results have been obtained using  $^{13}\text{C}$ -NMR spectroscopy). This approximation is consistent with the observation that acidification of the cellulose solutions does not result in any precipitation, as would be the case for lower-DS methyl celluloses [1].

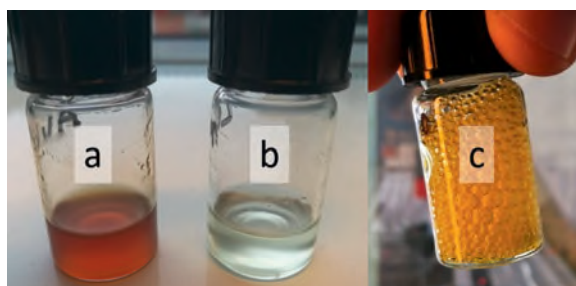


**Figure 1:** Left: photographs of solutions of 10 wt% Avicel (a) and 5 wt% LenCel (b) in roughly 1:1 w/w 40% Me<sub>3</sub>S-OH/DMSO, obtained via stirring at RT for 16 h. Right (c): photograph of a strongly effervescing solution of 10 wt% Avicel in 40% Me<sub>3</sub>S-OH at 60 °C.

In order to obtain more information about the accessible DS range, celluloses were dissolved in Me<sub>3</sub>S-OH electrolytes at 25, 60 and 100 °C using different reaction times, either in the absence or presence of a co-solvent (DMSO). At elevated temperatures, the methylation reaction should occur faster, and thus higher DS values are ought to be obtainable. However, if Me<sub>3</sub>S-OH quickly decomposes under these conditions, or the generated methyl cellulose precipitates

from solution due to lower critical solution temperature (LCST) phenomena, a higher DS does not necessarily ensue.

At RT, only experiments with DMSO as co-solvent led to dissolution of cellulose. Both **1** and **2** took on the form of clear solutions after approximately two hours.

When cellulose was reacted with Me<sub>3</sub>S-OH electrolytes at 60 °C (samples **3-6**), the material quickly dissolved, and the solutions soon took on a yellow color. In addition, excessive frothing took place (Fig. 1c), which is most likely attributable to the mixed effect of boiling dimethyl sulfide and the surfactant properties of methyl cellulose.

At 100 °C (samples **7** and **8**), cellulose dissolution and solution coloration (from light yellow to almost black) were very fast. In contrast to experiments conducted at 60 °C, the cellulosic material precipitated from solution after some time and formed a gel, irrespective of whether DMSO was used as a co-solvent or not. Such behavior is attributable to either reaching the LCST, or to increasing the product's DS over the water-soluble threshold (generally accepted for DS > 2.5 [1]).

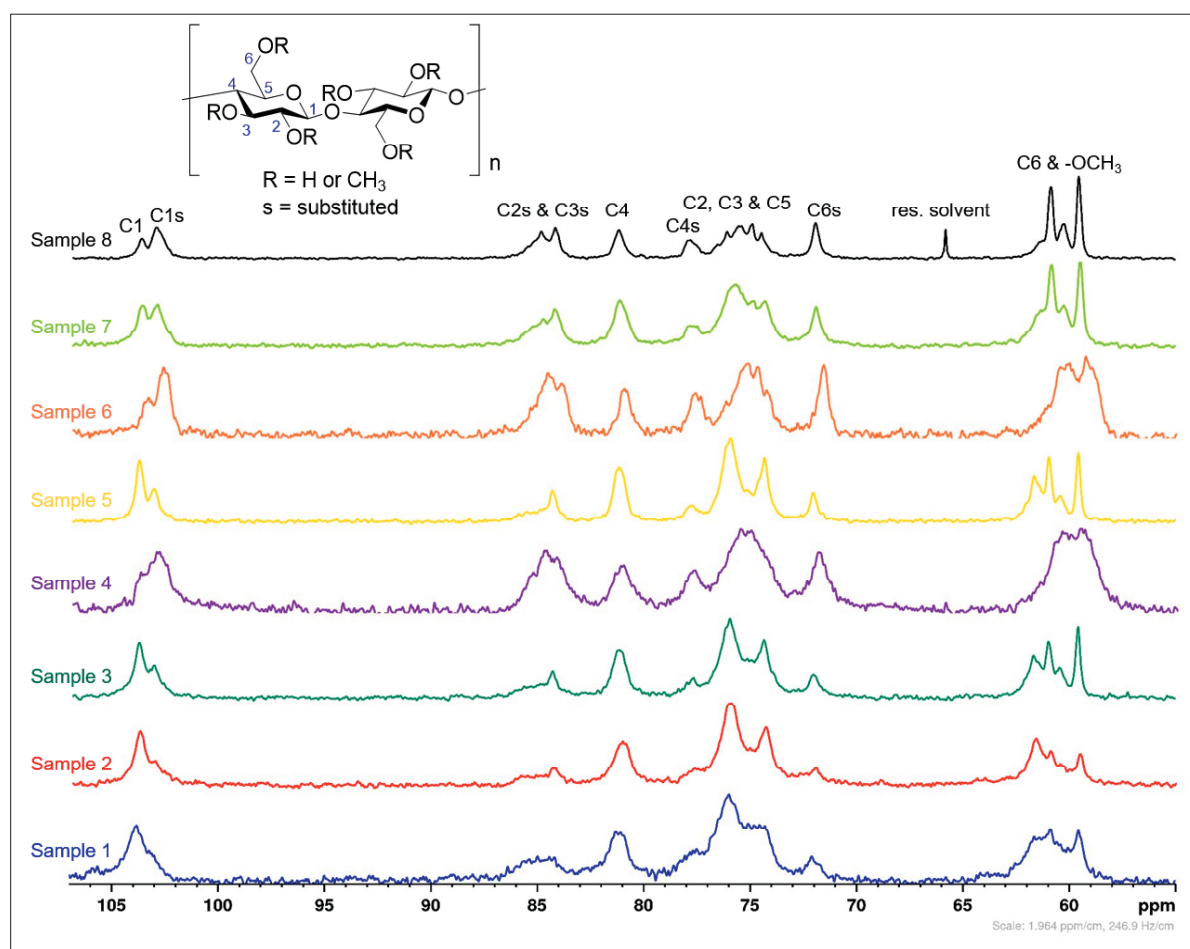


**Figure 2:** Quantitative <sup>13</sup>C-NMR spectra of the cellulosic region of samples **1-8** with signal assignment [20].

Via quantitative solution-state  $^{13}\text{C}$ -NMR experiments and deconvolution of the spectra, the total DS values of the products were determined (Table 2). In Fig. 2, the  $^{13}\text{C}$ -NMR spectra of samples **1-8** (bottom to top) are displayed. Due to some samples (in particular **1**, **4** and **6**) exhibiting severely broadened peaks, deconvolution of the spectra was necessitated. The spectra are all comprised of peaks typically observed in methyl celluloses [1, 20, 21], with sample **8** having been dried insufficiently and thus showing an additional solvent peak at 65 ppm. Fortunately, it does not overlap with any product peaks and therefore does not negatively impact integration accuracy.

Setting sample **3** with a DS of 0.82 aside, the RT samples **1** (LenCel) and **2** (Avicel) exhibit the lowest DS values with 1.22 and 0.88, respectively (specific to the respective cellulose type). While it was expected that the methylation would take place slightly faster at LenCel, due to its arguably lower degree of crystallinity, the discrepancy between **1** and **2** is still remarkable. After considering sample concentrations and  $\text{Me}_3\text{S-OH}$  to anhydrous glucose unit (AGU) ratios, this circumstance is readily explained: for **1** (0.1 g LenCel + 0.9 g 40%  $\text{Me}_3\text{S-OH}$  + 1 g DMSO), 6.20 eq. of  $\text{Me}_3\text{S-OH}$  were available per AGU, whereas for **2** (0.2 g Avicel + 0.8 g 40%  $\text{Me}_3\text{S-OH}$  + 1 g DMSO), only 2.75 eq. of  $\text{Me}_3\text{S-OH}$  per AGU were employed.

The 60 °C sample series highlights the effect of the co-solvent: compared to the very low DS of **3** (0.1 g LenCel + 0.9 g 40%  $\text{Me}_3\text{S-OH}$ ), the DS of **4** (0.1 g LenCel + 0.9 g 40%  $\text{Me}_3\text{S-OH}$  + 1 g DMSO) is more than twice as high with 1.70. It should be noted that the change in cellulose concentration through addition of a co-solvent might also play a role. For **5** (0.2 g Avicel + 0.8 g 40%  $\text{Me}_3\text{S-OH}$ ) and **6** (0.2 g Avicel + 0.8 g 40%  $\text{Me}_3\text{S-OH}$  + 1 g DMSO), a similar effect is observed with DS = 1.02 vs. 1.54. Comparison of **1** and **4** reveals that when all other parameters are equal, the methylation reaction does indeed proceed much faster at higher temperatures; the same is true between **2** and **6**.

In the 100 °C Avicel series (**7** and **8**), the above-observed trends are applicable as well: implementation of a co-solvent raises the DS from 1.29 to 1.81. Additionally, regardless of whether a co-solvent is used or not, DS values after treatment at 100 °C are higher than those obtained at 60 °C (1.29 vs. 1.02 and 1.81 vs. 1.54). Owing to the comparatively high DS, sample **8** is the only one that displays good solubility in organic solvents; a 1:1 v/v mixture of ethanol and chloroform proved to be particularly suitable.

**Table 2:** DS values of samples 1-8, determined via quantitative solution-state  $^{13}\text{C}$ -NMR experiments (Fig. 2).

Sample	DS
<b>1</b>	1.22
<b>2</b>	0.88
<b>3</b>	0.82
<b>4</b>	1.70
<b>5</b>	1.02
<b>6</b>	1.54
<b>7</b>	1.29
<b>8</b>	1.81

From these preliminary results, it appears safe to claim that further enhancing the  $\text{Me}_3\text{S-OH}$  to AGU ratio is likely to enable the synthesis of high-DS methyl celluloses in a matter of a few hours, provided DMSO is used as a co-solvent and reaction temperatures are within a reasonable range.

It should be noted that in addition to the research pertaining to  $\text{Me}_3\text{S-OH}$  electrolytes, initial experiments regarding the use of trimethylsulfoxonium hydroxide ( $\text{Me}_3\text{SO-OH}$ ) electrolytes and alicyclic sulfonium hydroxide electrolytes have been conducted as well. In particular,  $\text{Me}_3\text{SO-OH}$  electrolytes should theoretically be exceedingly interesting derivatizing cellulose solvents. The methylating action of  $\text{Me}_3\text{SO-OH}$  has been well-documented [22, 23], and the only reaction byproduct is DMSO, which would then act as co-solvent to further speed up the solubilization and derivatization of cellulose. Additionally, and in contrast to dimethyl sulfide, DMSO is essentially odorless. However, during preparation of  $\text{Me}_3\text{SO-OH}$  solutions, it was observed that concentrated solutions seem to be markedly less stable than  $\text{Me}_3\text{S-OH}$ , perhaps because of quicker ylide formation. Yet, the authors are certain that the use of more dilute  $\text{Me}_3\text{SO-OH}$  electrolytes as derivatizing cellulose solvents should give fascinating results, and we explicitly invite interested researchers to further pursue this hypothesis.

## Conclusions

By using aqueous/mixed electrolytes of the highly basic methylating agent  $\text{Me}_3\text{S-OH}$ , a simple, effective and convenient approach to methyl celluloses of tunable DS was devised. The cost-effective, quasi-homogeneous reaction is advantageous over the com-

monly used biphasic, heterogeneous system, since it allows for a more even distribution of the methyl moieties, as is suggested by the water solubility of products with a DS < 1. While this one-pot-one-reagent method lends itself best to the lab-scale preparation of various methyl celluloses, the use of other, more easily controllable and recyclable reactants such as Me<sub>3</sub>SO-OH might even be fit for industrial applications. Further synthesis options comprise the preparation of high-DS methyl celluloses, mixed cellulose ethers and the application of other stable sulfonium or sulfoxonium hydroxide electrolytes.

## Acknowledgments

Financial support was provided by the Austrian government, the provinces of Lower Austria, Upper Austria, and Carinthia as well as by Lenzing AG. The authors also express their gratitude to the Johannes Kepler University, Linz, the University of Natural Resources and Life Sciences (BOKU), Vienna, and Lenzing AG for their in-kind contributions.

## References

- [1] Nasatto, P.; Pignon, F.; Silveira, J.; Duarte, M.; Nosedá, M.; Rinaudo, M., Methylcellulose, a Cellulose Derivative with Original Physical Properties and Extended Applications. *Polymers* 2015, 7, 777–803 and references therein.
- [2] Yamauchi, K.; Tanabe, T.; Kinoshita, M., Trimethylsulfonium hydroxide: a new methylating agent. *J. Org. Chem.* 1979, 44, 638–639.
- [3] Drechsel, D.; Dettmer, K.; Engewald, W., Studies of thermally assisted hydrolysis and methylation-GC-MS of fatty acids and triglycerides using different reagents and injection systems. *Chromatographia* 2003, 57, S283-S289.
- [4] Huang, Z.; Zhang, P.; Sun, Y.; Huang, Y.; Pan, Z.; Wang, L., Determination of glyceride and free fatty acid residuals in biodiesel by thin layer chromatography combined with on-line pyrolytic methylation gas chromatography. *J. Anal. Appl. Pyrol.* 2015, 113, 288–295.
- [5] Purcaro, G.; Tranchida, P. Q.; Dugo, P.; La Camera, E.; Bisignano, G.; Conte, L.; Mondello, L., Characterization of bacterial lipid profiles by using rapid sample preparation and fast comprehensive two-dimensional gas chromatography in combination with mass spectrometry. *J. Sep. Sci.* 2010, 33, 2334–2340.
- [6] Reinnicke, S.; Bernstein, A.; Elsner, M., Small and reproducible isotope effects during methylation with trimethylsulfonium hydroxide (tmsh): a convenient derivatization method for isotope analysis of negatively charged molecules. *Anal. Chem.* 2010, 82, 2013–2019.
- [7] Shadkani, F.; Helleur, R., Use of an injection port for thermochemolysis-gas chromatography/mass spectrometry: rapid profiling of biomaterials. *J. Chromatogr. A* 2009, 1216, 5903–5910.
- [8] Shadkani, F.; Sithole, B. B.; Helleur, R., Rapid screening of hardwood and softwood lignin using low temperature thermochemolysis with a GC injection port. *Org. Geochem.* 2010, 41, 586–594.
- [9] Kühbandner, S.; Ruther, J., Solid phase micro-extraction (spme) with in situ transesterification: an easy method for the detection of non-volatile fatty acid derivatives on the insect cuticle. *J. Chem. Ecol.* 2015, 41, 584–592.
- [10] Corey, E. J.; Chaykovsky, M., Dimethyloxosulfonium Methylide ((CH<sub>3</sub>)<sub>2</sub>SOCH<sub>2</sub>) and Dimethylsulfonium Methylide ((CH<sub>3</sub>)<sub>2</sub>SCH<sub>2</sub>). Formation and Application to Organic Synthesis. *J. Am. Chem. Soc.* 1965, 87, 1353–1364.
- [11] Johnson, A. W.; LaCount, R. B., The Chemistry of Ylids. VI. Dimethylsulfonium Fluorenylide—A Synthesis of Epoxides I. *J. Am. Chem. Soc.* 1961, 83, 417–423.
- [12] Gololobov, Y.G.; Nesmeyanov, A. N.; Iysenko, V. P.; Boldeskul, I. E., Twenty-five years of dimethylsulfoxonium ethylide (Corey's reagent). *Tetrahedron* 1987, 43, 2609–2651.
- [13] Liebert, T., Cellulose Solvents – Remarkable History, Bright Future, in: Liebert, T. F.; Heinze, T. J.; Edgar, K. J. (Eds.), *Cellulose Solvents: For Analysis, Shaping and Chemical Modification*. ACS Symposium Series, Washington, DC: American Chemical Society, 2010, 20103–54.
- [14] Richard S. Shutt, Method of producing solution containing cellulosic material. US2371259, 1945.
- [15] Peydecastaing, J.; Vaca-Garcia, C.; Borredon, E., Accurate determination of the degree of substitution of long chain cellulose esters. *Cellulose* 2009, 16, 289–297.
- [16] Phillion, D. P.; Andrew, S. S., A new method for preparing aqueous solutions of trialkylsulfonium and trialkylsulfoxonium hydroxides. *Tetrahedron Lett.* 1991, 32, 3621–3622.

- [17] Corey, E. J.; Chaykovsky, M., Dimethylsulfonium Methylide, a Reagent for Selective Oxirane Synthesis from Aldehydes and Ketones. *J. Am. Chem. Soc.* 1962, 84, 3782–3783.
- [18] Heinze, T.; Koschella, A., Solvents applied in the field of cellulose chemistry: a mini review. *J. Am. Chem. Soc.* 2005, 127, 84–90.
- [19] Kunnen, K., Trimethylsulfonium hydroxide, in: Paquette, L. A. (ed.): *Encyclopedia of reagents for organic synthesis*, Chichester: Wiley, 1995, 3621.
- [20] Takahashi, S.-I.; Fujimoto, T.; Barua, B. M.; Miyamoto, T.; Inagaki, H., <sup>13</sup>C-NMR spectral studies on the distribution of substituents in some cellulose derivatives. *J. Polym. Sci. A Polym. Chem.* 1986, 24, 2981–2993.
- [21] Kono, H.; Fujita, S.; Tajima, K., NMR characterization of methylcellulose: chemical shift assignment and mole fraction of monomers in the polymer chains. *Carbohydr. Polym.* 2017, 157, 728–738.
- [22] Yamauchi, K.; Nakamura, K.; Kinoshita, M., Methylation of pyrimidines, the corresponding nucleosides, and inosine with trimethyloxosulfonium hydroxide. *J. Org. Chem.* 1978, 43, 1593–1595.
- [23] Kuhn, R.; Trischmann, H., Trimethyl-Sulfoxonium-Ion. *Liebigs Ann. Chem.* 1958, 611, 117–121.



# Alkali-Blau (Anilin-Blau) für die Färbung textiler PAC-Fasern

**Dr. Manfred Hähnke**

Manfred Hähnke, D-65779 Kelkheim, email: m.a.haehnke@t-online.de

## Zusammenfassung

Die Anwendung der Weltmarkt-Produkte aus der Familie der N-arylierten Triphenylmethan-Farbstoffe wie Alkali-Blau (früher als Anilin-Blau bezeichnet) auf textilen, sauer modifizierten Polyacrylnitril(PAC)-Fasern scheint eigentlich nicht möglich zu sein. Das beiderseitige Eigenschaftsprofil schließt auf den ersten Blick eine Vereinbarkeit aus. Aber die vorliegende Arbeit zeigt, dass eine färberische Anwendung von (unsulfoniertem) Alkali-Blau auf PAC-Fasern tatsächlich möglich ist. Es gibt sogar mehrere Varianten der Applikation.

Das Grundverhalten beider „Partner“ d. h. ihre chemischen und sonstigen Eigenschaften werden kurz diskutiert, soweit dies für das „Miteinander“ hilfreich erscheint.

## Die Acryl(PAC)-Faser

Innerhalb der aktuellen Weltproduktion (1) von textilen Chemie-Fasern (ca. 65 Mio to/a) dominieren deutlich die Polyester(PES)-Fasern (ca. 39 Mio to/a = 60 %), diese Menge ist weiterhin steigend. Aber auch die Polyacrylnitril(PAC)-Fasern haben eine ziemlich große Bedeutung, ihre Menge liegt allerdings nur konstant bei ca. 2 Mio to/a.

Die textilen PAC-Fasern sind im wesentlichen Copolymerisate mit mindestens 85 % Polyacrylnitril-Anteil (2). Die Polymerketten enthalten darüber hinaus Anteile von Comonomeren wie z. B. Vinylalkohol, Vinylchlorid, Vinylacetat, Acrylsäure/Methacrylsäure, Acrylsäure-/Methacrylsäureester. In den ganz überwiegenden (üblichen) Fällen sind textile PAC-Fasern sauer modifiziert, sie enthalten zusätzlich einpolymerisierte oder aufgepfropfte Comonomer-Anteile mit sauren Gruppen wie z. B. Sulfo (-SO<sub>3</sub>H), Sulfato (-O-SO<sub>3</sub>H) oder Carboxy (-COOH). Diese Gruppen führen in wässriger Umgebung zu einem an-

ionischen Verhalten. Daher sind sie verantwortlich für die Färbbarkeit der Fasern mit kationischen Farbstoffen (C. I. Basic Dyes).

Produktionstechnisch wird das PAC-Polymer aus einer Lösung in Dimethyl-formamid (DMF), Dimethylacetamid (DMAC), Dimethyl-sulfoxid (DMSO) oder in wässriger Na-rhodanid-Lösung in ein wässriges Koagulationsbad ausgesponnen (extrudiert). Ein solches Koagulationsbad besteht z. B. aus einer 40 – 60 % igen Lösung der genannten Lösungsmittel. Hier erfolgt die Koagulation des Polymers zu einem Faser-Gel, welches zunächst noch viele und große wasser-gefüllte Porenräume aufweist. Erst durch das Trocknen und Verstrecken entsteht die fertige PAC-Faser mit ihren fasertypischen Eigenschaften. Im Fall von Dimethyl-formamid ist auch ein Trocken-Verspinnen in einen Heißluftschacht möglich, in welchem das Lösungsmittel dann verdampft.

Die Colorierung der PAC-Faser kann generell an 3 Stellen des Herstellungsprozesses erfolgen: in der Spinnmasse, im Gel-Zustand (beide beim Faserhersteller) und im fertigen Zustand (in einer textilen Färberei oder Druckerei).

## Der Farbstoff

Grundsätzlich kommen für die Colorierung von PAC-Fasern a) Farb-Pigmente und b) kationische Farbstoffe in Betracht.

Die Pigmente weisen allerdings bestimmte Nachteile auf (3). Beim Verspinnen ist oft ein Verstopfen und eine mechanische Abnutzung der Spinnndüsen und folglich eine gewisse Titer-Ungenauigkeit nicht zu vermeiden. Farbpigmente lassen sich weiterhin nicht immer mit gleichbleibender Feinverteilung und in gesicherter Kristallstruktur herstellen. Darüber hinaus führen Farbpigmente (insbesondere bei hohen Kon-

zentrationen, d. h. hohen Farbtiefen) oft zu Einbußen an Faserglanz. Falls die Farbpigmente hohe Anteile an farblosen Bestandteilen (Stellmittel, Dispergiermittel, Gegenionen wie z. B. Heteropolysäuren) enthalten, ist die maximal erreichbare Farbtiefe auch noch merklich eingeschränkt.

Neben den Farbpigmenten gibt es weltweit eine Vielzahl von Klassen und von Einzelindividuen kationischer Farbstoffe (C. I. Basic Dyes). Praktisch immer können im Fall eines ausreichenden Gehalts der PAC-Faser an anionischen Gruppen höchste Farbtiefen und eine maximale Brillanz erreicht werden, gleichgültig ob in der Spinnmasse, im Gel-Zustand oder später in einer textilen Färberei/Druckerei coloriert wird.

Die kationischen Farbstoffe bestehen jeweils aus einem (kationischen) Chromophor und einem farblosen (anionischen) Gegenion. Je nach molekularer Größe des Gegenions kann eine merkliche Absenkung der Farbstärke eines handelsüblichen Farbstoffs resultieren.

Aus der Sicht der Anwendung wäre die Form einer freien Farb-Base auch deshalb nützlicher als die Form eines Farb-Salzes, weil die marktüblichen Anionen wie z. B.  $\text{ZnCl}_3^-$ ,  $\text{CNS}^-$ ,  $\text{CH}_3\text{OSO}_3^-$ ,  $\text{BF}_4^-$  zu Unverträglichkeiten der Farbstoffe untereinander (z. B. bei einer Trichromie-Färbung) führen können. Leider ist aber die Basen-Form der allermeisten kationischen Farbstoffe chemisch nicht über eine längere Zeit und bei höheren Temperaturen stabil.

Glücklicherweise gibt es aber auch Typen von tendenziell kationischen Farbmitteln, deren Basen-Form leicht herstellbar und außerordentlich stabil ist. Hierzu gehören mehrere Individuen aus der Familie der Alkaliblau-Produkte (4).

Grundsätzlich ist der molare Extinktionskoeffizient (Ausdruck für die molekulare Farbstärke) von Alkaliblau mit einem Wert von über 70 000 außergewöhnlich hoch (5). Andere Farbmittel erreichen eine solche Farbstärke zumeist bei weitem nicht.

In Abhängigkeit von der definitiven chemischen Konstitution/Substitution können mit der Familie der Alkaliblau-Produkte in industriellem Maßstab rotstichige, neutrale oder grünstichige Blaus erzeugt werden, alle mit sehr hoher Farbton-Reinheit. Auch Rotviolett-, Blauviolett- und Grün-Töne sind zugänglich. Interessant ist auch die erzielbare Lichtechtheit. Im Vergleich zu den verwandten wasserlöslichen Triphenylmethan-Farbstoffen (Malachit-Grün, Fuchsin und Rosanilin), welche auf PAC-Fasern nur zu Lichtechtheitswerten in 1/1-RTT im Bereich von 2 – 4 führen, erreichen Alkaliblau-Produkte Werte bis zu 5 – 6 (auf der 8-teiligen Blau-Skala), was für Oberbekleidung und Kinderkleidung völlig ausreicht (6).

Es ist darüber hinaus höchst interessant, dass man mittels „Schönung“ von Ruß-basierten Schwarz-Pigmenten durch den Zusatz von bestimmten Mengen von Alkaliblau-Produkten ein wirkliches Tiefschwarz erzielen kann, auf Papier mit einer Lichtechtheit bis

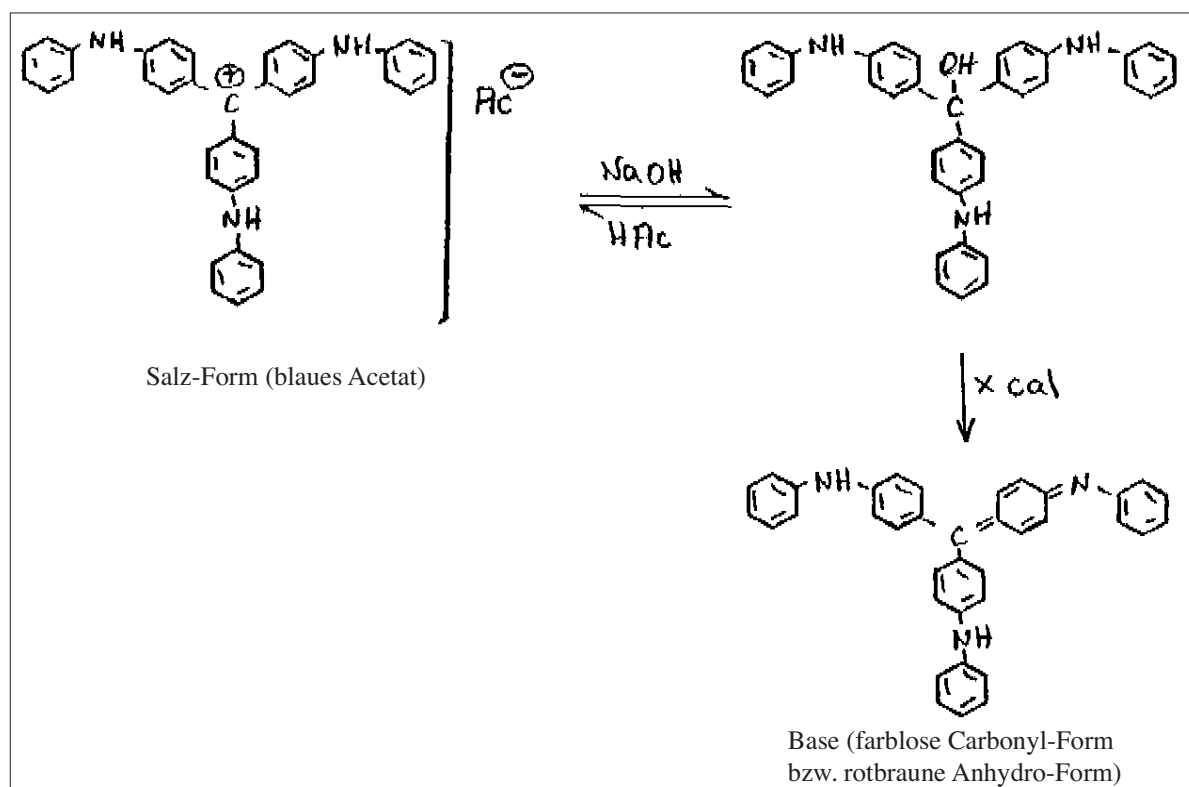


**Bild 1:** Die Chemischen Formen von Alkali-Blau

über Note 6. In diesem Fall werden bestimmte einfallende Lichtquanten durch den Kohlenstoff des Rußes so weitgehend adsorbiert, dass keine große Lichtschädigung des Alkali-Blaus mehr geschehen kann.

Die Verfügbarkeit von (unsulfoniertem) Alkali-Blau, d. h. seine Produktion zu günstigen Herstellkosten ist absolut gesichert. Es gibt ältere und neue Synthese-Varianten (7), welche großtechnisch in mehreren Ländern praktiziert wurden (USA, Deutschland, Indien, China) und immer noch werden. Die modernsten Synthese-Varianten führen zu weiteren Verbesserungen, insbesondere bezüglich Farbton und Herstellkosten (8).

Darüber hinaus landen Tausende von to/a (in mono- oder höher sulfonierter Form) im Blaupigment-Bereich (wie auch in Schwarz-Mischungen), auf Papier, daneben in Sanitär-Farbmitteln, in der Düngemittel-Markierung sowie in Schreibtinten.

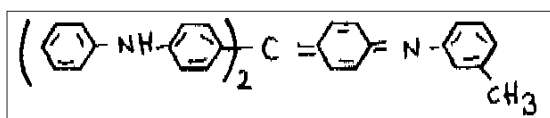
Wie bereits angedeutet ist die Basen-Form von (unsulfoniertem) Alkali-Blau chemisch außergewöhnlich beständig, sowohl bei höheren Temperaturen als auch über längere Lagerzeiten. Darüber hinaus ist die Umsetzung der Farb-Salze zu den Farb-Basen und umgekehrt „kinderleicht“. Einfach durch eine pH-Änderung lassen sich die verschiedenen Formen ineinander überführen (Bild 1).

Für die coloristische Anwendung führt letzten Endes ausschließlich die Salz-Form zum farbigen Resultat. Die beiden dargestellten Basen-Formen sind farblos bzw. rotbraun/ farbschwach.

## Die PAC-Färbung mit Alkali-Blau in der Spinnmasse

Wie bereits erwähnt wird PAC häufig aus einer Lösung in DMF oder DMAC versponnen. In diesen Lösungsmitteln ist auch (unsulfoniertes) Alkali-Blau sehr gut molekular löslich, auch bereits bei Raumtemperatur. Insbesondere gilt dies für die Farbkörper in Basen-Form. Es ist problemlos möglich, hochkonzentrierte Lösungen der Farb-Basen in DMF oder DMAC zu erzeugen und diese dann direkt der PAC-Spinnlösung zuzusetzen (9).

Beispiel a: 1 Gewichtsteil einer 10 %igen Lösung der Alkaliblau-Anhydrobase der Formel



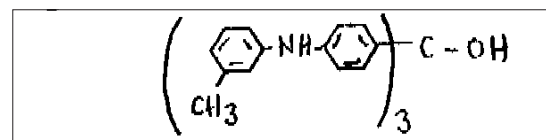
in DMAC wird einer PAC-Spinnlösung (28 %ig in

DMAC) zugesetzt. Die zuvor rötlich-braune Farbkörper-Lösung führt augenblicklich zu einer tiefblauen, voll transparenten Spinnmasse. Nach gutem Homogenisieren wird die gefärbte Spinnmasse dann wie üblich nach dem Nass-Spinnverfahren versponnen. Es entstehen tiefblaue PAC-Fasern ohne ein durch den Farbkörper verändertes Eigenschaftsprofil.

Die in Beispiel (a) erwähnte Farb-Base kann über eine kostengünstige Synthese-Variante hergestellt werden (4). Auch durch Umsetzen eines entsprechenden Alkaliblau-Salzes in Methanol mit NaOH und anschließendes wässriges Aufarbeiten erhält man die genannte Farb-Base. Noch einfacher gestaltet sich die Zubereitung der Farbbasen-Lösung direkt in DMAC mittels Umsetzung des Alkaliblau-Salzes mit einer passenden Menge NaOH.

Einen beträchtlichen praktischen Nutzen kann auch die im nachfolgenden Beispiel beschriebene Verwendung einer Alkaliblau-Farbbase bringen:

Beispiel b: Zu 100 Gewichtsteilen einer 28 %igen PAC-Spinnlösung in DMF werden die für eine Schwarz-Spinnfärbung übliche Menge eines handelsüblichen Ruß-Pigments (mittlerer Teilchendurchmesser von 15  $\mu$ , spezifische Oberfläche von 450  $\text{m}^2/\text{g}$ , gemessen nach BET) sowie 0.1 Gewichtsteile der Alkaliblau-Carbinolbase der nachfolgenden Formel gerührt



Die homogenisierte Spinnmasse liefert nach dem Trocken-Spinnverfahren blaustichig tiefschwarze PAC-Fasern mit guter Lichtechtheit.

Durch eine solche „Schwarzsönung“ kann man den ursprünglich bräunlich schwarzen Ruß-Grundton ganz merklich verbessern. Das Alkali-Blau wird hierbei sowohl an die aciden Gruppen im PAC-Polymer als auch an die vorhandenen aciden Gruppen des Rußes gebunden.

Beim Zusatz des Alkali-Blaus in Basen-Form zu der Spinnlösung entstehen keine salzartigen Nebenprodukte, es können also höchst mögliche Farbtiefen erzielt werden.

Anstelle der Farb-Basen kann das Alkali-Blau zwar auch in Salz-Form (z. B. als Chlorid, Sulfat oder Acetat) verwendet werden, die etwas geringere Löslichkeit der Salz-Form muss aber beachtet werden.

Bei der Spinnfärbung nach dem Nass-Spinnverfahren mit üblichen kationischen Farbstoffen bluten stets gewisse Mengen unfixiert in das wässrige Koagulationsbad aus, da diese Farbstoffe gut wasserlöslich sind. Wird (unsulfoniertes) Alkali-Blau verwendet, tritt ein solches Ausbluten in den Hintergrund, da diese Farbkörper wasserunlöslich sind.

## Die PAC-Färbung mit Alkali-Blau im Gel-Zustand

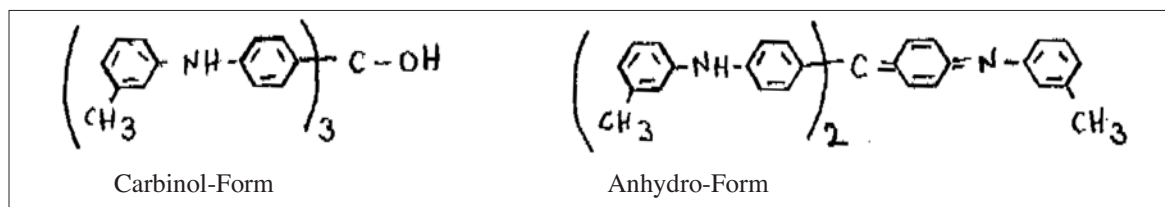
Wie weiter vorn beschrieben bildet sich beim Nass-Spinnverfahren von PAC unabhängig vom verwendeten Spinnlösemittel im wässrigen Koagulationsbad ein außerordentlich offenes Porensystem aus. Die wassergefüllten Poren ermöglichen ein leichtes und rasches Eindiffundieren von molekular gelösten kationischen Farbstoffen (C. I. Basic Dyes) und in direkter Folge eine chemische (ionische) Farbstoffbindung an die anionischen/aciden Anker-Gruppen des Polymers (10, 11)). Viele Hersteller von textilen PAC-Fasern gehen mehr oder weniger erfolgreich diesen Weg. Üblicherweise werden hierbei solche „normale“ kationische Farbstoffe verwendet. Im Fall von Alkali-Blau bleibt die Frage: wie bekommt man ein von Natur aus wasserunlösliches

Produkt in molekularer Feinverteilung in das wässrige Koagulationsbad? Nun, dies ist recht einfach: Das Alkali-Blau ist (auch in Form des Farbsalzes) löslich in Spinnlösemitteln wie DMF oder DMAC. Man kann eine Lösung des unsulfonierten Alkali-Blaus (z. B. als Acetat) als Stammlösung dem Koagulationsbad in der gewünschten Menge zudosieren. Der hohe DMF- bzw. DMAC-Gehalt des ersten Koagulationsbades reicht aus, den Farbkörper molekular für eine ausreichende Zeit in Lösung zu halten. Eine Verbesserung der Löslichkeit kann man erzielen, indem man der Farbkörper-Stammlösung eine gewisse Menge eines geeigneten nichtionogenen Dispergiermittels zusetzt.

## Die traditionelle PAC-Färbung mit Alkali-Blau im Ausziehverfahren

Beim Auszieh-Färbeverfahren textiler PAC-Fasern werden großtechnisch seit jeher wasserlösliche kationische Farbstoffe (C. I. Basic Dyes) eingesetzt. Notwendig sind hierbei (neben einer reproduzierbaren und kostengünstigen Herstellung) eine gute Wasserlöslichkeit, eine gute chemische Beständigkeit unter den in Frage kommenden Färbebedingungen, eine optimale Kombinations-Kennzahl K (um eine hohe

Beispiel c: 10 Gewichtsteile einer Alkalilau-Anhydrobase oder -Carbinolbase der chemischen Formel



werden unter Erhitzen auf ca. 80 °C in 40 Gewichtsteilen eines Addukts von 25 mol Ethylenoxid an 1 mol Stearylalkohol gelöst. Nach dem Erkalten erhält man ein wachsartiges rotbraunes Präparat, welches sehr gut lagerstabil ist. Anstelle des Stearylalkohol-Derivats kann man auch z. B. ein Addukt aus 20 mol Ethylenoxid an 1 mol Rizinusöl einsetzen. Dann entsteht ein entsprechendes flüssiges Präparat mit nahezu dem gleichen Eigenschaftsprofil.

Färbeegalität sicherzustellen) und natürlich ein ausreichendes Echtheitsniveau.

Für die textile Anwendung von Alkali-Blau im Ausziehverfahren scheint die fehlende Wasserlöslichkeit völlig prohibitiv zu sein. Überraschenderweise wurde inzwischen eine interessante Möglichkeit erarbeitet, nach der man dieses Problem überwinden kann.

Man kann (unsulfoniertes) Alkali-Blau in Form der Carbinol- oder der Anhydrobase in einem geeigneten nichtionogenen Tensid aus der Reihe der Ethylenoxid-Addukte von z. B. Fettalkoholen, Alkylphenolen oder Fettsäuren molekulardispers lösen (12).

Beim Aufnehmen solcher Färbepreparate mit angesäuertem Wasser, z. B. Essigsäure in färberisch üblicher Konzentration, bildet sich eine tiefblaue Farblösung, welche direkt einer PAC-Auszieh-Färbeflotte zugesetzt werden kann. Die Basen-Form des Farbkörpers geht hierbei sofort und quantitativ quantitativ in das kationische Farbsalz (Acetat) über, das Tensid solubilisiert dieses in situ in molekulardisperser Form. Die Verwendung eines optimalen Tensids bzw. einer Tensid-Mischung führt zu einer recht stabilen blauen Färbeflotte. Bei der Ausziehfärbung von üblichen textilen PAC-Fasern hiermit nach den praxisüblichen

Färbeverfahren resultieren brillante blaue Färbungen, auch sehr hohen Farbtiefen sind erreichbar. Die Kombinationskennzahl (K-Wert) beträgt beim beschriebenen Beispiel (c) K=3. Die Kombinierbarkeit mit „normalen“ kationischen Farbstoffen ist daher voll gegeben. Die Färbeproduktion ist hoch. Je nach ausgefärbter Farbtiefe erzielt man Lichtechtheitswerte zwischen 4 - 5 und 6.

Eine weitere Optimierung erzielt man durch den Zusatz von gewissen Mengen Ammonium-rhodanid zum beschriebenen Färbepreparat. Die Rekristallisationsgefahr wird hierdurch weiter verringert.

## Übersicht über die in Frage kommenden Alkaliblau-Produkte

Eine gewisse Variation der chemischen Konstitution verändert die chemischen, physikalischen und färbereigenschaften nur wenig. Alle geeigneten Individuen müssen aber Phenylamino-Gruppen tragen und stets frei sein von wasserlöslich machenden Substituenten wie z. B. Sulfo (-SO<sub>3</sub>H), Carboxy (-COOH), Sulfato (OSO<sub>3</sub>H) (Bild 2).

Beispiele:

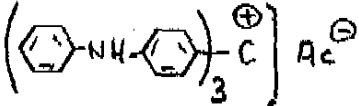
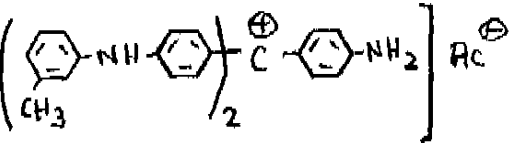
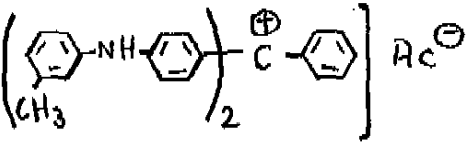
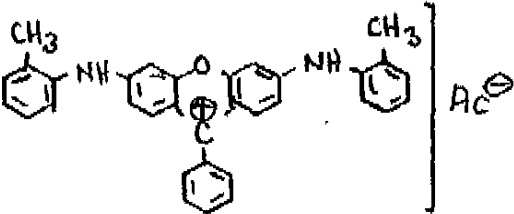
Chemische Konstitution	Farbton
	brilliantblau
	blauviolett
	grün
	rotviolett

Bild 2: Konstitution und Farbspektrum geeigneter Produkte (dargestellt in Salz-Form)

**Literatur:**

- (1) Lenzing AG, The Fiber Year 2018
- (2) Chemie in unserer Zeit, Wiley-VCH Verlag 52 (2018), 178
- (3) Farbwerke Hoechst, DE 2413299
- (4) M. Haehnke, Lenzinger Berichte 93 (2017), 31
- (5) Herbst und Hunger, Industrielle Organische Pigmente (1995)
- (6) Farbwerke Hoechst, DE 1644619
- (7) Polytechnisches Journal (1878), Über Anilinblau
- (8) E. Vekariya, Project report on micro inks (2014)
- (9) Farbwerke Hoechst, DE 2359466
- (10) US 3242243
- (11) DE 2132030
- (12) DE 2308210

*Dedicated to my dear teacher Prof. Dr. Herbert Sixta to his 65th anniversary*

# Lyocell fibers from pulps with high mannan and xylan content - Part 1: Fiber cross section

**Gabriele Schild\***, **Martina Opietnik\***, **Sandra Schlader\***

\* Lenzing AG, A-4860 Lenzing, Austria; corresponding author: g.schild@lenzing.com

## Abstract

For the first time, lyocell fibers with increased hemicellulose content were produced on mill scale. Mannan and xylan were present as an original constituent of the pulp and processed in the lyocell process using NMMO as a solvent. This study was focused on the elucidation of the structure of the fiber cross section. Mannan appeared to be the more stable hemicellulose in the lyocell process when compared to xylan. By enzymatic peeling analysis and fluorescent staining, evidence was found that suggested an even pore structure and an even distribution of hemicelluloses over the fiber cross section. Hemicelluloses appeared to hinder crystallization of the cellulose and gave rise to an increased uptake of water - a water retention value of up to 82.9% was measured. The shape of the hemicellulose rich fibers was also observed to be more circular. Lastly, the results showed that the hemicellulose rich fibers had significantly decreased fiber tensile strength and that the fiber elongation was also slightly reduced.

**Keywords:** *NMMO, lyocell, mannan, xylan, fiber cross section, fiber structure, fiber strength*

## Introduction

Due to an enormous demographic growth and the corresponding increasing prosperity, a shortage in fossil fuel oil is expected across the globe. As a result, it is desired to produce novel types of sustainable regenerated cellulosic fibers with new properties aligned with their area of application.

It is known that the production capacities for natural cellulosic fibers such as cotton are close to reaching their limits and the structure of these fibers grown by nature can hardly be altered according to customer's request. Inherently, they exhibit the morphology of plant cells - depending on the raw material, they have different fiber lengths varying from 1 mm for hardwood pulp to 5 cm for cotton lint. For fibers grown by nature, cell walls are built up by different layers which comprise of a hollow space referred to as a lumen. These cells are closed at their ends and partly connected by pits.

In contrast to pulp and lint, the structure of regenerated cellulosic fibers, such as viscose fibers or lyocell fibers, differs significantly from fibers grown by nature. The cellulose of regenerated fibers is present in the more stable form of cellulose II, while cotton, pulp, wood and annual plants are built up of cellulose I. Viscose fibers are mostly solid without a lumen, except for special applications with small market shares where hollow fibers are produced by special process modifications. The length of the fiber depends on the cut during final processing.

The structure of the cross section has been described in literature in detail. For viscose fibers, the profile is oval and cloud-like and a dense skin surrounds the sponge-like porous structured core. The core to skin ratio is about 3:1, meaning that the skin of a viscose staple fiber with a titer of 1.3dtex is between 2.5 to 3µm thick. It has also been observed that the cellulose chains in the skin show a higher orientation with

smaller crystallites. The core has a lower orientation, but exhibits larger crystals.

On the other hand, the cross section lyocell fibers produced with NMMO as a solvent is close to circular. Using TEM- and SAXS-methods as well as fluorescent staining, Abu-Rous and co-workers describe the lyocell fibers as having a three-layered composition: comprising of a skin, a middle layer and a core which stands out from viscose fibers (*Abu-Rous et al. 2006a and b, Abu-Rous et al. 2007, Biganska 2002*). The final lyocell fiber depicts a very thin and compact skin of about 50 to 100nm in diameter, corresponding to a thickness of about 0.005 to 0.010 $\mu\text{m}$ . It was also found that the porosity increases with an average size from 2 to 5nm towards the middle layer. Pores and voids of the middle layer reach a size of 10 to 20nm. Interestingly, towards the center, the pore size decreases markedly and the core itself shows a very compact structure. Cellulose chains in lyocell fibers are made up of crystalline and amorphous regions organized as nano-, micro- and macro-fibrils.

The requirement for new cellulosic fibers is not only to fill the gap between production capacities and customer demands, but also to be able to supply the customer with a suitable and sustainable high quality material. The structure of regenerated cellulosic fibers influences the fiber properties markedly (*Wendler et al. 2011*). Therefore, shaping the structure of the fiber cross section would be an adequate mean to control and mimic fiber quality. At the same time, it is well known from the lyocell process that possibilities to vary process parameters to influence properties of the regenerated fibers are restricted to the variation of the molecular weight distribution, cellulose concentration in the spinning dope, as well as process temperature and/or stretch after extrusion. That being said, fiber properties can only be controlled to a minor extent during processing (*Biganska and Navard 2009*). Therefore, another method to adjust fiber properties would be the initial choice of raw material. The composition and nature of pulps used could be altered and an ecological and economical approach would be the application of other wood components like lignin and hemicelluloses as additional polymers in lyocell fibers.

Research has been reported on the addition of xylan to viscose fibers in pilot scale (*Schild et al. 2014a and b*). Together with an agglomeration of the hemicelluloses, a segregation of the cellulose and xylan polymers was observed with an enrichment of the xylan at the fiber surface. Changed properties were monitored such as the increased dyability and water retention at almost constant fiber strength. *Singh and Murthy (2017)* observed a slightly more circular cross section

after addition of xylan. These results cannot be transferred directly to the lyocell process due to the general differences of a direct solving system to the more complex viscose process.

An enrichment of lyocell fibers with hemicelluloses using NMMO as a solvent is discussed controversially in the literature. Predominantly, the hemicellulose used was xylan and results for the addition of mannan are not available so far. The reported results are also completely contradictory. *Wendler et al. (2011)* found no significant changes in either process performance or in fiber quality by adding short chain xylan to lyocell fibers. In contrast, *Fink et al. (2004)* observed a deterioration in the process behavior with very poor spinnability, but no changes were observed in fiber properties using unbleached organosolv pulps with an increased lignin and xylan content. *Chen et al. (2015)* correlated the poor spinnability directly with the concentration of hemicelluloses. Additionally to this, *Chen et al (2015)* also found a clear negative influence on fiber strength. Conversely, *Zhang et al. (2007 and 2008)* found only small changes in fiber quality by increasing the hemicellulose content of the pulp from 9.7% to 20.8%.

In the literature, the poor spinnability is ascribed to the fact that cellulose, hemicelluloses and lignin are present in the pulp. This lignin-carbohydrate-complex is not completely dissolved in any direct solvent system and as a result, gel-like structures occur in the spinning dope. This inhomogeneity leads to problems at the spinning devices and lowers the mechanical properties of the final fiber. For the lyocell process using ionic liquids, a solution was proposed by *Ma et al. (2018)* who applied an electron beam treatment to the pulp to crack lignin-carbohydrate bonds before processing. Applying this method, they overcame the spinning problems.

A very important point to consider is that hemicelluloses are not a homogeneous polymer. In fact, their structures and compositions vary enormously depending on the wood species and the process applied. It is well known that xylan associates with lignin while mannan more often associates with cellulose. So far, no investigations have been made using mannan and xylan as additional polymers in lyocell fibers and therefore, we can still expect new and surprising results using different hemicelluloses together with cellulose as a raw material. In this report, for the first time, the influence of increased mannan and xylan contents in lyocell fibers was investigated. This study was focused on the elucidation of the structure of the fiber cross section and strength properties of a pulp with increased mannan and xylan content, processed on a mill scale with NMMO as a solvent.



## Experimental

### Material

Two different market pulps were chosen according to their hemicellulose composition for the production of lyocell fibers. Market pulp A is a standard dissolving pulp for lyocell fiber production made from *Eucalyptus ssp.*. The pulping process applied was the acid sulfite process combined with elemental chlorine free (ECF) bleaching. Market pulp B on the other hand, with its increased mannan and xylan content, was produced by a modified kraft process with subsequent ECF bleaching. The raw material used was *Pinus ssp.*. Both pulps were processed in the lyocell process in mill scale using NMMO as a solvent without major changes in production parameters. For this study, textile fibers with a titer of 1.3dtex and non-wovens fibers with a titer of 1.8dtex were produced.

### Methods

All analyses of pulps and fibers were performed according to Tappi-, ISO- and SCAN-standards.

The method of enzymatic peeling as described by *Sjöberg et al. (2005)* was also employed, where fibers were peeled in layers by an enzyme mixture and the dissolved polysaccharides were analyzed by HPLC. Additionally, the degree of crystallinity (CrI) was determined by FT-Raman measurements with a Bruker IFS66, calibrated by WAX-measurements (*Röder et al. 2006*).

For fluorescent staining, fibers were dyed with Uvitex BHT from 5 min to 24h, according to the method described by *Abu-Rous et al. (2007)*. The samples were embedded by Technovit 7100™ and cross sections of 10µm to 20µm were cut with a microtome Fa. Reichert-Jung. Fluorescent pictures were then taken with an Olympus BX 51 Microscope at a magnification of 1000x and an exposure of 50 to 200ms. Aspect ratios were determined with the same light microscope using two different samples with ten fibers each.

The determination of neutral sugar monomers was performed by anion exchange chromatography (AEC) with pulsed amperometric detection (PAD) after a total hydrolysis with sulfuric acid (H<sub>2</sub>SO<sub>4</sub>) according to *Sixta et al. (2001)*.

## Results and discussion

### Pulp characterization

The properties of both market pulps were very similar in terms of viscosity levels, residual lignin (measured as kappa number) and brightness (tab. 1). Even inor-

ganics, organic extractives, carbonyl- and carboxyl-groups (measured as COOH and Cu number) were comparable. For these reasons, it could be concluded that these parameters would not induce any differences in the processing of the pulps in the lyocell process.

	Market pulp A	Market pulp B
Wood species	<i>Eucalyptus ssp.</i>	<i>Pinus ssp.</i>
Pulping process	Sulfite	Kraft
Viscosity [ml/g]	400	370
Brightness [%ISO]	93.7	91.6
Kappa No. [-]	0.3	0.3
R10 [%]	88.6	83.7
R18[%]	95.4	87.4
Glucan [%]	95.5	82.2
Xylan [%]	2.3	8.3
Mannan [%]	0.2	5.7
Arabinan [%]	<0.1	0.3
Rhamnan [%]	<0.1	<0.1
Galactan [%]	<0.1	0.2
Total hemicellulose [%]	2.4	14.5
Mn [kg/mol]	49	60
Mw [kg/mol]	200	349
PDI [-]	4.1	5.9
w DP<50 [%]	2.9	1.6
w DP<100 [%]	6.5	5.8
COOH [µmol/g]	42	44
Copper No. [-]	1.1	1.4
Extractives [%]	0.05	0.03
Ash [%]	0.05	0.04
Fe [ppm]	0.8	1.6
Si [ppm]	13.0	2.1
Ca [ppm]	3.3	8.4
Mg [ppm]	1.0	9.3

**Table 1:** Properties of the different market pulps for lyocell fiber production.

As intended, the major difference between the two pulps was the mannan and xylan content. While market pulp A showed the low content of hemicelluloses required for a standard lyocell pulp of 2.3% xylan, market pulp B had a high mannan content of 5.7% and a high xylan content of 8.3%.

Likewise, the molecular weight distributions of the two market pulps were different (fig. 1). Market pulp A presented the broad molecular weight distribution of a sulfite dissolving pulp with a poly dispersity index (PDI) of 4.1. It depicted the typical shoulder at lower molecular weights caused by the sulfite process. Polymers with  $DP < 100$  accounted for 6.5% of the pulp and therefore it could be concluded that this shoulder did not only comprise of low Mw hemicelluloses (2.3%) but also of low Mw cellulose as known from literature. In contrast, market pulp B showed the typical fingerprint of a kraft pulp in the low molecular region. The part was smaller compared to the sulfite pulp and there was no enrichment of low molecular weight polymers either as cellulose or as hemicellulose. This was an indication that mannan and xylan had a longer chain length after modified kraft pulping which could be attributed to the process as well as the choice in raw material (softwood). The PDI of 5.9 was very high indicating that no acidic prehydrolysis step was applied at the beginning of the production process.

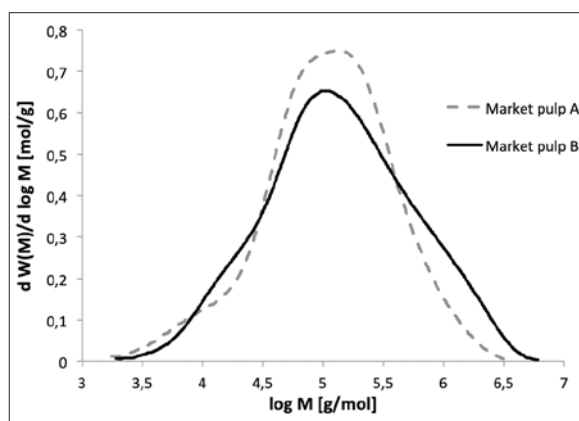


**Figure 1:** Molecular weight distribution of market pulp A, a standard lyocell dissolving pulp compared to market pulp B with a high mannan and xylan content.

## Fiber morphology

### Shape of fiber cross section

There are two main factors that influence the shape of man-made cellulosic fiber cross sections: the first being the applied fiber production process itself, and second being the variation of process parameters therein. The direct dissolving process with the addition of air gap spinning does not require any chemical reaction during precipitation. It is faster and the crystallites are smaller when compared to the viscose process. These fibers, like lyocell fibers, depict a more circular shape. On the other hand, the velocity of chemical reactions during regeneration in wet spinning of the viscose process is driven by mass transfer. The forming of fibers is much slower compared to the lyocell process and the shape of the fibers is more oval.

The aspect ratio is defined as the relationship between different dimensions and describes the geometric shape of the fiber cross section. For fibers, it is the ratio of the longer diameter to the shorter diameter. Microscopic pictures of a standard lyocell fiber from the production process (A) and a hemicellulose rich fiber (B) were taken and analyzed (fig. 2). The aspect ratio of the standard fiber A was 1.60 and it was significantly lower for the hemicellulose rich fiber B which had an aspect ratio of 1.44. Considering that the process conditions were comparable for both fibers during the large scale mill production, this result indicates that hemicellulose rich fibers yield more circular shapes of the fiber. For comparison, the aspect ratio of a standard viscose staple fiber C was measured to be 2.34.

These findings are in good accordance with that described in literature. *Singh and Murthy (2017)* observed a decreasing aspect ratio from 1.67 to 1.46 for viscose fibers spun in the lab with addition of

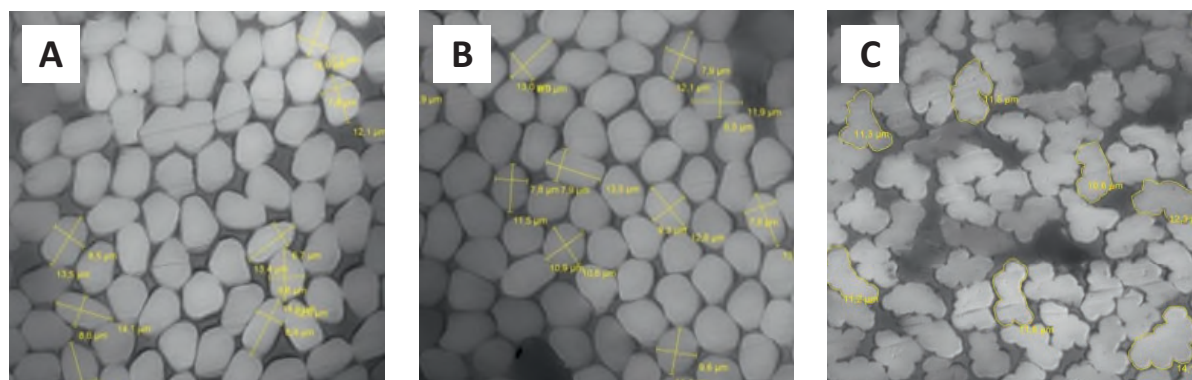


**Figure 2:** Cross section of mill samples of standard lyocell fibers (A) and hemicellulose rich lyocell fibers (B) compared to a standard viscose fiber (C) with a titer of 1.3dtex.

10% xylan. The effect on lyocell fibers was comparable to that observed with viscose fibers even though the values the authors reported were in a different range, probably due to spinning with lab equipment. Lyocell fibers are known to be more circular when compared to other regenerated cellulosic fibers. Therefore, the contact area between fibers is lower and subsequently the friction between the fibers is also lower. Besides avivage, finishes, enzyme treatment and others, this is one factor that lowers the pill-

ing of textiles and the liberation of single fibers from the garment by friction. The total surface area compared to the diameter has a significant impact on fiber friction and consequently, hemicellulose rich lyocell fibers may have a positive effect on lowering friction and therefore reducing pilling which should be subject of further investigations. It should however be noted that the structure of the fiber surface is not considered in this parameter such as the cloudy structure for viscose fibers.

	Fiber A 1.3	Fiber A 1.8	Fiber B 1.3	Fiber B 1.8
Pulp	Market pulp A		Market pulp B	
Titer [dtex]	1.3	1.8	1.3	1.8
CrI [%]	44	47	37	40
WRV [%]	69.6	65.3	82.8	82.1
Glucose [%]	95.8	94.3	86.6	85.6
Xylan [%]	1.8	1.9	6.8	6.9
Mannan [%]	0.3	0.4	5.2	5.3
Arabinan [%]	<0.1	<0.1	0.3	0.2
Rhamanan [%]	<0.1	<0.1	<0.1	<0.1
Galactan [%]	<0.1	<0.1	0.2	0.2
Total hemicellulose [%]	2.1	2.3	12.5	12.6

**Table 2:** Properties and composition of hemicellulose rich lyocell fibers compared to standard lyocell fibers.

### **Crystallinity and water retention value**

For standard lyocell fibers, a low water retention value (WRV) is known to be combined with a very high orientation of the polymer chains and a high crystallinity. This phenomena was observed for the standard fibers produced from the market pulp A which had a low xylan content (see tab. 2). The fibers produced from the hemicellulose rich market pulp B showed higher WRVs for both titers (82 and 83%).

Since swelling is a result of hydrophilicity and structure, the data can be explained by an increased ability of hemicelluloses to form H-bonds and adsorb water. Simultaneously, this result may indicate an increased pore size and increased pore number. For the fibers rich in xylan and mannan, the crystallinity index (CrI) also decreased significantly (40 and 37%) underlining a lower orientation of the polymer chains giving rise to an enhanced pore volume.

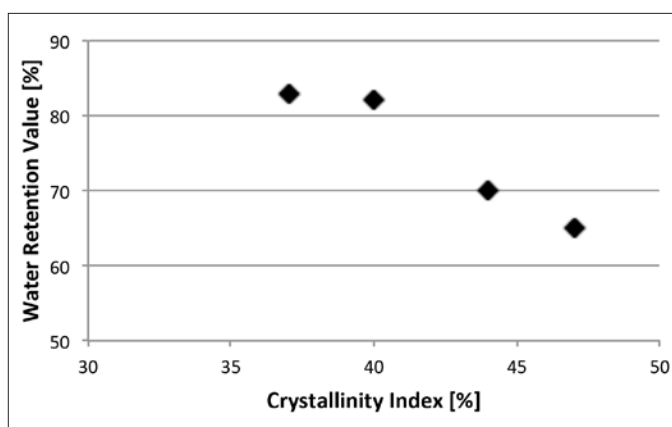


Figure 3 shows a linear correlation between CrI and WRV of different lyocell fibers types with different titers (1.3 and 1.8dtex) and different hemicellulose content. Based on the results in the figure, it can be concluded that the crystallinity index and WRV are independent of titer or diameter of the final lyocell fiber in the context of these investigations.

**Figure 3:** Correlation between water retention values and crystallinity index of lyocell fibers with different titers and different hemicellulose content.

It is obvious that hemicelluloses interfere with the alignment of cellulose chains to form crystals. Due to their chemical structure, hemicelluloses cannot build crystals with cellulose although they have a high tendency to form hydrogen bonds. As a result, hemicelluloses build up discontinuities during fiber forming and disrupt crystallization of cellulose polymers. The same effect was described for xylan enriched fibers from the Ioncell-F process using ionic liquids (Nypelö *et al.* 2018) and for viscose staple fibers after xylan addition (Singh and Murthy 2017; Schild and Liftinger 2014b).

Revisiting the data presented in tab. 2, the xylan content of the fibers was lower than that of the market pulps. As a matter of fact, 78% of the original xylan content of market pulp A was preserved in the fiber, compared to a preservation of 82% of the original xylan content in market pulp B. Only a relative yield can be determined because the total polymer yield physically cannot be measured in mill scale production. In contrast, 93% of the original content of the mannan was preserved for market pulp B, which indicated that mannan was more stable in the lyocell process and/or mannan was more easily incorporated in the fiber when compared to xylan. Thus, it can be concluded

that the stability of the woody carbohydrates in NMMO under alkaline mill conditions were in the following order: cellulose > mannan > xylan. It should however be noted that xylan and xylan degradation products may end up partly in the spinning bath and other process streams.

#### **Fluorescent staining and enzymatic peeling**

The WRV and CrI give an average value over the whole fiber cross section and do not differentiate between the different fiber layers. For this reason, fluorescent staining and enzymatic peeling were chosen to elucidate the structure of the cross sectional area.

During fluorescent staining, coloring is restricted to areas with larger pore volumes due to the large size of the fluorescent dye molecules. The intensity of the color results in optical indications concerning the number of pores and voids, their size as well as the chemical bonding of the dye molecules to the inner surface of the fiber pores. Chemical bonding is mainly attributed to hemicelluloses and non-crystalline cellulosic regions. In Figure 4, a comparison is made between a hemicellulose rich fiber B, a standard lyocell fiber A and a standard viscose fiber C, accompanied with schematic drawings of their dye uptake.

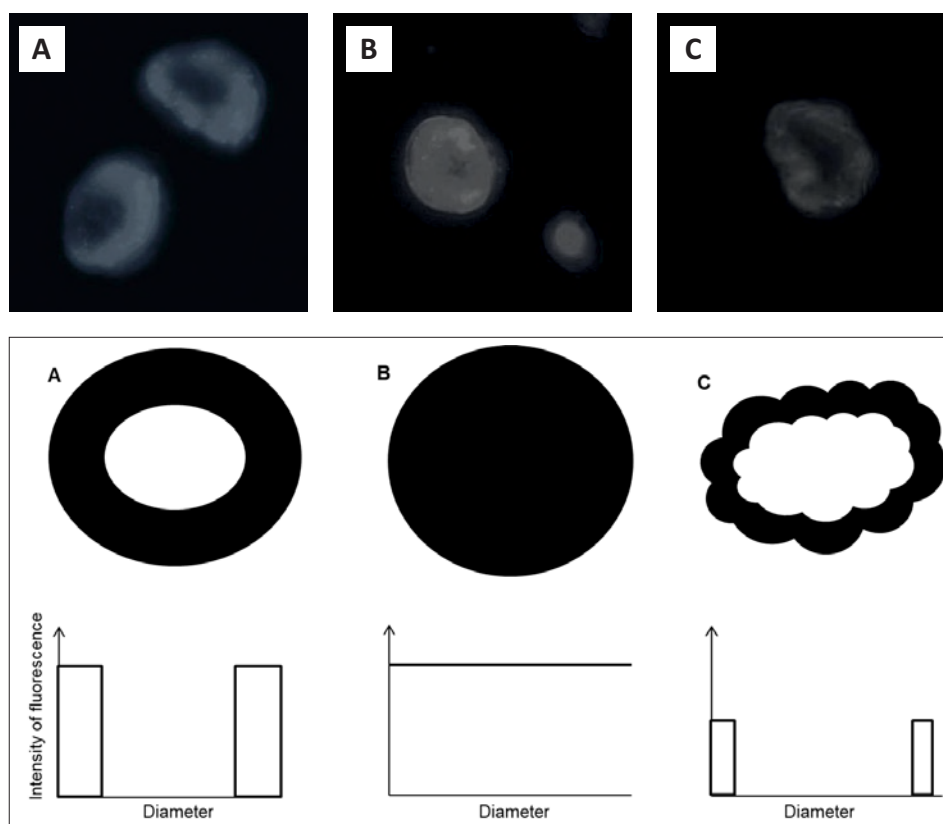


**Figure 4:** Fibers after fluorescent staining at maximum dye uptake, microscopic pictures as well as schematic drawings of the intensity and location of the staining: standard lyocell fiber (A), hemicellulose rich lyocell fiber (B), standard viscose fiber (C).

The standard lyocell fiber A reacted at mean velocity and the reaction was limited to the skin and middle layer, and yet resulted with the same deep coloring as that of the hemicellulose rich lyocell fiber B. In contrast, the viscose fiber C was only lightly stained at the outer regions of the shell which was even smaller than the colored region of the standard lyocell fiber A. It was also noted that the dye uptake was very slow and ceased after 3 hours. These results were in good accordance with those published by *Abu-Rous et al. (2007 and 2006b)*.

The mannan and xylan rich lyocell fiber showed a fast, intensive and complete staining of the entire cross section of the fiber (fig. 4, fiber B). The fiber was more easily penetrated by the dye, indicating increased accessibility due to larger pore sizes, increased pore numbers, a lower crystallinity and a higher hemicellulose content over the whole fiber cross section. As a result, skin, middle and core layers could not be differentiated and the compact and un-colored core of the conventional lyocell fiber was no longer visible (compare fig. 4, fiber A and C). The layers described in the literature were resolved. As expected, the precipitation of the spinning dope in the spinning bath slowed down due to the higher mannan and xylan content. This led to a completely different structure of the inner layers and the fiber cross section of the hemicellulose rich fiber appeared to be more homogenous.

The lyocell fibers were subjected to an enzymatic peeling test. For comparison, a viscose fiber with an enhanced xylan content of 7.5% from the paper by *Schild and Liftingner (2014)* was selected because the xylan content was close to the hemicellulose content of the hemicellulose enriched lyocell fiber of this study (6.8%). The test elucidates the xylan distribution over the cross section of fibers including information relating to different densities and structures of layers as denser layers show a slower response. These layers have smaller pore sizes and higher crystallinity.

At the very beginning, during the first 60min, the peeling rates for all tested fibers were comparable in velocity. The standard lyocell fibers (fiber A 1.3) slowed down after about 1500min as well as the xylan enriched viscose fibers after about 500 min of reaction time (fig. 5). This deviating effect compared to the hemicellulose rich lyocell fiber (fiber B 1.3) was even more pronounced for prolonged peeling times. The enzyme mixture contained different cellulases and xylanase aiming to completely degrade the fibers. Additionally, no inhibitors like lignin were present. Therefore, the material itself was not

restricting to the peeling reaction. Obviously, the structure of the fibers was the most important parameter, taking into consideration the distribution of the different polymers in the ordered and unordered regions as well as pore shape and volume. It is well known that enzymes first attack amorphous and less ordered areas of the material which explains the different behavior of the two lyocell fibers in this study. The hemicellulose enriched lyocell fiber (fiber B 1.3) was degraded at almost constant velocity rate which correlated well to the homogeneous structure of the fiber cross section. The results from enzymatic peeling tests indicated that hemicelluloses were evenly spread over the cross section. They underline an even distribution of pore volumes and size as well as crystallinity. At the same time, the standard lyocell fiber had low accessibility for the enzymes after about 40% mass loss. This can be attributed to the denser core and higher crystallinity of standard fibers.

Nevertheless, viscose fibers should be degraded more rapidly because they have a lower crystallinity index of about 30% compared to lyocell fibers with 40% or more. In addition to the above, the amorphous regions of viscose fibers depict a lower orientation compared to lyocell fibers and a faster degradation would be expected. However this was not the case. After 24h (1440min) the xylan rich viscose fiber showed only a mass loss of 30% while the xylan rich lyocell fiber showed a mass loss of close to 60%. Evidently, the core-shell structure of the viscose fibers was dominating the degradation process. It can therefore be concluded that a denser skin structure and a core with smaller pores hindered the attack of the enzymes. This was the same effect that was observed during the staining of the fibers.

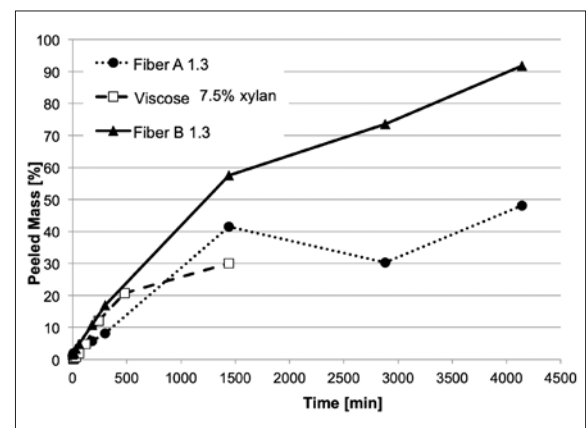


**Figure 5:** Velocity of enzymatic peeling for the lyocell fiber B with increased hemicellulose content compared to a standard lyocell fiber A and a xylan enriched viscose fiber (data from *Schild and Liftingner (2014)*) with a titer of 1.3dte.

When comparing the xylan loss to the loss in total mass, the hemicellulose enriched lyocell fiber showed an even distribution of the xylan content over the entire cross section (fig. 6) while the standard lyocell fiber featured only a low xylan concentration with a sharp increase in the outermost region. For viscose fibers, even a segregation of xylan and cellulose was reported (Schild and Liftinger 2014b). These viscose fibers clearly exhibited a decrease in xylan concentration towards the core.

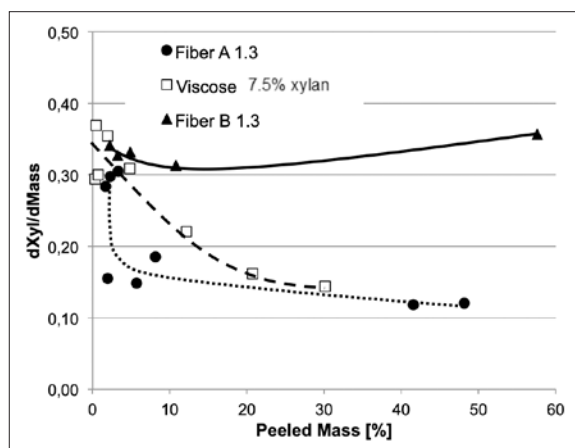


**Figure 6:** Xylan concentration over the fiber cross section of the lyocell fiber B with increased hemicellulose content compared to a standard lyocell fiber A and a xylan enriched viscose fiber (data from Schild and Liftinger (2014)) with a titer of 1.3dtex.

Nevertheless, the results only describe the xylan distribution and the enzyme mixture applied contained only very small amounts of mannanase. From the study conducted, it was observed that mannan was preserved in the lyocell fibers with increasing hemicellulose content during testing. Thus, the peeling results are only valid for the distribution of xylan.

From enzymatic peeling and fluorescent staining, it can be concluded that the structure of the hemicellu-

lose rich lyocell fibers was completely different to conventional lyocell and viscose fibers. The fiber cross section was more homogeneous and showed a higher porosity with a more even distribution of xylan. Standard regenerated cellulosic fibers from both the viscose and lyocell processes have always been described as being built up by layers in a core-shell structure. In an effort to confirm these results, Nypelö *et al.* (2018) recently observed a homogenous cross section lacking a core-shell structure for regenerated cellulosic fibers from the IONCEL-F process when adding xylan and/or lignin.

## Mechanical properties

The tensile strength decreased when pulp with a high hemicellulose content was used (tab. 3). The difference of 5.8cN/dtex for a titer of 1.3dtex and 4.0cN/tex for a titer of 1.8dtex was deemed as significant abliet that the data was at a high level known for lyocell fibers - 30.9cN/dtex for a titer of 1.3dtex and 28.1cN/dtex for a titer of 1.8dtex. These findings match exactly with the literature published by Nypelö *et al.* (2018) and Ma *et al.* (2017b). Nypelö *et al.* (2018) correlated the strength reduction with the lower cellulose content claiming that the lower cellulose content lead to a decrease in polymer orientation and therefore a loss in strength. At the same time, the authors described the elongation of the lyocell fibers as almost constant, using a lyocell process with an ionic liquid as the solvent.

Within the range of this study, the hemicellulose content slightly lowered the fiber elasticity, decreasing to about 89% of the value for lyocell fibers with low hemicellulose content after the lyocell process using NMMO.

Sample	Sum of hemicelluloses [%]	Titer [dtex]	Tensile strength [cN/tex]	Elongation [%]
Fiber A 1.3	2.1	1.3	36.1	13.5
Fiber B 1.3	12.5	1.3	30.9	12.1
Fiber A 1.8	2.3	1.8	32.1	12.9
Fiber B 1.8	12.6	1.8	28.1	11.5

**Table 3:** Mechanical properties of hemicellulose rich lyocell fibers compared to standard lyocell fibers.

## Conclusion

The structure of the cross section of lyocell fibers was altered successfully by selecting a softwood kraft pulp with a higher content of mannan and xylan. A lyocell fiber with lower crystallinity, larger pore size and an even distribution of the hemicelluloses was produced for the first time on a mill scale. A homogeneous cross sectional area was achieved with only minor deterioration of the mechanical properties. Knowing these potential impacts, suitable raw material selection and process optimization could overcome this issue.

Raw materials with additional natural wood polymers like hemicelluloses could be a key to designing lyocell fibers with altered properties that could break into new markets. Using additional hemicelluloses without removing them from the wood by means of pulping and/or bleaching is an important eco-credential and an important contribution to economic success. Softwood pulps could be favored as a raw material for this new type of fiber because their hemicelluloses are composed of xylan and mannan and in this study, it was found that the latter was more stable in the lyocell process, and more easily incorporated into the fiber.

## Literature

1. Abu-Rous M, Varga K, Bechtold T, Schuster K C (2007): A new method to visualize and characterize the pore structure of Tencel (Lyocell) and other man-made cellulosic fibers using a fluorescent dye molecular probe. *J Appl Polym Sci* 106:2083-2091.
2. Abu-Rous M, Ingolic E, Schuster K C (2006a): Visualisation of the fibrillary and pore morphology of cellulosic fibres applying transmission electron microscopy. *Cellulose* 13:411-419.
3. Abu-Rous M, Ingolic E, Schuster K C (2006b): Visualisation of the nano-structure of TENCEL® (Lyocell) and other cellulosics as an approach to explaining functional and wellness properties in textiles. *Lenzinger Berichte* 85:31-37.
4. Biganska O, Navard P (2009): Morphology of cellulose objects regenerated from cellulose-N-methylmorpholine N-oxide-water solutions. *Cellulose* 16:179-188.
5. Biganska O (2002): Etude physico-chimique des solutions de cellulose dans la N-Methylmorpholine-N-Oxyde. PhD Thesis, Ecole Nationale des Mines de Paris, France.
6. Chen J-H, Wang K, Xu F, Sun R (2015): Properties of regenerated bamboo fibers prepared from raw materials with different hemicellulose content. Abstracts of Papers, 249th ACS National Meeting & Exposition, Denver, CO, United States, March 22-26.
7. Fink H-P, Weigel P, Ganster J, Rihm R, Puls J, Sixta H and Parajo JC (2004): Evaluation of new organosolv dissolving pulp. Part II: Structure and NMMO processability of the pulps. *Cellulose* 11:85-98.
8. Ma Y, Stubb J, Kontro I, Nieminen K, Hummel M, Sixta H (2018): Filament spinning of unbleached birch kraft pulps: Effect of pulping intensity on the processability and the fiber properties. *Carb Polym* 179:145-151.
9. Ma Y, Hummel M, Kontro I, Sixta H (2017): High performance man-made cellulosic fibres from recycled newsprint. *Green Chem* DOI: 10.1039/c7gc02896b.
10. Nypelö T, Asaadi S, Kneidinger G, Sixta H, Konnerth J (2018): Conversion of wood-biopolymers into microfibrils with tunable surface energy via dry-jet wet-spinning. *Cellulose* 25:5297-5307.
11. Röder T, Moosbauer J, Fasching M, Bohn A, Fink H-P, Baldinger T, Sixta H (2006): Crystallinity determination of native cellulose—comparison of analytical methods. *Lenzinger Berichte* 86:85–89.
12. Schild G, Borgards A, Sixta H (2014a): Verfahren zur Herstellung eines cellulosischen Formkörpers. WO2014086883.
13. Schild G, Liftinger E (2014b): Xylan enriched viscose fibers. *Cellulose* 21:3031–3039.
14. Singh C S, Murthy Z V P (2017): Study of cellulosic fibres morphological features and their modifications using hemicelluloses. *Cellulose* 24:3119-3130.
15. Sixta H, Schelosky N, Milacher W, Baldinger T, Röder T (2001): Characterization of alkali-soluble pulp fractions by chromatography. In: Proceedings of the 11th ISWPC, Nice, France. pp 655–658.
16. Sjöberg J, Potthast A, Rosenau T, Kosma P, Sixta H (2005): Cross-sectional analysis of the polysaccharide composition in cellulosic fiber materials by enzymatic peeling/highperformance capillary zone electrophoresis. *Biomacromolecules* 6:3146–3151.
17. Wendler F, Persin Z, Stana-Kleinschek K, Reischl M, Ribitsch V, Bohn A, Fink H-P, Meister F (2011): Morphology of polysaccharide blend

fibers shaped from NaOH, N-methylmorpholine-N-oxide and 1-ethyl-3-methylimidazolium acetate. *Cellulose* 18:1165-1178.

18. Zhang H, Tong M (2007): Influence of Hemicelluloses on the Structure and Properties of Lyocell Fibers. *Polym Eng Sci* 47:702-706.
19. Zhang H, Zhang H, Tong M, Shao H and Hu X (2008): Comparison of the Structure and Properties of Lyocell Fibers from High Hemicellulose Pulp and High –Cellulose Pulp. *J of Appl Polym Sci* 107:636-641.



# Processing of metal sulfide/cellulose nanocomposite fibers in *core-shell* configuration

Michael Weißl<sup>1</sup>, Mike Pelzmann<sup>1</sup>, Armin Zankel<sup>2</sup>, Brigitte Bitschnau<sup>3</sup>, Helmar Wiltzsche<sup>4</sup>, Gregor Trimmel<sup>5</sup>, and Stefan Spirk<sup>1\*</sup>

<sup>1</sup> Institute of Paper, Pulp and Fiber Technology, Graz University of Technology, Inffeldgasse 23, A8010 Graz, Austria

<sup>2</sup> Institute of Electron Microscopy and Nanoanalysis, NAWI Graz, Graz University of Technology and Centre for Electron Microscopy Graz, Steyrergasse 17, A-8010 Graz, Austria

<sup>3</sup> Institute of Physical and Theoretical Chemistry, Graz University of Technology, Stremayrgasse 9, A8010 Graz, Austria

<sup>4</sup> Institute of Analytical Chemistry and Food Chemistry, Graz University of Technology, Stremayrgasse 9, A8010 Graz, Austria

<sup>5</sup> Institute for Chemistry and Technology of Materials, Graz University of Technology, Stremayrgasse 9, A8010 Graz, Austria

Correspondence: Stefan Spirk, stefan.spirk@tugraz.at, +43 (316) 873 – 30763

## Abstract

This work describes a simple and straightforward processing of *core-shell* structured nanocomposite fibers, consisting of a metal sulfide shell and a viscose fiber core. The metal sulfide shell forms by the addition of the corresponding metal salt precursor into the sulfuric acid regeneration bath; any further reactants are not needed. A reaction of the dissolved metal cations (Ag, Cu, Sn) with sulfur sources present in the viscose spinning dope leads to the formation of (nano)crystalline metal sulfide particles (CuS, Ag<sub>2</sub>S, SnS) on the viscose fibers. The metal loading on the fibers and the thickness of the formed shell depends on the type of precursor salt and concentration and can reach up to 10 wt% under the chosen conditions. The formation of metal sulfides exclusively takes place on the fiber surface and some metal sulfides (CuS and Ag<sub>2</sub>S) unexpectedly come in phase pure configurations. The materials have been characterized by SEM (morphology), XRD (metal sulfide phase) and ICP-MS (amount of metal sulfide on fiber).

**Keywords:** Cellulose xanthate, viscose process, metal sulfide, fiber functionalization, core-shell structure, nanocomposite, hybrid material

## Introduction

The basic idea behind the viscose process is to convert cellulose into a soluble derivative that can be processed and shaped into fibers or films. The conversion to a soluble precursor proceeds via the formation of alkali cellulose which is then reacted with CS<sub>2</sub> to give cellulose xanthate (CX). The properties of the resulting CX dope are adjusted by the ripening procedure which exploits reactivity differences of the hydroxyl groups leading to favored xanthate substitution at the C6 position in an industrial context.<sup>1,2</sup>

However, the reaction of the alkali cellulose and CS<sub>2</sub> is not straightforward. A wealth of other reaction products are formed as well, which comprise sulfur containing species such as sulfides, thiolates and thio-carbonates.<sup>3-5</sup> In the course of the spinning procedure into sulfuric acid, these species decompose to give, among others, H<sub>2</sub>S, CS<sub>2</sub>, and Na<sub>2</sub>SO<sub>4</sub> while converting the CX to a cellulose fiber or film. The properties of the obtained cellulose fibers can be further tuned by either incorporating additional functionality into the

CX dope or by post-treatment of the fibers.<sup>6,7</sup> Crosslinking, hydrophobization, amination or physicochemical deposition of functional molecules and inorganic particles are common routes to extend the application range of fibers.<sup>8</sup> Such fibers often carry inorganic nanoparticles with antibacterial (e.g., Ag, Cu), magnetic (e.g., Fe<sub>2</sub>O<sub>3</sub>) or self-cleaning properties (e.g., TiO<sub>2</sub>) for instance.<sup>7,9,10</sup> One class of inorganic nanoparticles that has not been extensively investigated in this context are metal sulfides. Metal sulfides find applications in various fields. For instance, some metal sulfides (e.g. Bi<sub>2</sub>S<sub>3</sub>, CuInS<sub>2</sub>) have a narrow band gap, i.e. they can generate a current when they are exposed to light.<sup>11,12</sup> This can be exploited in thin film solar cells and optoelectronics for instance.<sup>13-15</sup> As a consequence of the low HOMO-LUMO gap, metal sulfides are also employed in photocatalysis (e.g., Ag<sub>2</sub>S for hydrogen production or degradation of organic pollutants).<sup>16,17</sup> Fluorescence is another feature of many metal sulfides (e.g. ZnS, CdS) that can be used in quantum dot based sensing applications.<sup>18,19</sup> Some sulfides (Li<sub>2</sub>S, Na<sub>2</sub>S) in turn are used as active electrode material in batteries and energy storage systems<sup>20</sup> while antibacterial properties are provided by Ag<sub>2</sub>S and CuS.<sup>21</sup> CuS and SnS are further used in lubricants and friction stabilizers, for instance in braking systems in automotive industry. There, the metal sulfides provide high durability, prevent break fading and produce only a limited amount of rim dust.<sup>22,23</sup> While for many nanoparticles it is rather simple to deposit them on cellulosic materials, for the metal sulfides the preparation is a challenge since most manufacturing methods require elevated temperatures (>200°C) to generate these.<sup>24</sup> However, most metal ions form binary as well as complex sulfides when they come in contact with sulfur containing anions (e.g. S<sup>2-</sup>, CS<sub>3</sub><sup>2-</sup>) in aqueous solution. The tendency to form sulfides is the more pronounced, the softer the character of the metal ion is according to the HSAB concept.<sup>25</sup> In general, metal sulfides decompose under strongly acidic conditions to the corresponding metal sulfate and SO<sub>2</sub>.<sup>26</sup> The decomposition depends on the temperature and the type and molarity of the used acid. Further, the solubility of the metal sulfide under the chosen conditions determines whether the process

proceeds fast or rather slow since decomposition is limited by mass transport into the acidic solution.<sup>27</sup> Here, we aim at exploiting the sulfur containing reaction products in the viscose dope to serve as a sulfur source in the generation of metal sulfides in the presence of metal cations during the regeneration process. For the proof of principle, we selected three metal ions of different softness according to the HSAB concept (Ag: soft, Cu: intermediate, Sn: hard) and study their influence on sulfide formation on the viscose fiber *in situ*.

## Experimental Part

### Materials and fiber processing

CuCl<sub>2</sub> and SnCl<sub>2</sub> were purchased from Aldrich, and AgNO<sub>3</sub> was obtained from Roth. Deionized water was obtained from an Elga PURELAB Prima (Bucks, United Kingdom) water treatment system. Lenzing AG (Lenzing, Austria) kindly provided a cellulose xanthate (CX) spinning dope with 10% cellulose content, 6% NaOH, a gamma number of 52 and a DP of 550, which was used as stock solution. The stock solution was diluted with water (1:2 w/w), vigorously shaken on a vortex and evaporated for at least 20 minutes in a desiccator before fiber spinning. The dope was injected into a 15% sulfuric acid (VWR chemicals, v/v) bath through two injection needles (diameter 450 μm) with a speed of 1.2 m/min and collected on a rotating polypropylene (PP) cylinder (v = 8 m/min) on the opposite direction of the regeneration bath. After injecting the viscose solution completely, the fibers were rotated in the acid bath for additional 15 minutes. After spinning, the fibers were cut from the PP role and washed two times in water for 15 minutes each. The fibers were dried overnight at room temperature under ambient conditions. The core-shell formation of a metal sulfide layer on a viscose fiber filament was realized by addition of metal salts (CuCl<sub>2</sub>: 2.5, 5.0, 10 g/L spinning bath, SnCl<sub>2</sub>: 5.0 g/L spinning bath, AgNO<sub>3</sub>: 5.0 g/L spinning bath) into the regeneration bath and injecting the spinning dope as described (Table 1).

Spinning bath additive	Concentration [g/L]	Concentration [mM]
CuCl <sub>2</sub>	2.5	26
CuCl <sub>2</sub>	5.0	52
CuCl <sub>2</sub>	10.0	104
AgNO <sub>3</sub>	5.0	16
SnCl <sub>2</sub>	5.0	15

**Table 1.** Overview on type and amount of added metal salts to the spinning bath

The setup is shown in Figure 1 at the example of  $\text{CuCl}_2$  as spinning bath additive. Finally, the fibers are collected on a rotating PP cylinder.

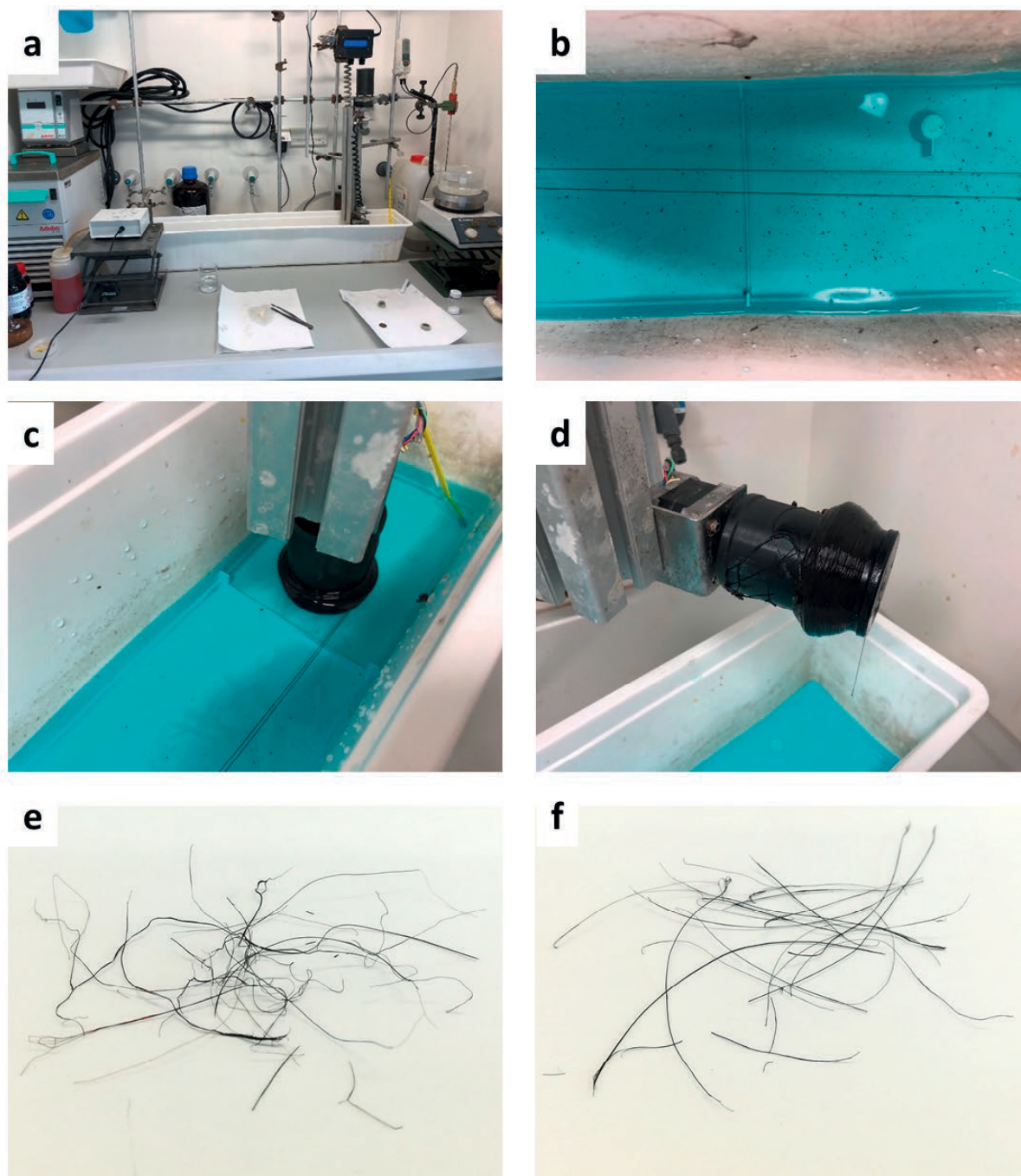


**Figure 1.** Manufacturing of CuS coated viscose fibers a) lab scale fiber spinning equipment b) development of a CuS layer on the regenerating fibers in the spinning bath ( $c=10$  g/L), c) collecting the CuS fibers at the end of the spinning bath d) CuS coated fibers after removal from the spinning bath e/f) CuS coated fiber after washing and drying (26 and 104 mM  $\text{CuCl}_2$ ).

### Attenuated total reflection: infrared spectroscopy (ATR-IR)

The infrared spectra were recorded with an ALPHA FT-IR spectrometer (Bruker; Billerica, MA, U.S.A.). For the measurement, an attenuated total reflection (ATR) attachment was used with 64 scans at a resolution of  $4\text{ cm}^{-1}$  and a scan range between  $4000$  and  $400\text{ cm}^{-1}$ . The samples were prepared on Au-coated glass slides (SPR102-AU). The data were analyzed with OPUS 4.0 software.

### Scanning electron microscopy (SEM)

The fibers were imaged in the low vacuum mode of the environmental scanning electron microscope ESEM Quanta 600 FEG equipped with a Schottky emitter (FEI, Eindhoven, The Netherlands). In this mode it is possible to investigate electrically non-conductive specimens at conventional electron energies without additional coating like carbon or gold. An acceleration of voltage of  $7\text{ kV}$  was applied to the primary electrons and water vapor was used as imaging gas. In order to get topographic contrast, the large field detector (LFD, dedicated SE detector of the low vacuum mode) was used for the detection of secondary electrons (SE). At each position synchronously, an image with backscattered electrons (BSE) was recorded in order to get material contrast (Z-contrast; i.e. the higher the atomic number  $Z$  of the material the brighter the imaged region).

### Inductively coupled plasma – optical emission spectroscopy (ICP-OES)

$100\text{ mg}$  sample were dissolved in a mixture of  $4\text{ ml HNO}_3$  and  $1\text{ ml HCl}$  under microwave assistance at  $40\text{ bar}$  and  $230^\circ\text{C}$  (Multiwave 3000, Anton Paar; HF-Vials). After dissolution and restocking to a total volume of  $50\text{ ml}$  quantification with ICP-OES (Spectro Ciros Vision EOP;  $1350\text{ W}$  RF power;  $0.6\text{ L/min}$  assist gas;  $12\text{ L/min}$  cool gas;  $0.83\text{ L/min}$  nebulizer gas, Cross-flow nebulizer in Scott- spray chamber) was carried out. Calibration was done with 5-points between  $0,04$  and  $4\text{ mg/L}$  with a Roth 28 elements standard; Sc was used as internal standard ( $1\text{ mg/L}$ ).

### X-ray powder diffraction (XRPD)

The samples were analyzed by powder X-ray diffraction using a Bruker D8 Advance diffractometer (Bragg Brentano geometry,  $\text{CuK}\alpha$  radiation) with LynxEye Detector. Patterns were recorded with a step size of  $0.02^\circ$  in the  $2\theta$ -range  $10^\circ$  to  $100^\circ$ ,  $2\text{ s}$  per step. Rietveld refinement was carried out using X'PertHigh-ScorePlus (Panalytical).

## Results and discussion

We used a simplified setup for the fiber spinning experiments, with a syringe pump operating at  $1.2\text{ m/min}$ , spinning nozzles (diameter  $450\text{ }\mu\text{m}$ ), a regeneration bath ( $15\%\text{ H}_2\text{SO}_4$ ) and a cylinder to collect the fibers. White cellulose fibers with an average diameter of  $50\text{ microns}$  were obtained after washing them in hot water and subsequent drying.

The addition of metal salts ( $\text{CuCl}_2$ ,  $\text{SnCl}_2$ ,  $\text{AgNO}_3$ ) to the regeneration bath led to strong coloration of the formed fibers directly after injection of the CX. The resulting fibers featured a brownish to black color, which can be associated to the respective metal sulfides (Figure 1 e,f). Extensive washing of the fibers even at elevated temperatures ( $60^\circ\text{C}$ ) did not lead to any leaching or decoloration of fibers, i.e. the metal sulfides irreversibly stick to the cellulose surface. The fiber diameter for all the samples was between  $45$  and  $55\text{ }\mu\text{m}$  as determined by optical microscopy.

The amount of the deposited metals was determined using ICP-OES. Table 2 shows how the different metal concentrations influence the amount of metal sulfide on the surface. The increase in copper chloride concentration from  $26$  to  $104\text{ mmol/L}$  in the spinning bath led only to a doubling of the deposited copper on the fiber surface ( $0.47$  vs  $1.05\text{ mmol Cu/g}$  fiber).

The use of a softer metal ion according to the HSAB concept (i.e.  $\text{Ag}^+$ ) led to a much higher deposition on the fiber ( $0.64\text{ mmol/g}$ ) at much lower metal salt concentration in the spinning bath, while in the

	Ag [mmol/g]	Cu [mmol/g]	Sn [mmol/g]
No salt added	< LOQ	< LOQ	< LOQ
$\text{CuCl}_2$ (26 mM)	< LOQ	$0.47\pm 0.01$	< LOQ
$\text{CuCl}_2$ (52 mM)	< LOQ	$0.55\pm 0.02$	< LOQ
$\text{CuCl}_2$ (104 mM)	< LOQ	$1.05\pm 0.05$	< LOQ
$\text{AgNO}_3$ (16 mM)	$0.64\pm 0.01$	< LOQ	< LOQ
$\text{SnCl}_2$ (15 mM)	< LOQ	< LOQ	$0.23\pm 0.02$

**Table 2.** Influence of metal salt concentration (mmol/L) in the spinning bath on the amount of deposited metal on the fiber (mmol metal/g fiber). LOQ: limit of quantification.

case of a harder ion (i.e. Sn) deposition was lower (0.22 mmol/g at 16 mM SnCl<sub>2</sub> concentration in the spinning bath).

XRD was used to elucidate the type of material that was created on the surface. It also allows for distinguishing between different polymorphs of the same compound. This is important since copper and silver sulfide come in various polymorphs, if they are synthesized by non-specific procedures.<sup>21,24,28-30</sup> The XRD patterns confirmed that for silver and copper the corresponding sulfides have been exclusively formed (Figure 2). Additionally, they appear in a phase pure form (CuS: covellite, Ag<sub>2</sub>S: acanthite) as the diffraction pattern perfectly matches those of the reported ones for these polymorphs. The XRD patterns also showed that the crystals are smaller in the case of the CuS compared to the Ag<sub>2</sub>S (ca 20 vs 35 nm, calculated by the Scherrer equation). In the case of tin, XRD revealed that a mixture of different sulfur containing salts is present consisting of 66% orthorhombic and 10% cubic tin sulfide as well as 24% tin sulfate, the hydrolysis product of the sulfide.

SEM provided morphological information about the crystalline structures developing on the fiber surface during the regeneration procedure. The amount of crystallites visible on the fiber surface depends on the amount of the metal salt concentration in the spinning bath. The shell becomes thickest at the highest used CuCl<sub>2</sub> concentration. High concentrations of CuCl<sub>2</sub> (52 and 104 mM) in the spinning bath result in full coverage of the fibers (Figure 3ab). The lowest concentration of CuCl<sub>2</sub> (26 mM) in the regeneration bath does not lead to complete coverage of the fiber surface (Figure 3c). The morphology of the CuS particles is disk-like and comparable to literature reports on covellite (Fig. 3c).<sup>28</sup> The reference fibers spun in the absence of any metal cations possess a smooth and regular fiber surface with an obviously dense and closed structure (Figure 3d). The cross sectional analysis further confirms that the metals sulfides are only present at the surface of the fibers, forming a shell, while in the bulk of the fiber no CuS was detected. For SnCl<sub>2</sub> as additive, particles with different shapes are present in the fibers surface (Fig. 3e) which can be assigned to the different tin sulfide phases and the formed SnSO<sub>4</sub>. The deposited materials do not form continuous layers on the fiber surface and inhomogeneous spots are present on the fiber.

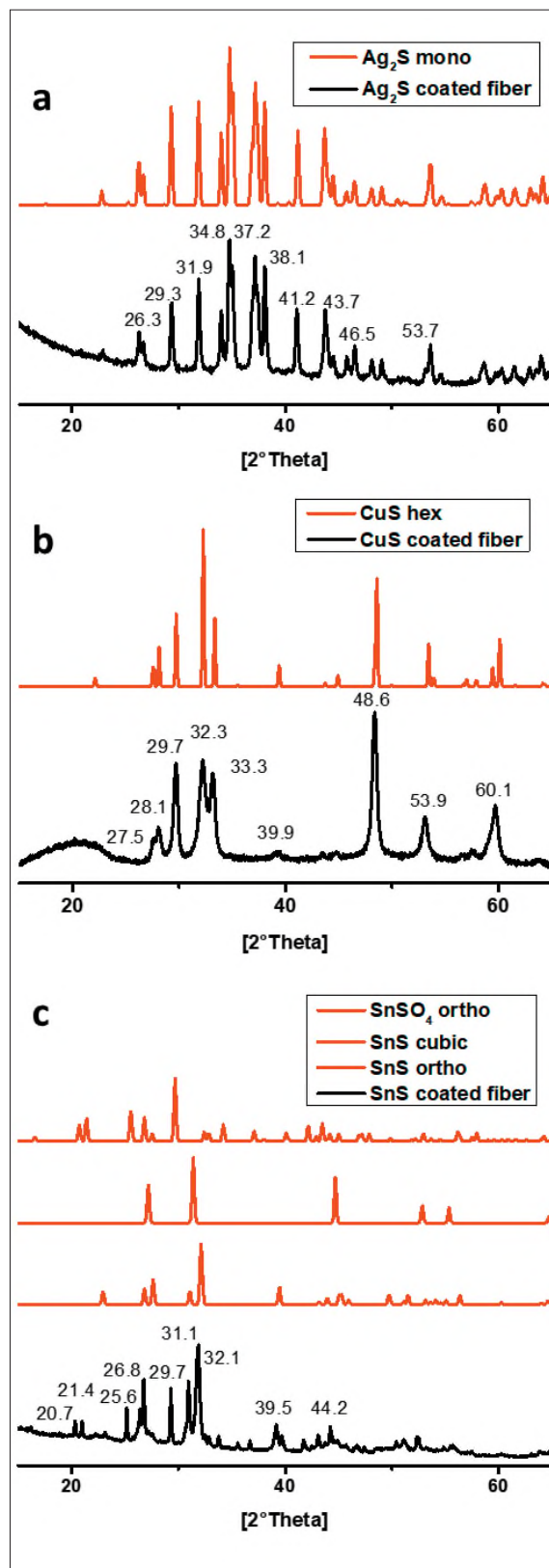


**Figure 2.** X-ray diffraction patterns of a) CuS coated fiber and CuS (hexagonal, 32106-ICSD) reference pattern b) Ag<sub>2</sub>S coated fiber and Ag<sub>2</sub>S (monoclinic, 44507-ICSD) reference pattern c) SnS/SnSO<sub>4</sub> coated fiber and reference patterns of SnS (orthorhombic, 106028-ICSD; cubic, 651015-ICSD) and SnSO<sub>4</sub> (orthorhombic, 245904-ICSD)

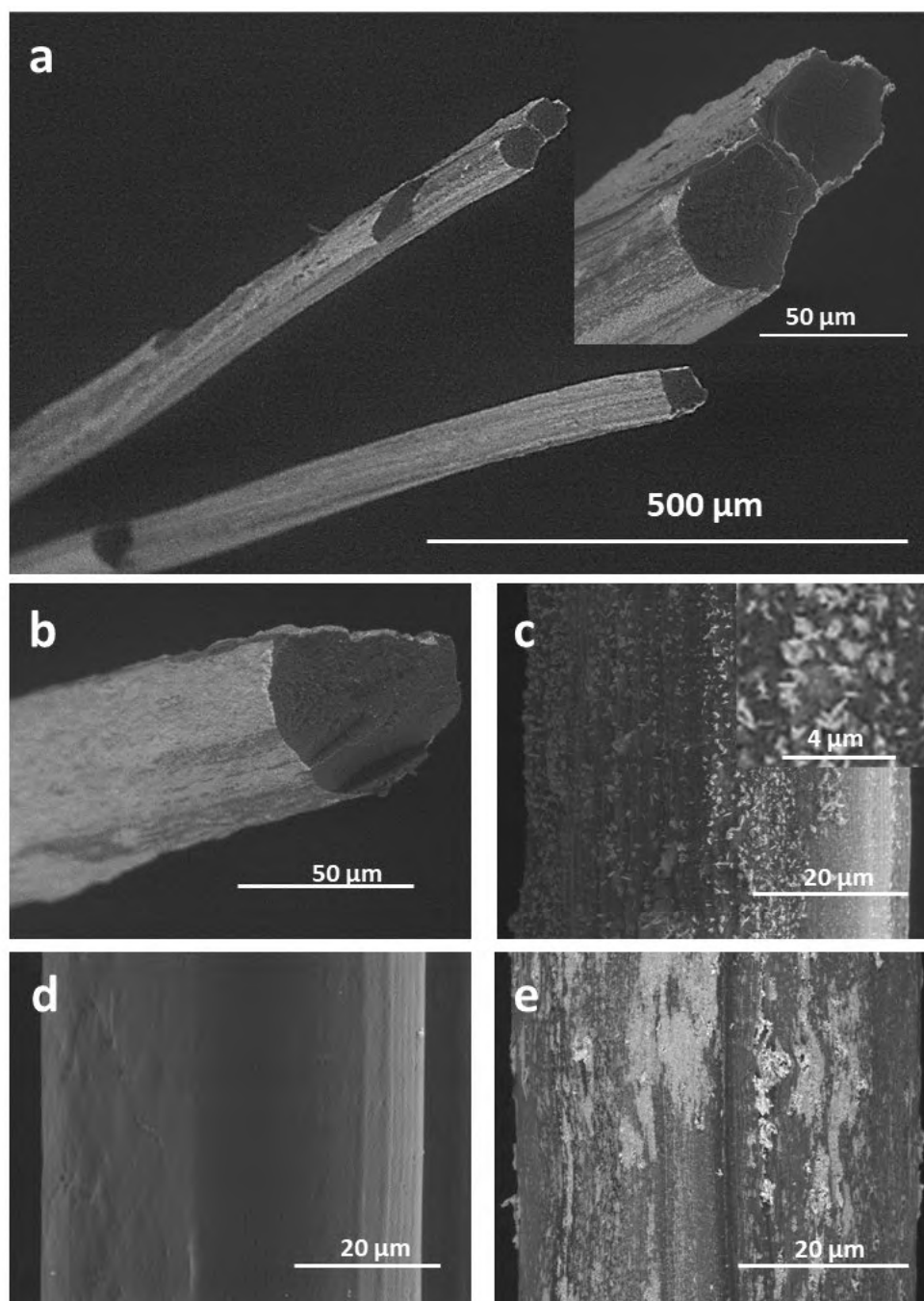


**Figure 3.** SEM surface and cross section images of a) Overview image of CuS coated fiber (104 mM) with an insert showing the core-shell structure b) CuS coated fiber (56 mM) with full coverage and any CuS particles in the fiber core, c) CuS coated fiber (26 mM CuCl<sub>2</sub>) with an insert showing the morphology of the CuS particles d) uncoated reference fiber e) SnS/SnSO<sub>4</sub> coated fiber (15 mM SnCl<sub>2</sub>)

The influence of the metal salts in the spinning bath on the regeneration process was investigated by ATR-IR spectroscopy. A comparison of the spectra of dry CX used as spinning dope, a spun fiber without metal salt additive in the spinning bath and one with CuCl<sub>2</sub> (104 mM) and AgNO<sub>3</sub> (15 mM) is shown in Figure 4. The spectrum of the dried CX is complex and consists of cellulose xanthate as well as of decomposition and side products present in the provided CX solution. As

dominating side products, sodium sulfide (intensive bands at 1420 and 920 cm<sup>-1</sup>), sodium trithiocarbonate (1670, 1427, 925 and 880 cm<sup>-1</sup>) and sodium hydroxide with intense bands at 1452 cm<sup>-1</sup> and 1380 cm<sup>-1</sup> could be identified.<sup>3-5</sup> The series of intense bands between 1200 and 950 cm<sup>-1</sup> can be assigned to the vibrations of the pyranose ring, overlapping with the C-S and C=S vibrations of the xanthate, reported in the same region.

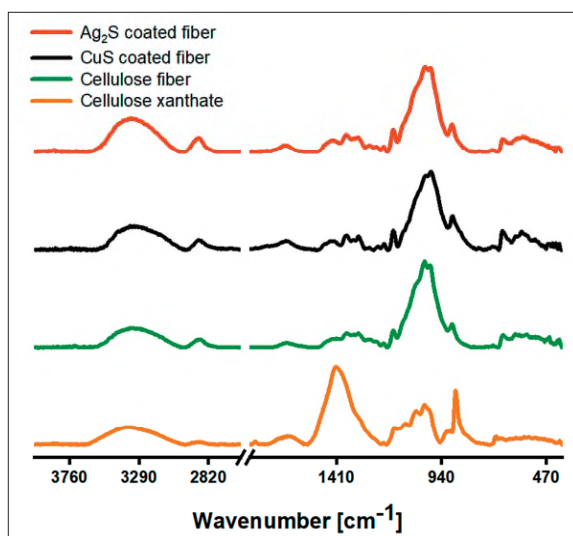


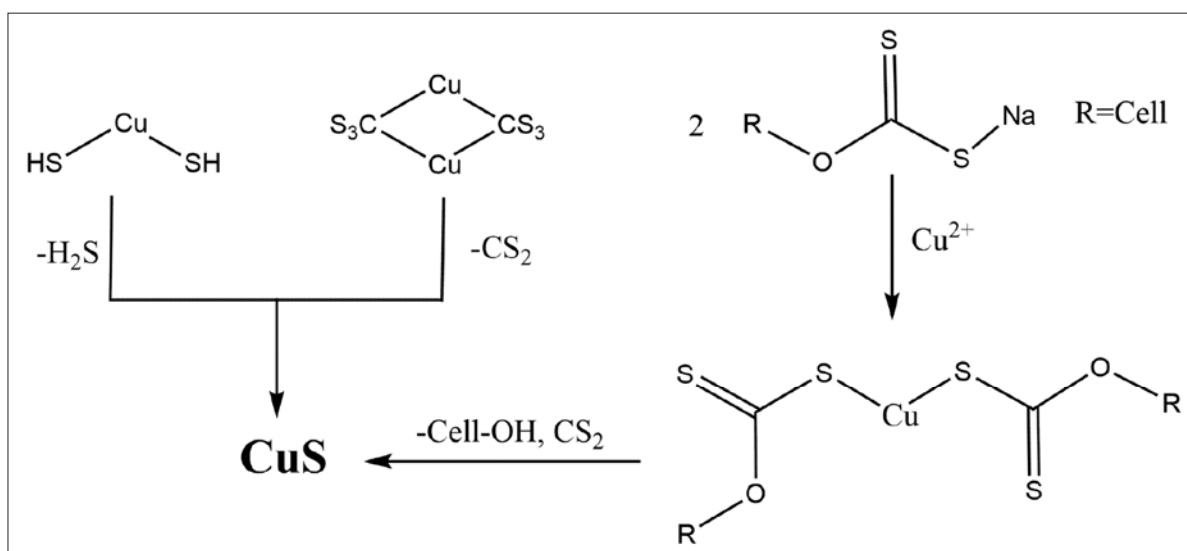
**Figure 4.** ATR-IR spectra of dried viscose (yellow), regenerated cellulose fiber as reference material (green), CuS (black) and Ag<sub>2</sub>S (red) coated fibers after spinning and washing

After fiber spinning and processing, the uncoated cellulose reference fibers display bands at 3600 to 3000 cm<sup>-1</sup> (OH vibration), at 2850 cm<sup>-1</sup> (CH vibration), a series of less intense bands from 1430 to 1180 cm<sup>-1</sup> (C-O-H bending at 1430 cm<sup>-1</sup>, C-H deformation at 1372 cm<sup>-1</sup>, OH in plane deformation at 1330 and at 1200 cm<sup>-1</sup>) and strong overlapping bands from 1150 to 950 cm<sup>-1</sup> (C-O-C vibration at 1155 cm<sup>-1</sup>, O vibration at 1060 cm<sup>-1</sup> and C-O stretching at 1035 cm<sup>-1</sup>) accompanied by a small band at 899 cm<sup>-1</sup> (C-O-C vibration at 1155 cm<sup>-1</sup>).<sup>31</sup> The bands described for the cellulose reference fibers are all related to cellulose II vibrations and hence confirm a full regeneration of the cellulose xanthate under the chosen conditions.<sup>32</sup> The

presence of different metal cations in the spinning bath does not impact the regeneration of cellulose xanthate to cellulose. Since the metal sulfides are not absorbing in the investigated area of the spectrum, identical spectra compared to the cellulose reference are obtained.

The IR spectra confirm the presence of several sulfur containing species in the CX. A complication is the hydrolytic sensitivity of metal sulfides under acidic conditions that leads to the corresponding sulfates and SO<sub>2</sub>. The tendency to hydrolyze increases with increasing hardness of the metal ion. This is observed in our case for Sn, which is considered hard according to the HSAB concept and which already shows significant amounts of tin sulfate on the surface of the fiber (24%, according to XRD). Further, the rate constants for the formation of the sulfides are in general higher for soft ions than for harder ones.<sup>33</sup> Also this behavior has been observed in our experiments, since even low amounts of silver in the spinning bath led to significant sulfide formation on the surface of the cellulose fibers, while comparable amounts of the harder tin yielded lower amounts.

The mechanism and the species which are responsible for the generation of the metal sulfide are challenging to reveal in detail. However, there are various plausible ways how the sulfides are formed during the processing step (Scheme 1). For instance, thiocarbonates (i.e. dithio- and trithiocarbonates) that are either present already in the CX or are formed during the spinning process can provide sulfur species for sulfide formation under formation of COS and CS<sub>2</sub>, respectively. Thiolates may provide sulfur by elimination of H<sub>2</sub>S in acidic medium to give the corresponding sulfide as well. Also cellulose sodium xanthate itself



**Scheme 1.** Formation of metal sulfides at the example of CuS, based on a reaction of the added metal cations with thiols, trithiocarbonates present as by products in viscose, or the cellulose xanthates itself.

is capable to act as sulfur source by exchange of the sodium by the metal ion as soon as the spinning dope comes into contact with the spinning bath. The formed metal-xanthate complex may decompose as in other cases to the metal sulfides and organic leaving groups, here cellulose.<sup>34</sup> Independent of the mechanism, the formation of the metal sulfides is diffusion controlled since the sulfides are only present on the fiber surface. So far it is unclear why CuS and Ag<sub>2</sub>S come phase pure when they are synthesized on the fibers. Particularly copper sulfides have a large variation of different phases, both copper and sulfur rich ones. Even for synthetic routes where mainly covellite is obtained usually other phases are present in minor amounts.<sup>28</sup> The same applies for Ag<sub>2</sub>S, where often sulfur rich phases are observed (typical ratio Ag:S= 1.92), particularly when particle size reaches the nanometer regime.<sup>30</sup>

## Conclusion

We presented a facile approach to produce metal sulfide decorated viscose fibers by addition of metal salts to the spinning bath. The amount of material on the fiber can be either tuned by the concentration as well as by the hard/softness of the metal ions. The procedure works best for soft ions since they feature higher affinity towards sulfide formation. Further, they show higher stability towards hydrolysis, the counter reaction that results in the formation of the corresponding sulfates and SO<sub>2</sub>, respectively, under the conditions present in the spinning bath. The mechanism for metal sulfide formation remains unclear so far. However, there are different options which species may provide the sulfur for the sulfide formation, which include thiolates, thiocarbonates and the xanthates. An intriguing observation was that CuS and Ag<sub>2</sub>S come in a phase pure form (covellite and acathite, respectively) which is an unexpected result given the wealth of known polymorphs, particularly for copper sulfide. This could be an advantage for future applications where phase pure covellite could be used in optoelectronic applications. However, the fiber properties (tensile strength, water uptake etc.) are of course influenced by the metal sulfide layer. Further, we did not investigate in detail how the presence of the employed metal salts in the spinning bath influences coagulation and regeneration of the fibers; this will be done in scale up experiments.

We just presented a part of our work on metal sulfide decoration of cellulose fibers produced via the viscose route. We have evidence that the procedure works for a wide range of metal ions, whereas soft metals pref-

erentially form sulfides on the fibers and survive the acidic conditions. Since metal sulfides have a large potential for various applications, such nanocomposites may serve as new interesting materials for advanced applications.<sup>35</sup>

## Acknowledgements

Lenzing AG is gratefully acknowledged for providing viscose spinning dope. Dr. Josef Innerlohinger, Dr. Thomas Röder (both Lenzing AG) and Dr Ingo Berndt are gratefully thanked for the fruitful discussion and their support. Chris Corner is acknowledged for inspiration during the writing of this paper.

## References

- (1) Götze, K. *Chemiefasern nach dem Viskoseverfahren*; 2nd ed.; Springer Verlag: Heidelberg, Germany, 1951.
- (2) Wöss, K.; Weber, H.; Grundnig, P.; Röder, T.; Weber, H. K. Rapid determination of  $\gamma$ -value and xanthate group distribution on viscose by liquid-state <sup>1</sup>H NMR spectroscopy. *Carbohydr. Polym.* **2016**, *141* (Supplement C), 184.
- (3) Andrews, D. A.; Hurtubise, F. G.; Krassig, H. The Presence of Monothiocarbonate Substituents in Cellulose Xanthates. *Can. J. Chem.* **1960**, *38* (8), 1381.
- (4) Dautzenberg, H.; Philipp, B. Über Bildungsweise und Verhalten des Natriumdithiocarbonats. *Z. Anorg. Allg. Chem.* **1970**, *375* (2), 113.
- (5) Ogura, K.; Sobue, H. Studies on the derivatives of sodium cellulose xanthate. Part I. Infrared absorption spectra and characteristic frequencies of C-S and C=S groups in sodium cellulose xanthate and its stable derivatives. *J. Polym. Sci., Part B: Polym. Lett.* **1968**, *6* (1), 63.
- (6) Weber, F.; Koller, G.; Schennach, R.; Bernt, I.; Eckhart, R. The surface charge of regenerated cellulose fibers. *Cellulose (Dordrecht, Neth.)* **2013**, *20* (6), 2719.
- (7) Malucelli, G. Surface-Engineered Fire Protective Coatings for Fabrics through Sol-Gel and Layer-by-Layer Methods: An Overview. *Coatings* **2016**, *6* (3).
- (8) Klemm, D.; Philip, B.; Heinze, T.; Heinze, U.; Wagenknecht, W. *Comprehensive Cellulose Chemistry, Volume 2: Derivatization of Cellulose*; Wiley, 1998.
- (9) Breitwieser, D.; Moghaddam, M. M.; Spirk, S.; Baghbanzadeh, M.; Pivec, T.; Fasl, H.; Ribitsch,



- V.; Kappe, C. O. In situ preparation of silver nanocomposites on cellulosic fibers – Microwave vs. conventional heating. *Carbohydr. Polym.* **2013**, *94* (1), 677.
- (10) Hribernik, S.; Sfiligoj-Smole, M.; Bele, M.; Gyergyek, S.; Jamnik, J.; Stana-Kleinschek, K. Synthesis of magnetic iron oxide particles: Development of an in situ coating procedure for fibrous materials. *Colloids Surf., A* **2012**, *400*, 58.
- (11) Weißl, M.; Rath, T.; Sattelkow, J.; Plank, H.; Eyley, S.; Thielemans, W.; Trimmel, G.; Spirk, S. Multi-layered nanoscale cellulose/CuInS<sub>2</sub> sandwich type thin films. *Carbohydr. Polym.* **2019**, *203*, 219.
- (12) Reishofer, D.; Ehmman, H. M.; Amenitsch, H.; Gspan, C.; Fischer, R.; Plank, H.; Trimmel, G.; Spirk, S. On the formation of Bi<sub>2</sub>S<sub>3</sub>-cellulose nanocomposite films from bismuth xanthates and trimethylsilyl-cellulose. *Carbohydr. Polym.* **2017**, *164*, 294.
- (13) Fradler, C.; Rath, T.; Dunst, S.; Letofsky-Papst, I.; Saf, R.; Kunert, B.; Hofer, F.; Resel, R.; Trimmel, G. Flexible polymer/copper indium sulfide hybrid solar cells and modules based on the metal xanthate route and low temperature annealing. *Sol. Energy Mater. Sol. Cells* **2014**, *124*, 117.
- (14) Reishofer, D.; Rath, T.; Ehmman, H. M.; Gspan, C.; Dunst, S.; Amenitsch, H.; Plank, H.; Alonso, B.; Belamie, E.; Trimmel, G. et al. Biobased Cellulosic-CuInS<sub>2</sub> Nanocomposites for Optoelectronic Applications. *ACS Sustain. Chem. Eng.* **2017**, *5*, 3115.
- (15) Rath, T.; Kaltenhauser, V.; Haas, W.; Reichmann, A.; Hofer, F.; Trimmel, G. Solution-processed small molecule/copper indium sulfide hybrid solar cells. *Sol. Energy Mater. Sol. Cells* **2013**, *114*, 38.
- (16) Shi, E.; Xu, Z.; Wang, W.; Xu, Y.; Zhang, Y.; Yang, X.; Liu, Q.; Zeng, T.; Song, S.; Jiang, Y. et al. Ag<sub>2</sub>S-doped core-shell nanostructures of Fe<sub>3</sub>O<sub>4</sub>@Ag<sub>3</sub>PO<sub>4</sub> ultrathin film: major role of hole in rapid degradation of pollutants under visible light irradiation. *Chem. Eng. J. (Amsterdam, Neth.)* **2019**, *366*, 123.
- (17) Yu, W.; Yin, J.; Li, Y.; Lai, B.; Jiang, T.; Li, Y.; Liu, H.; Liu, J.; Zhao, C.; Singh, S. C. et al. Ag<sub>2</sub>S Quantum Dots as an Infrared Excited Photocatalyst for Hydrogen Production. *ACS Appl. Energy Mater.* **2019**, *2* (4), 2751.
- (18) Yang, J.; Wang, J.; Zhao, K.; Izuishi, T.; Li, Y.; Shen, Q.; Zhong, X. CdSeTe/CdS Type-I Core/Shell Quantum Dot Sensitized Solar Cells with Efficiency over 9%. *J. Phys. Chem. C* **2015**, *119* (52), 28800.
- (19) Pons, T.; Pic, E.; Lequeux, N.; Cassette, E.; Bezdetnaya, L.; Guillemin, F.; Marchal, F.; Dubertret, B. Cadmium-Free CuInS<sub>2</sub>/ZnS Quantum Dots for Sentinel Lymph Node Imaging with Reduced Toxicity. *ACS Nano* **2010**, *4* (5), 2531.
- (20) Manthiram, A.; Fu, Y.; Chung, S.-H.; Zu, C.; Su, Y.-S. Rechargeable Lithium-Sulfur Batteries. *Chem. Rev.* **2014**, *114* (23), 11751.
- (21) Sadovnikov, S. I.; Gusev, A. I. Universal Approach to the Synthesis of Silver Sulfide in the Forms of Nanopowders, Quantum Dots, Core-Shell Nanoparticles, and Heteronanostructures. *European Journal of Inorganic Chemistry* **2016**, *2016* (31), 4944.
- (22) Koteeswara Reddy, N.; Devika, M.; Gopal, E. S. R. Review on Tin (II) Sulfide (SnS) Material: Synthesis, Properties, and Applications. *Crit. Rev. Solid State Mater. Sci.* **2015**, *40* (6), 359.
- (23) Österle, W.; Dmitriev, I. A. The Role of Solid Lubricants for Brake Friction Materials. *Lubricants* **2016**, *4* (1), 5.
- (24) Gorai, S.; Ganguli, D.; Chaudhuri, S. Synthesis of Copper Sulfides of Varying Morphologies and Stoichiometries Controlled by Chelating and Nonchelating Solvents in a Solvothermal Process. *Crystal Growth & Design* **2005**, *5* (3), 875.
- (25) Pearson, R. G. Hard and Soft Acids and Bases. *J. Am. Chem. Soc.* **1963**, *85* (22), 3533.
- (26) Narasagoudar, R. A.; Johnson, J. W.; O'Keefe, T. J. The anodic dissolution of ZnS electrodes in sulfuric acid solutions. *Hydrometallurgy* **1982**, *9* (1), 37.
- (27) Biswas, A. K.; Mohan, N. P. Kinetics of dissolution of copper(II) sulphide in aqueous sulphuric acid solutions. *Journal of Applied Chemistry and Biotechnology* **1971**, *21* (1), 15.
- (28) Jiang, X.; Xie, Y.; Lu, J.; He, W.; Zhu, L.; Qian, Y. Preparation and phase transformation of nanocrystalline copper sulfides (Cu<sub>9</sub>S<sub>8</sub>, Cu<sub>7</sub>S<sub>4</sub> and CuS) at low temperature. *Journal of Materials Chemistry* **2000**, *10* (9), 2193.
- (29) Freymeyer, N. J.; Cunningham, P. D.; Jones, E. C.; Golden, B. J.; Wiltrout, A. M.; Plass, K. E. Influence of Solvent Reducing Ability on Copper Sulfide Crystal Phase. *Crystal Growth & Design* **2013**, *13* (9), 4059.
- (30) Sadovnikov, S. I.; Gusev, A. I.; Rempel, A. A. Nonstoichiometry of nanocrystalline monoclinic silver sulfide. *Physical Chemistry Chemical Physics* **2015**, *17* (19), 12466.
- (31) Weißl, M.; Niegelhell, K.; Reishofer, D.; Zankel, A.; Innerlohinger, J.; Spirk, S. Homogeneous cellulose thin films by regeneration of cellulose xanthate: properties and characterization. *Cellulose* **2018**, *25* (1), 711.

- (32) Široký, J.; Blackburn, R. S.; Bechtold, T.; Taylor, J.; White, P. Attenuated total reflectance Fourier-transform Infrared spectroscopy analysis of crystallinity changes in lyocell following continuous treatment with sodium hydroxide. *Cellulose* **2010**, *17* (1), 103.
- (33) Luther, G. W.; Rickard, D. T.; Theberge, S.; Olroyd, A. Determination of Metal (Bi)Sulfide Stability Constants of Mn<sup>2+</sup>, Fe<sup>2+</sup>, Co<sup>2+</sup>, Ni<sup>2+</sup>, Cu<sup>2+</sup>, and Zn<sup>2+</sup> by Voltammetric Methods. *Environ. Sci. Technol.* **1996**, *30* (2), 671.
- (34) Rath, T.; Edler, M.; Haas, W.; Fischereder, A.; Moscher, S.; Schenk, A.; Trattnig, R.; Sezen, M.; Mauthner, G.; Pein, A. et al. A Direct Route Towards Polymer/Copper Indium Sulfide Nanocomposite Solar Cells. *Adv. Energy Mat.* **2011**, *1* (6), 1046.
- (35) Liu, Y.; Li, Y.; Kang, H.; Jin, T.; Jiao, L. Design, synthesis, and energy-related applications of metal sulfides. *Materials Horizons* **2016**, *3* (5), 402.

# Effect of packing density on zeta potential of cellulosics

Adisak Jaturapiree, Avinash P. Manian\* and Thomas Bechtold

Research Institute of Textile Chemistry/Physics, Hoechsterstrasse 73, 6850 Dornbirn, Austria

\* Corresponding author: Tel. +43 5572 28533; Fax: +43 5572 28629; Email: avinash.manian@uibk.ac.at

## Abstract

The zeta potential and zeta potential corrected for plug conductance as function of pH were measured on modal on cotton fibers under varying fiber packing densities. The cotton and modal exhibited very similar magnitudes at the same packing density. And, modal fibers measured at different packing densities, exhibited different magnitudes. These differences however were negated by corrections for plug conductance. It is to be noted though, that the process of correction for plug conductance has the potential for altering the sample packing and therefore the results.

## Introduction

Solid substrates in contact with aqueous solutions acquire a surface charge due to: dissociation (or ionization) of surface functional groups; adsorption of ions from solution; and/or dissolution of ions from the substrate into solution [1]. Differences in dielectric permittivity between the solid and liquid may also result in the solid surface acquiring a charge (Coehn's rule) [2]. But in general, ionic effects exert the greatest influence in determining the degree and nature of charge on solid surfaces. Ions in liquid accumulate in the vicinity of the solid (largely counter-ions) and compensate for the charge on the solid surface. This system of charges across the solid-liquid interface, comprised of surface charges on the solid and ions in liquid, is termed the 'electrical double layer'. A schematic representation of an idealized model of the electrical double layer, redrawn from reference [3], is shown in Figure 1.

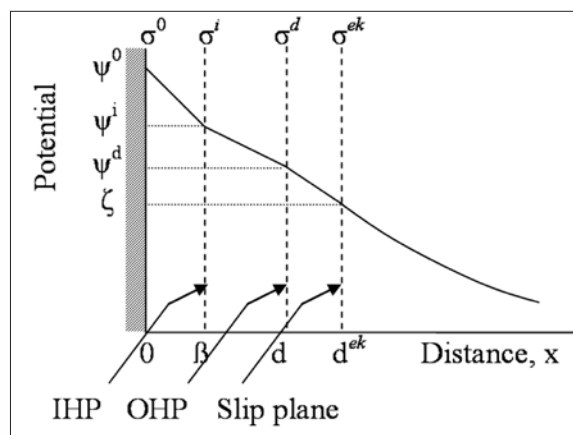


**Figure 1.** Schematic representation of electrical double layer, showing change in electric potential ( $\psi$ ) with increasing distance ( $x$ ) from solid surface (at 0) into bulk liquid, beginning from:  $\psi^0$ , the potential at the solid surface;  $\psi^i$ , the potential at the Inner Helmholtz Plane (IHP) located at distance ' $\beta$ ';  $\psi^d$ , the potential at the Outer Helmholtz Plane (OHP) located at distance ' $d$ '; and  $\zeta$ , the potential at the slip plane located at distance ' $d^{ek}$ ' (also referred to as the electrokinetic or zeta potential). All potentials are defined with respect to that in bulk liquid. The corresponding charge densities ( $\sigma$ ) are also shown. Redrawn from Reference 3.

The electrical double layer is envisaged as being comprised of: the Inner Helmholtz Layer delineated by the IHP, the Outer Helmholtz Layer delineated by the OHP, and the slip plane. Ions in liquid that have a specific affinity for the solid (also referred to as ‘specifically adsorbing ions’) are believed to be localized at the IHP; while the OHP is the locale for ‘indifferent ions’, i.e. those counter-ions that have no specific affinity for the solid and adsorb purely through coulombic interactions. The inner and outer Helmholtz layers together comprise what is known as the ‘Stern layer’, beyond which is the ‘diffuse layer’ that begins from the OHP. Relative motion between the solid and bulk liquid (induced mechanically or electrically) occurs at the slip plane, also known as the shear plane. The liquid in the region between the solid surface and the slip plane, which includes the Stern layer, is immobile and referred to as the ‘hydrodynamically stagnant layer’.

Of the different potentials defined in the electrical double layer, only the electrokinetic or zeta potential (ZP) can be experimentally determined. The ZP is often regarded as an estimate of the potential at the OHP,  $\psi^d$  (also referred to as the ‘diffuse layer potential’), and experimental conditions are designed to minimize differences between the electrokinetic and diffuse layer potentials.

One method of measuring ZP in fibers is the ‘streaming potential’ method. An electrolyte solution is forced by external pressure through a plug of fibers placed in a measurement cell, resulting in the development of a streaming potential across the fiber plug. The potential across the fiber plug, and its resistance, are measured with electrodes placed at either end of the plug; and the ZP is derived from the Helmholtz-Smoluchowski equation (equation 1):

$$\zeta = \frac{dU}{dp} \times \frac{\eta}{\varepsilon \times \varepsilon_0} \times \frac{L}{Q \times R_s} \quad (1)$$

where,  $\zeta = \text{ZP (V)}$ ;  $dU/dp = \text{change in streaming potential with change in external pressure (V/Pa)}$ ;  $\eta = \text{electrolyte viscosity (Pa.s)}$ ;  $\varepsilon = \text{dielectric constant of electrolyte}$ ;  $\varepsilon_0 = \text{permittivity of free space (F/m)}$ ;  $L$  and  $Q = \text{length and cross-sectional area of fiber plug}$ ; and  $R_s = \text{electrical resistance } (\Omega) \text{ of fiber plug flushed with the streaming solution}$ .

It is difficult to measure the length and cross-sectional area of fiber plugs, but the term  $L/Q$  maybe estimated with equation 2 (the Fairbrother-Mastin method):

$$\frac{L}{Q} = R_s \times K_L \quad (2)$$

where,  $K_L = \text{conductivity of streaming solution (S/m)}$ ; which when substituted in equation 1, yields equation 3:

$$\zeta = \frac{dU}{dp} \times \frac{\eta}{\varepsilon \times \varepsilon_0} \times K_L \quad (3)$$

With increasing ionic strength of streaming solutions, there is a greater rate of decay in potential with increasing distance from the solid surface. This phenomenon, also referred to as a decrease in thickness or suppression of the electrical double layer [4, 5], leads to a widening of differences between the diffuse layer and zeta potentials. Hence, to promote sensitivity in measurements, the amount of electrolyte in streaming solutions is kept low (in the range of  $10^{-4}$ - $10^{-3}$  mol/l electrolyte). With dilute electrolyte solutions however, the magnitude of plug conductivity due to accumulation of ions may become significant, and lead to errors in ZP values as calculated with equation 3.

When the length and cross-sectional area of the fiber plug are estimated from the plug resistance (and solution conductivity) of fiber plug flushed with a concentrated electrolyte solution, the contribution of accumulated ions to total fiber plug conductivity becomes negligible in comparison to conductivity of the solution bulk; and the  $L/Q$  term maybe more accurately estimated with equation 4:

$$\frac{L}{Q} = R_s^c \times K_L^c \quad (4)$$

where,  $R_s^c = \text{electrical resistance } (\Omega) \text{ of fiber plug flushed with concentrated electrolyte solution}$ ; and  $K_L^c = \text{conductivity (S/m) of the concentrated electrolyte solution}$ .

In usual practice, ZP measurements are conducted using streaming solutions of low electrolyte concentration. The fiber plugs may then be flushed with a concentrated solution of electrolyte (usually 0.1 mol/l KCl) for estimation of the  $L/Q$  term. Equation 4 when substituted in equation 1 yields equation 5:

$$\zeta_{Corr} = \frac{dU}{dp} \times \frac{\eta}{\varepsilon \times \varepsilon_0} \times \frac{R_s^c \times K_L^c}{R_s} \quad (5)$$

where,  $\zeta_{Corr} = \text{ZP (V) corrected for plug conductance}$ .

In theory, the ZP magnitudes vary only with surface charge (as function of pH), electrolyte concentration, the electrolyte, and the solvent. However, they are susceptible to even minor amounts of impurities on substrates and also to measurement conditions. Charges adsorbed behind the layer of shear (in the stagnant layer) also influence the magnitudes. Hence,

there are variations in ZP magnitudes of the same substrate measured in different laboratories.

The aim of the work was to investigate the effect of varying the packing density on the resulting ZP values of one cellulosic fiber type (modal), and to compare the ZP values of two cellulosic fibers (modal vs. cotton) under similar packing densities.

## Materials and Methods

### Materials

The modal and cotton fibers were supplied pre-cleaned, i.e. scoured, and in case of cotton, also

bleached, and were used as received. All reagents used were of reagent grade, and deionized water was used in the formulation of solutions.

### Methods

The measurements were performed on an Electokinetic Analyzer from Anton Paar GmbH (Austria). It consists of a tubular measurement cell (2 cm inner diameter) in which fiber samples may be packed between two electrodes (Ag/AgCl) inserted in from both sides. The distance between the electrodes may be varied, and thus the fiber packing density may be altered. That feature was employed to perform four experimental sets as listed in Table I, with three replicate measurements each.

Set	Fiber type and mass	Distance between electrodes	Fiber packing density (nominal)
a.	Modal, 1.0 g	8 mm	0.40 g/cm <sup>3</sup>
b.	Modal, 1.0 g	14 mm	0.23 g/cm <sup>3</sup>
c.	Modal, 1.5 g	12 mm	0.40 g/cm <sup>3</sup>
d.	Cotton, 1.0 g	8 mm	0.40 g/cm <sup>3</sup>

**Table I.** The nominal packing densities employed in measurement sets

Pre-weighed amounts of the fibers were soaked for 1 h in 200 ml of the streaming solution ( $1 \times 10^{-3}$  mol/l KCl adjusted to ca. pH 10 with NaOH), before being loaded into the measurement cell. The cell was then flushed with the streaming solution from either direction multiple times to remove any entrapped air. The measurements were then performed by streaming the solution through the substrate plug in the tubular cell along both directions, with flow pressures of up to 35 kPa (350 mbar). The pH of the streaming solution was titrated down in regular decrements from ca. 10 to ca. 2, and the potential was measured 4 times at each pH change. The asymmetric potential in all measurements was in the range of  $\pm 3$  mV. At the end, the cell with fiber plug was flushed with 0.1 mol/l KCl, and the electrical resistance of the fiber plug and the solution conductance were re-measured for calculating the ZP corrected for plug conductance.

## Results

The profiles of the ZP ( $\zeta$ ) and ZP corrected for plug conductance ( $\zeta_{\text{Corr}}$ ) vs. pH are shown in Figure 2. All are characteristic of cellulose, with a plateau in the pH range of ca. 10–4 followed by a rise towards zero as the pH decreases below 4, which is attributed to the dissociation profile of cellulosic carboxyl groups as function of pH. With a  $pK_a$  of ca. 3.5–4 [6-8], the

groups are fully deprotonated above pH 4, and the levels of protonation rise as the pH decreases below 4.

There were differences of ZP magnitudes in the plateau regions between some experimental sets. In part A of the figure, it may be observed that  $\zeta$  magnitudes at the plateau were greater with a nominal packing density of 0.23 g/cm<sup>3</sup> (set b) as compared to 0.40 g/cm<sup>3</sup> (sets a and c). One reason may be that more of the fiber carboxyl groups become accessible to the streaming solution at lower packing densities. However, in part B of the figure it may be observed that the  $\zeta_{\text{Corr}}$  magnitudes at the plateau were similar between sets b and c, which suggests that the effect of accessibility differences becomes negligible when the values are corrected for plug conductance.

In part C of the figure, it may be observed that there were generally no differences between the  $\zeta$  vs. pH profiles of cotton and modal fibers when measured at the same nominal packing density (sets a, c and d). And in part D of the figure, it may be observed that there were also no differences in the  $\zeta_{\text{Corr}}$  vs. pH profiles between sets c and d. This suggests that different cellulosic fiber types measured under the same experimental conditions yield similar results.

There was an apparent anomaly with experimental set a, in that whereas the  $\zeta$  values matched those of set c,

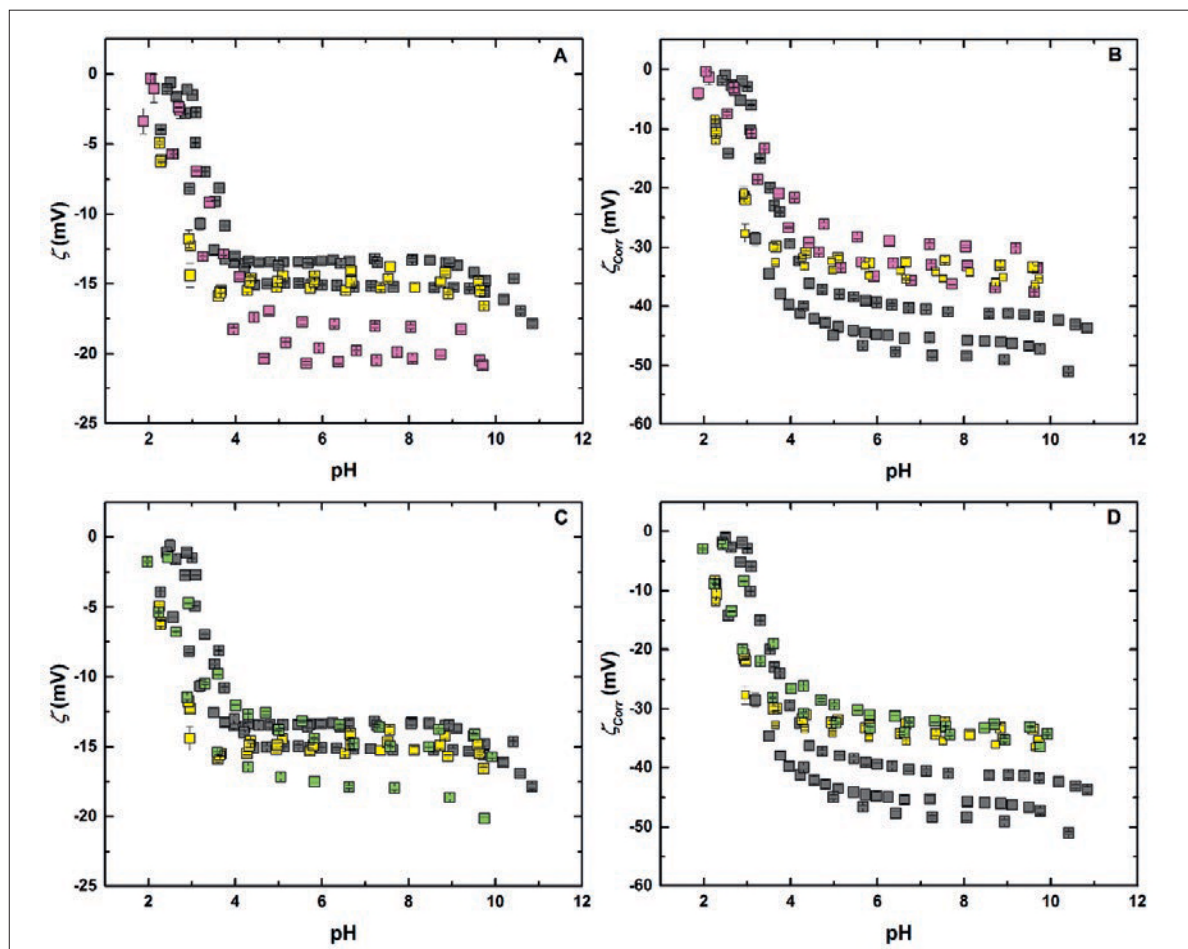


**Figure 2.** The ZP (parts A and C), and ZP corrected for plug conductance (parts B and D): set a (■); set b (■); set c (■); and, set d (■). The plots depict the results of all three replicate measurements per set. Note that the scale and range of values in the  $\zeta$  plots are not the same as in the  $\zeta_{\text{corr}}$  plots

the  $\zeta_{\text{corr}}$  magnitudes at the plateau region in set a, were greater. The fiber packing densities were the same in both sets, and thus it is difficult to understand the reasons for these differences. A possible cause of the apparent anomaly in set a, is that the fiber packing was somehow altered when the plug was flushed with the concentrated electrolyte solution (0.1 mol/l KCl). However, it is difficult to verify this hypothesis.

## Conclusions

It was observed that differences of packing densities in measurements on the same fiber produced a difference in the  $\zeta$  values. That may be because fiber functional groups have greater accessibility to the streaming solution when the packing density is lower. However, the effect of such packing densities appear to become negligible when the measured values are corrected for plug conductance. It is to be noted

though, that the process of correction for plug conductance has the potential for altering the sample packing and therefore the results.

## References

1. Jacobasch, H.-J., et al., *Problems and results of zeta-potential measurements on fibers*. Colloid & Polymer Science, 1985. **263**(1): p. 3-24.
2. Lyklema, J., *Electrokinetics after Smoluchowski*. Colloids and Surfaces A: Physicochemical and Engineering Aspects, 2003. **222**(1-3): p. 5-14.
3. Delgado, A.V., et al., *Measurement and Interpretation of Electrokinetic Phenomena (IUPAC Technical Report)*. Pure and Applied Chemistry, 2005. **77**(10): p. 1753-1805.
4. Bull, H.B., et al., *Studies on Electrokinetic Potentials. VI. Electrical Phenomena at Interfaces*. Journal of Physical Chemistry, 1931. **35**(1): p. 309-330.

5. Herrington, T.M., et al., *Adsorption of ions at the cellulose/aqueous electrolyte interface. Part 3.— Calculation of the potential at the surface of cellulose fibres*. Journal of the Chemical Society, Faraday Transactions 1: Physical Chemistry in Condensed Phases, 1984. **80**(6): p. 1553-1566.
6. Bagrovskaya, N.A., et al., *Influence of Solvent Acidity on Equilibrium Sorption of Zn(II) and Cd(II) by Cellulose-based Polymers*. Russian Journal of General Chemistry, 2002. **72**(3): p. 345-348.
7. Shet, R.T., et al., *Polyelectrolyte behavior of chemically modified cotton cellulose*. Journal of Applied Polymer Science, 1982. **27**(2): p. 631-636.
8. Frás, L., et al., *Determination of dissociable groups in natural and regenerated cellulose fibers by different titration methods*. Journal of Applied Polymer Science, 2004. **92**(5): p. 3186-3194.

